CHALMERS
UNIVERSITY OF TECHNOLOGY

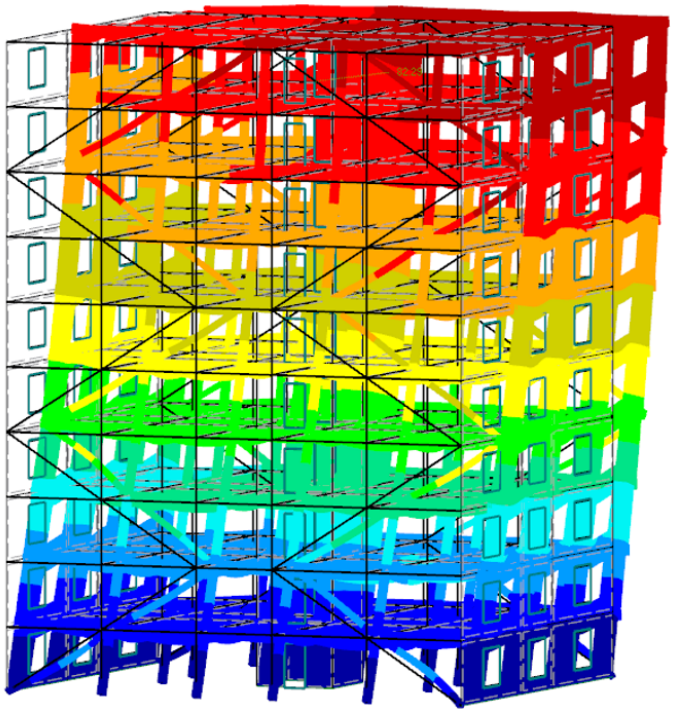

Modeling of Cross Laminated Timber in FE Analysis

A sensitivity study regarding different CLT modeling assumptions and their influence on high-rise timber buildings

Master's thesis in Master Programme Structural Engineering and Building Technology

CAROLINE JOHANSSON
ERIK JOHANSSON

DEPARTMENT OF ARCHITECTURE AND CIVIL ENGINEERING
CHALMERS UNIVERSITY OF TECHNOLOGY
Gothenburg, Sweden 2021
www.chalmers.se

Master's thesis 2021

Modeling of Cross Laminated Timber in FE Analysis

A sensitivity study regarding different CLT modeling assumptions and their influence on high-rise timber buildings

CAROLINE JOHANSSON
ERIK JOHANSSON

CHALMERS
UNIVERSITY OF TECHNOLOGY

Department of Architecture and Civil Engineering
Division of Structural Engineering
Lightweight Structures
Chalmers University of Technology
Gothenburg, Sweden 2021

Modeling of Cross Laminated Timber in FE Analysis
A sensitivity study regarding different CLT modeling assumptions and their influence on high-rise timber buildings
CAROLINE JOHANSSON
ERIK JOHANSSON

Supervisor: Linda Jakobsson, ELU
Examiner: Robert Jockwer, Structural Engineering, Lightweight Structures

Master's Thesis 2021
Department of Architecture and Civil Engineering
Division of Structural Engineering
Lightweight Structures
Chalmers University of Technology
SE-412 96 Gothenburg
Telephone +46 31 772 1000

Cover: Deformed shape of reference building under horizontal loads in *RFEM*.

Typeset in LaTeX
Printed by Chalmers Reproservice
Gothenburg, Sweden 2021

Modeling of Cross Laminated Timber in FE Analysis
A sensitivity study regarding different CLT modeling assumptions and their influence on high-rise timber buildings
CAROLINE JOHANSSON, ERIK JOHANSSON
Department of Architecture and Civil Engineering
Chalmers University of Technology

Abstract

The use of cross laminated timber (CLT) is steadily increasing due to its beneficial structural properties, but also due to the increased popularity of timber buildings in general. Timber elements, such as CLT, have a highly orthotropic behaviour that can be challenging to implement in finite element analysis, and the consequences of the orthotropic modeling could be more substantial for taller timber buildings. This thesis investigates different methods and assumptions regarding how CLT is modeled in FE-analysis, and which advantages or disadvantages certain modeling assumptions have in regards to results on both element level and system level.

In this thesis, different modeling assumptions for CLT shell elements were analysed both as independent elements and as parts of a 10-storey, all timber, reference building. The reference building was created in the finite element program *RFEM* with the aim to replicate properties of an existing high-rise timber building, while still maintaining a relatively simple geometry.

The stiffness parameters for the different modeling assumptions were extracted partly from recommendations and research, but they also include various simplifications of existing assumptions. The stiffness properties related to out-of-plane shear are in general more complicated than other stiffness properties, and many inhomogeneous recommendations therefore exists. The out-of-plane shear stiffness parameter was therefore investigated more thoroughly. The modeling assumptions were applied to CLT slabs and to CLT shear walls to investigate the behaviour of the elements both when exposed to bending and in-plane shear. Different reduction factors were also included in the sensitivity study.

The results show that many of the modeling assumptions yield similar results in regards to deflections and deformations in general, but certain simplified models show larger deviations. The reduction factor for in-plane shear that was investigated in the thesis resulted in large deformation differences in the sensitivity study.

Based on the results from the analyses, a number of general recommendations and conclusions regarding how CLT shells should be modeled in FE-analysis are presented in the small-scale study and in the final chapter of this thesis.

Keywords: Cross laminated timber, Finite element method, Bending stiffness, Shear stiffness, Reduction factors, Stiffness matrix.

Modellering av korslaminerat trä i FE-analys
En känslighetsanalys av olika modelleringsantaganden för KL-trä och dessas påverkan på höga trähus
CAROLINE JOHANSSON, ERIK JOHANSSON
Institutionen för arkitektur och samhällsbyggnadsteknik
Chalmers tekniska högskola

Sammanfattning

Användandet av korslaminerat trä (KL-trä) ökar ständigt i byggsektorn på grund av dess fördelaktiga bärighetsegenskaper, men även på grund av träbyggnaders generella populäritetsökning. Träelement, så som KL-trä, har ett ortotropt verkningssätt som kan vara svårt att representera i finit elementanalys, och ortotropin kan vara av särskilt stor betydelse för deformationerna i höga trähus. Detta examensarbete undersöker olika metoder och modelleringsantaganden som kan användas när KL-trä definieras i FE-program, men även för- och nackdelar både på elementnivå och strukturnivå för antagandena.

I denna rapport har olika modelleringsantaganden för KL-träelement analyserats både som oberoende element och som delar av ett tio våningar högt referenshus helt i trä. Referenshuset skapades i det finita elementprogrammet *RFEM* med målet att i så många avseenden som möjligt efterlikna ett existerande högt trähus, samtidigt som geometrin behålls relativt simpel.

Styvhetsparametrarna för de olika modelleringsantagandena har hämtats eller beräknats dels enligt rekommendationer och forskning, men vissa antaganden har också skapts genom att implementera förenklingar på de mer vedertagna modelleringsantagandena. Skjuvstyvheter vinkelrätt plattans plan är generellt mer komplicerade att definiera än andra styvheter, vilket resulterar i att många av de existerande rekommendationerna skiljer sig från varandra. Modelleringsantagandena applicerades på både KL-träbjälklag och KL-träskjuvväggar för att undersöka responsen av elementen när de är lastade i böjning och när de är lastade i sitt eget plan. Olika reduktionsfaktorer beträffande KL-trä har också inkluderats i känslighetsanalysen.

Resultaten från analyserna visar att många av modelleringsantagandena ger liknande deformationer och nedböjningar, med ett fåtal förenklade modeller som undantag. Reduktionsfaktorn för skjuvstyvhet i planet som undersöktes ger stora skillnader i deformationer beroende på vilket värde som antas för reduktionsfaktorn.

Baserat på analysernas resultat presenteras ett antal rekommendationer och slutsatser angående hur KL-trä bör modelleras i FEM.

Nyckelord: Korslaminerat trä (KL-trä), Finita elementmetoden, Böjstyvhet, Skjuvstyvhet, Reduktionsfaktorer, Styvhetsmatris.

Acknowledgements

This thesis was written as a part of the master's program *Structural Engineering and Building Technology* at Chalmers during the spring 2021. As a consequence of the restrictions due to Covid-19, the master's thesis work has been prohibited from being carried out as they have been other years, but we are very grateful for the people around us who has always tried to do the best of the situation.

A special thanks goes out to our supervisor Linda Jakobsson who has supported us both in the process of this thesis but also by introducing us to her coworkers at ELU during this very special year. We would also like to thank Johanna Riad for her help with FEM related questions.

Throughout the thesis, our examiner Robert Jockwer has provided us with feedback, invited us to FEM discussions and mediated our questions to experts within the field, all of which we have appreciated a lot. Gratitude also goes towards Patrik Aondio who has contributed with his expertise concerning material properties of CLT in FE analysis when we have gotten stuck at technical questions.

Finally we would like to thank our opponents Signý Ingólfsdóttir and Daníel Sæmundsson who has provided us with valuable feedback to help improve our thesis.

Caroline Johansson, Erik Johansson, Gothenburg, June 2021

Contents

List of Figures

List of Tables

1

Introduction

1.1 Background

The interest for cross laminated timber (CLT) is constantly increasing within the industry. The material has proven to be a good environmentally friendly material while still providing possibilities for a fast assembly at the building site and a good strength-density relationship at a reasonable price. Simultaneously with the development of massive timber products, there is an ongoing densification of many cities which requires taller and sometimes more complex buildings. For these kinds of projects the finite element (FE) method is an important tool for analysing, designing and assessing the structures, and the use of FE-programs is constantly extended.

Considering these three fields of strong development; environmentally friendly construction, densification of cities and extended use of FE-modelling, this thesis will make an attempt to distinguish how to make the FE-modelling of CLT in high-rise timber buildings more efficient in terms of sufficiently precise results for a reasonable amount of time spent on the model. This will be done by investigating which parameters associated with CLT that are the most crucial for an accurate result from a static analysis of the structure for a high-rise timber building.

1.2 Aims

The following section addresses the purpose of the thesis:

- To study how the load path and deformations of a high-rise timber building is affected by different parameters such as material stiffness, reduction factors and rigidity of connections.
- To create an increased understanding of how modeling choices associated with the orthotropy and connections of CLT elements affects the outcome of the analysis on element and structural level.

1.3 Objectives

The following section addresses the objectives of the thesis:

- To perform a sensitivity study of which modeling assumptions for CLT elements affects the outcome of an FE-analysis for a high-rise timber building, and draw conclusions of how each parameter affects the result.
- To compose recommendations of how to model CLT elements with respect to the orthotropy of the material.
- To highlight aspects of moment rigidity in connections for CLT slab elements which will have to be considered when modeling a timber structure in FE-software.

1.4 Limitations

The focus of this thesis is to evaluate how the structural behaviour is affected by different ways of modeling CLT elements and their connections in a finite element program. To avoid the focus to shift towards a dynamic study, the analysis of the building is made using static loads. The dynamic load effects are reduced by limiting the height of the building, and no dynamic studies is be performed.

To maintain the focus of the sensitivity study to the effects of the modeling itself, the geometry and load combinations are not changed within the sensitivity study. Furthermore, the load cases applied to the structure are simplified and thus may not represent the actual design loads of the structure. Requirements concerning fire safety and acoustics will not be treated.

The analysis is of linear nature with regards to material models. Second order geometrical effects are considered by the program *RFEM*, but they not investigated in detail.

The connections of the structure is not modeled or designed in detail. Ways of considering connections between CLT slab elements in floor structures are addressed, but with the simplification that connections are considered unable to resist moment.

For the purpose of maintaining focus on the analysis of the entire structure, 1D and 2D elements are used. By avoiding solid elements, internal stresses for the elements are represented in a less detailed way, but the structural behaviour remains the same and time consumption for the analysis is reduced.

The whole structural system of the reference building is protected by the facade and roof, thus the structural components is considered to be exposed to an indoor climate. Exposure to moisture in the production stage is addressed, and the environmental factors such as e.g. k_{mod} is therefore considered constant during the sensitivity study.

1.5 Method

The method consists of the following steps: A literature study, the modelling of a building to use as a reference design, analysing said building with FE-software, validate or verify the results and finally compile the results and make conclusions.

The literature study focuses on material properties for cross laminated timber products and how these are translated into the input data used when modeling timber structures in an FE-program. Connections between CLT slabs are also investigated to determine how they can be represented in FE analysis. To increase the understanding of different modeling techniques, one part addresses the theory behind FE-modeling. The aim is that the literature study should make it possible to delimit the project and make the outcomes from the analysis as interesting and relevant as possible. Therefore, one important aspect is to determine which structural behaviours that are most important for a high-rise timber building, and how the modeling of CLT and CLT connections affects these aspects. Conclusions can whereafter be made of in which detail these aspects should be modelled to capture the real behaviour without spending an unnecessary amount of time on constructing the model.

The reference building is modeled in the FE-software *RFEM 5*, and used as a reference design in the sensitivity study. Hand calculations in *Mathcad Prime 6* or scripts written in *MATLAB* are used to produce necessary input data for the FE-model. The reference design is a high-rise timber building with many CLT elements and glulam beams. It is not a replication or copy of an already existing structure, but rather a combination of parts of different existing structures where the goal is to capture different behaviours and effects that this thesis aims to analyse, while still maintaining a relatively simple geometry. The model is verified against hand calculations.

The sensitivity study is focused on changing different modeling assumptions which are used to describe the structure in the FE-model, and observing the consequences these changes have on the structural behaviour. Parameters that are altered are chosen considering the result from the literature study, but also with respect to conclusions drawn in the small scale studies conducted in chapter 5. Finally, the observations are compiled into meaningful results, and conclusions regarding how to efficiently model the CLT components of a timber building in an FE-program are made.

1.6 Current research

The field of timber construction has developed rapidly over the past few years. When aiming to build higher, new problems occur and there is plenty of ongoing research covering everything between CLT shear stiffness calculations and connection rigidity to dynamic earthquake loads and implementation of FEM.

Regarding the assumptions for CLT shear stiffness, several models exists and has been developed over the last few years. The large number of models depends on the

lack of standardization globally, which results in local variations of which methods are used. For example, both the German and the Swiss annex to the Eurocode includes recommendations of how to assume stiffness for CLT and which reduction factors that should be applied on the stiffness parameters. The Swedish annex does not contain any specific recommendations regarding CLT besides the analysis of *Mechanically jointed beams*, which is a method presented in the annex of Eurocode 5. The method for *Mechanically jointed beams* has however been further developed by Swedish Wood in the Swedish CLT handbook, where suggestions for how to calculate the stiffness of CLT based on this method is presented. For in-plane shear deformations in CLT, a thorough report was published in 2019 by Lukacs et al. (2019), investigating the effects of using different methods to determine the deformations in a single CLT element.

Besides the fact that there are no standardized methods for determining the stiffness for CLT, there is also a lack of guidelines for how FEM should be implemented when designing or evaluating timber buildings. In the field of steel construction, a new part the Eurocode called EN 1993-1-14 is in development and is soon to be put into use (Al-Emrani, 2019). A similar project for the timber construction field has been started with the aim to investigate a suitable approach for developing recommendations for finite element analysis of timber structures. When it comes to CLT in FE programs, Aondio et al. (2020) have contributed with a very useful article addressing how to determine the stiffness of the material in a form that can easily be used as input data in the analysis.

The effects of connections in CLT structures is a field that has not yet been fully charted. Current research investigates how the in-plane flexibility of a diaphragm floor is influenced by connections and how the flexibility in its turn affects the load distribution to the supports (D'Arenzo et al., 2019), and the transferring of moment between CLT slabs is addressed by Asselstine et al. (2021), but further investigations of the subject are needed.

There are a lot of ongoing studies of earthquake loads on timber buildings, since the connections for CLT elements usually have a too brittle behaviour to manage the dynamic loads from earthquakes. One of the reports newly published addressing how this problem can be treated is *Axial slip-friction connections for cross-laminated timber* (Fitzgerald et al., 2021). While this is a very interesting and modern subject for timber construction in large parts of the world, Sweden is not significantly exposed to earthquakes and thus the load case is rarely considered in design.

2

CLT construction

2.1 Development of CLT

Even though timber has a long history as a construction material, it has traditionally rarely been used for taller buildings. Since the second half of the 20th century to the beginning of the 21st century, the other conventional building materials, such as steel and concrete, have simply been cheaper and more effective (Voulpiotis et al., 2021). Timber materials have however seen a large increase in technological advancements, making it possible to utilize the material in a more efficient way. One of those important advancements is the development of cross laminated timber, which was first developed in Austria in the late 1990's (Gustafsson et al., 2019). CLT is built up by sawn timber laminates and utilized as plates or panels which can carry load in two directions.

2.2 CLT as a construction material

Cross laminated timber is produced by stacking timber boards in layers and orientating the fibers in the different layers orthogonal to each other (Popovski et al., 2019). The layers are glued together and form panels which can be used as, for example, slab or wall elements. The boards on the top and bottom of the CLT element are usually orientated in the same direction, which gives the panel a main direction for carrying load and the other direction thus becomes the secondary load carrying direction. The ability to have two load carrying directions is what makes CLT a good plate material, and the distributions of the stiffness in each load carrying direction could be designed to suit specific situations. A cut of a three layer and five layer CLT element can be seen in Figure 2.1.

CLT panels are produced in factories and transported in prepared sections to the building site (Crocetti et al., 2016). This contributes to the efficiency of the construction process but also limits the maximum size of each panel. Furthermore, the majority of the connections between CLT panels are assumed unable to resist moment (Gustafsson et al., 2019), meaning that transportation limits often affect the structural system.

The strength and properties of CLT are dependent on the sawn timber of which the panel is made, but also how the boards in the panel are assembled, for example how they are glued together (Gustafsson et al., 2019). To understand the behavior of

the CLT panels, a basic knowledge about wood as a raw material and sawn timber as a construction material is required.

Figure 2.1: Cut of a three layer and five layer CLT element. "Cross laminated timber blocks" by ODF is licensed under CC BY 2.0.

2.3 Mechanical properties of timber

Structural timber is graded and classified into strength classes by measuring e.g. the elasticity modulus of the wood. Timber is also a heavily orthotropic material, and it is prone to time and moisture dependant effects such as creep and shrinkage (Johansson, 2016).

The maximum member sizes of structural timber is limited by the available dimensions of timber logs. This limitation has to be taken into consideration when designing structures using sawn timber members.

2.3.1 Orthotropy

Just like concrete, timber has different capacity when exposed to tension compared to when it is exposed to compression, but the capacity also differs between the directions in the material. The fibers of the wood, which are oriented along the growth direction of the tree, provide a high capacity both in tension and compression when the stress is parallel to the grain. According to Johansson (2016), it is common practise and also necessary to assume the strengths in the directions perpendicular to the grains (the radial and tangential direction) to be equal, even though they differ somewhat in the actual material. The strength used for both perpendicular directions is notated $f_{t,90}$ when the material is exposed to tensile stresses and $f_{c,90}$ when the material is in compression. The strengths in the direction of the fibers are notated with a 0 instead of 90 since the index refers to the angle between the stress direction and the direction of the grains.

The tension stiffness and the compression stiffness are assumed to be equal for the material, and therefore only two different values of the elasticity modulus is required, E_0 and E_{90}.

The shear strength of timber is also dependant on the direction of the shear loading. The two longitudinal shear strengths τ_{RL} and τ_{TL} are usually assumed to be equal for engineering purposes (Johansson, 2016), and the longitudinal strength can be denoted as $f_{v,090}$ or f_v. The third shear direction, τ_{RT}, is called rolling shear and has approximately half the strength of longitudinal shear. Rolling shear is rare for rectangular timber beams, but it can be common for different glulam cross-sections or CLT. Rolling shear can be denoted as $f_{v,9090}$ or f_r. The stiffness difference between rolling shear and longitudinal shear can be even larger than the strength difference (Gustafsson et al., 2019). The shear directions and their naming conventions are presented in Figure 2.2.

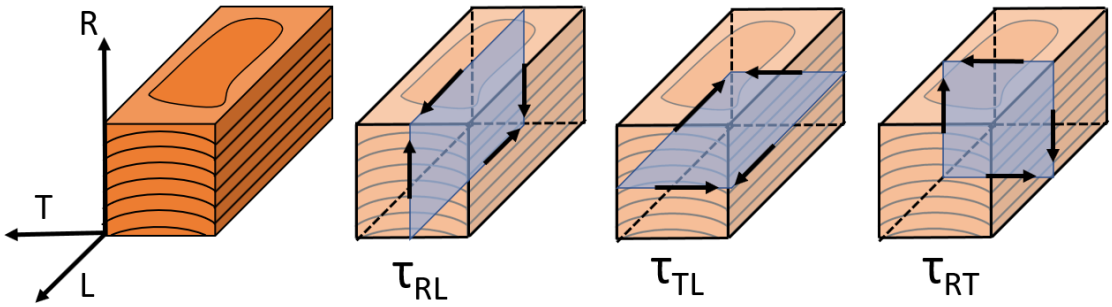

Figure 2.2: Shear directions for timber.

2.3.2 Time and moisture dependant effects

Timber is affected by both creep, shrinkage and moisture variations. Loss of strength over time is very apparent in timber, and were first modeled in the 1950's by a so called Madison curve that had a logarithmic relationship (Johansson, 2016). This phenomenon is compressed and simplified for structural engineering into five load duration classes that are defined in Eurocode 5. Moisture effects are in a similar manner simplified into three service classes in Eurocode 5, dependant on the expected average moisture content of the structure.

The effects of load duration and moisture variations in timber are with the use of load duration classes and service classes combined into a single reduction factor k_{mod}, that reduces the strength of the material. Creep deformation is further treated in Eurocode 5 by an additional reduction factor k_{def}.

2.4 Mechanical properties of CLT

The determination of the characteristics for a CLT plate is not standardized or regulated in the Eurocodes, neither is the procedure described in the Swedish national annex. This has resulted in various ways of calculating the characteristic strengths

and stiffnesses for CLT. The shear stiffnesses are particularly affected of this phenomenon. A selection of methods used for calculating the stiffnesses is presented in section 4.1.

The Swedish CLT handbook, published by Swedish Wood (Gustafsson et al., 2019), proposes the Gamma-method for hand calculations of deflections in CLT members. The method is proposed in Eurocode 5 to compensate for shear deformations which are not usually accounted for when using beam theory.

2.4.1 Orthotropy

The notations of sectional forces and moments for CLT panels differs throughout the literature. For simplicity, the conventions in this report are chosen to be the same as the FE-program *RFEM* uses. The convention is presented in Figure 2.3

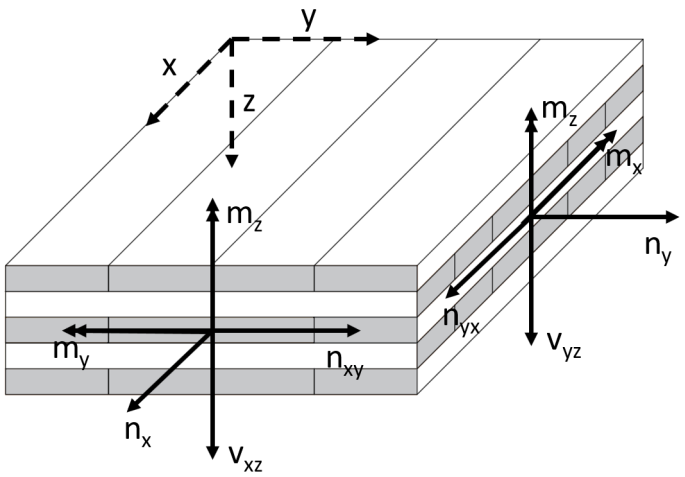

Figure 2.3: Definition of directions in a CLT element.

Instead of relating the direction of the stiffnesses to the direction of the grain, as in sawn timber, the directions are refereed to using the coordinate system for the CLT panel. In this coordinate system, x is the strong direction, y is the weak direction, and z is out-of-plane. The stiffnesses of the plate thus becomes: E_x, E_y, G_{xz}, G_{yz} and G_{xy}. These stiffnesses are explained in further detail in chapter 4.

2.4.2 Stress distribution over the cross section

When calculating stresses in CLT plates, the net cross section of the plate is used instead of the gross cross section. This means that only the boards that are spanning in the loaded direction should be considered when evaluating cross sectional constants such as inertia or moment resistance. This is based on the assumption that the cross layers are not edge-glued, and that their stiffness in bending therefore is negligible. An illustration of this is shown in Figure 2.4, where a plate is loaded in bending in both the major and minor direction.

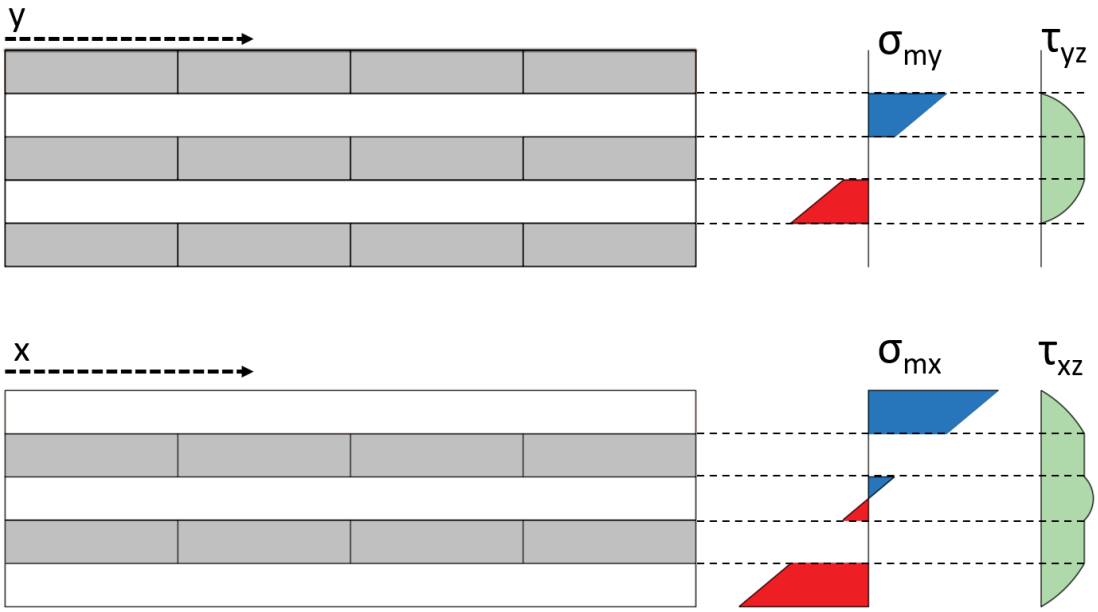

Figure 2.4: Stress distribution over a CLT cross section loaded in bending.

2.5 CLT connections

Since CLT elements are delivered to the building sites in modules and separate structural members, there is a large need for connections to assemble the structures. In this section, spline connections commonly used for joining CLT-slab elements are addressed, since these elements are of particular significance for the sensitivity study. Several other types of connections are also of importance for the reference building, but are in this thesis left out as a limitation.

For slab-slab connections made on site, a convenient method is to use surface splines as seen in Figure 2.5. The splines can be applied on one or two sides of the slab. The single spline connections is less time consuming but provides less rigidity than a double spline connection (Mohammad et al., 2019). Double surface splines can be considered to transfer some out of plane moment, which is not the case for the single surfaces spline connection.

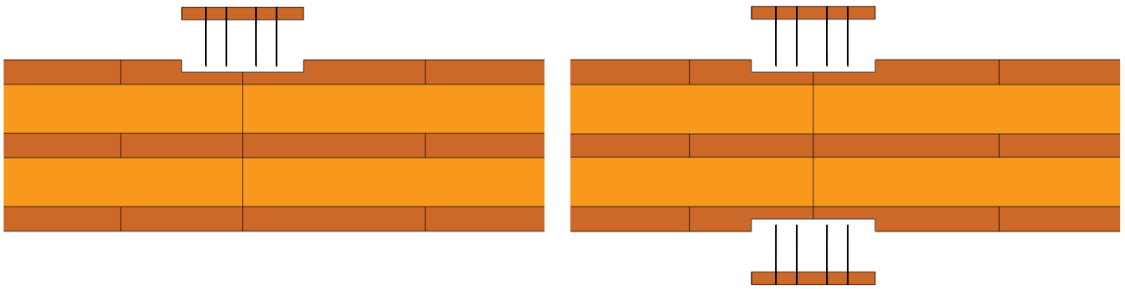

(a) Single spline connection

(b) Double spline connection

Figure 2.5: Singe and double spline connections.

Another important aspect of the connection characteristics is how large slip that can be expected. This affects the rigidity of the system and the ability to transfer in-plane forces between CLT elements. The transition of out-of-plane shear force is also limited by the capacity of the connection. Both slip and out-of-plane shear capacity are excluded for the sake of delimiting the thesis, but are interesting aspects to investigate in further research.

3

General FE theory

The methods that are used in FE analysis depends on which modeling choices are made, such as what element types are used, and on the settings used for the analysis, such as if the material input parameters are of a linear or a non-linear type. To better understand how different modeling choices affects the analysis, this chapter addresses the theory behind certain aspects of finite element analysis. A fundamental understanding of FE theory is also crucial to avoid the famous "Black box problem", which refers to the implied risk that is correlated with using a software without knowledge about the underlying calculations.

3.1 Element types

When a structure is to be represented in a FE model, each member in the structure is modeled with an individual element. Which element type that is suitable depends on the type of the member and its expected behaviour under the given loads. In the sections below, different element types are presented, together with how they are treated in an FE-software and what kinds of behavior they can represent. Element types are defined in their own plane.

3.1.1 Truss element

The truss element is one of the simplest types of elements used in FE-analysis. The element has a length and a cross section, and is only able to deform along its length-axis (u_x). This means that a truss element only has one degree of freedom per node as seen in Equation 3.1, and a typical truss element therefore has two total degrees of freedom (Liu & Quek, 2013). A truss element is also commonly referred to as a bar element.

$$\mathbf{d} = [u_x] \tag{3.1}$$

3.1.2 Beam element

A beam element is, just like the truss element, a one-dimensional element. The difference between the beam element and the previously defined truss element is that the beam element can deform vertically (u_y) and by rotation (θ_{xy}).

$$\mathbf{d} = \begin{bmatrix} u_y \\ \theta_{xy} \end{bmatrix} \tag{3.2}$$

Different literature uses different definitions for which degrees of freedom a beam consists of. Liu and Quek (2013) and Ottosen and Petersson (1992) defines the beam element as having two degrees of freedom per node (u_y and θ_{xy}) as seen in Equation 3.2, while the software *RFEM* defines a beam element as having three degrees of freedom per node (u_x, u_y and θ_{xy}) which could be seen as a combination of the truss element and the beam element according to Equation 3.3. The latter definition of three degrees of freedom per node is defined as a frame element in Liu and Quek (2013). The frame element (or beam element) is the most common and useful one-dimensional element type in FE-analysis.

$$\mathbf{d} = \begin{bmatrix} u_x \\ u_y \\ \theta_{xy} \end{bmatrix} \tag{3.3}$$

A distinction between 2D and 3D space is also necessary when defining the degrees of freedom for a beam element. For 3D space problem, a superimposition of a secondary beam element in the perpendicular plane is possible, while the shear stiffness properties of the beam are used to determine the torsional properties that are necessary in 3D.

3.1.3 Membrane element

A membrane element is a two-dimensional element where the loading and deformation only occurs in-plane (Liu & Quek, 2013). If a 2D model is to be analysed, the distinction between plane stress elements and plane strain elements is made. Plane stress elements have a very small thickness and the out-of-plane stresses can be assumed to be zero. Plane strain elements have a very large thickness where the out of plane strain can be assumed to be zero. Plane strain elements are very common in geotechnical engineering when analysing earth and water pressures. For 3D models the membrane elements are useful for, for example, shear walls where in-plane loading is relevant.

A membrane element has two transversal degrees of freedom per node (u_x and u_y) as presented in Equation 3.4.

$$\mathbf{d} = \begin{bmatrix} u_x \\ u_y \end{bmatrix} \tag{3.4}$$

3.1.4 Plate element

The plate element is a two-dimensional element that can be loaded and deformed out of plane and is therefore a well suited element for bending. There are two commonly used theories for plates, Kirchhoff theory and Mindlin theory (Larsson & Runesson, 2014). Kirchhoff theory assumes that the transverse shear strains are very small (zero), and is therefore well suited for thin plates. Mindlin plate theory considers that vertical fibres of the plate can rotate so that it is not perpendicular to the mid-plane of the plate (Liu & Quek, 2013). This rotation results in the out-of-plane shear strain components γ_{xz} and γ_{yz}.

A plate element usually has three degrees of freedom, two rotational and one transversal (θ_x, θ_y and u_z) as presented in Equation 3.5. However in certain applications (like *RFEM*), the out of plane shear strain components are treated as separate degrees of freedom, resulting in a total of five degrees of freedom per node for a plate element. The five degrees of freedom plate element can be transformed into a three degrees of freedom element by combining the displacements, but for calculation purposes the five degrees of freedom element can be used.

$$\mathbf{d} = \begin{bmatrix} \theta_x \\ \theta_y \\ u_z \end{bmatrix} \tag{3.5}$$

3.1.5 Shell element

Shell elements are a combination of membrane elements and plate elements. It is the most commonly used two dimensional element since it considers most effects, and many commercial FE softwares like ABAQUS only has the shell element type available for surfaces (Liu and Quek, 2013). The degrees of freedom for each node in a shell element are presented in Equation 3.6.

$$\mathbf{d} = \begin{bmatrix} u_x \\ u_y \\ u_z \\ \theta_x \\ \theta_y \end{bmatrix} \tag{3.6}$$

Direction definitions and degrees of freedom for membrane elements, plate elements and shell elements are presented in Figure 3.1.

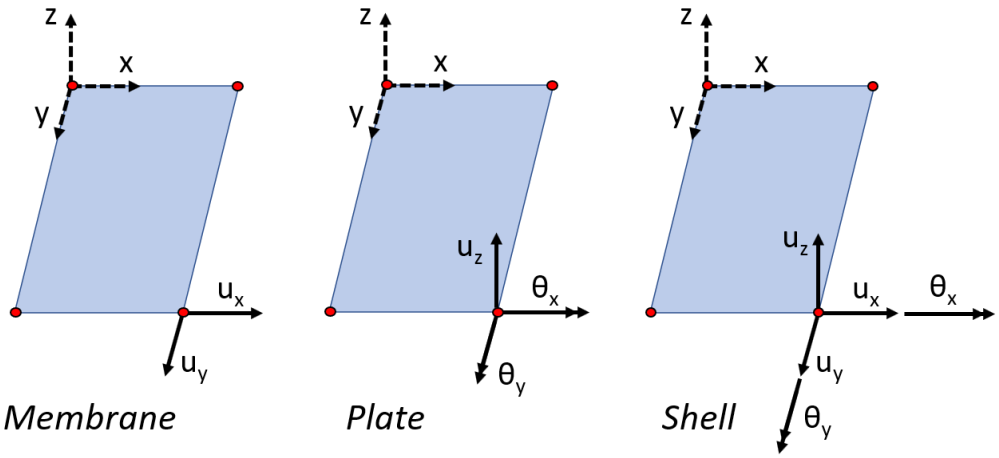

Figure 3.1: Degrees of freedom and directions for 2D elements.

3.2 Singular points

Stress singularities occur when a force is applied on an infinitely small area of a surface, for example when a column represented by a beam element connects to a shell element through a node. In the actual structure, the force is distributed over a certain area and yields lower stresses within the structure. A singularity point is recognized by showing a larger maximum value as the mesh is refined, while the area for the high stress values decreases as the mesh is made finer. A small analysis of this phenomena was made and the geometry and resulting moments from the analysis is presented in Figure 3.2 and 3.3. A simply supported slab with a supporting column in its mid-point was loaded by a uniformly distributed load. It can be seen that the maximum moment is not converging for finer meshes.

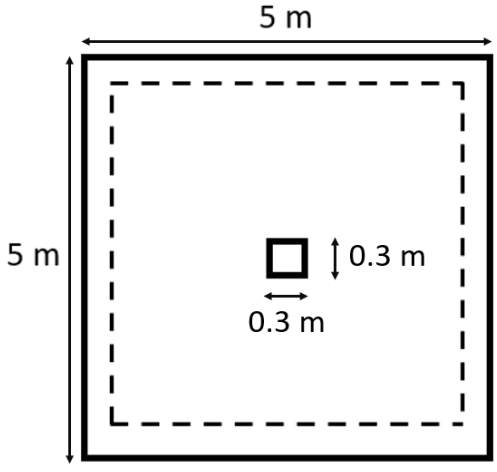

Figure 3.2: Geometry of the slab in the small analysis regarding singular points.

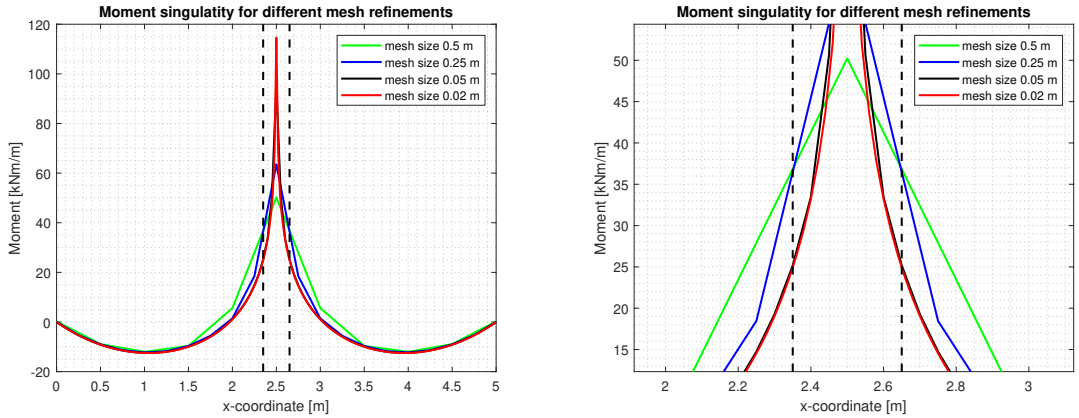

(a) Moment distribution over entire span. **(b)** Zoomed-in figure of (a).

Figure 3.3: Moment distribution with different mesh sizes involving a singular point. The dashed lines marks the column width.

There are several methods to obtain more reasonable stresses and sectional moments in areas affected by singularity issues, where these methods can be used in design or for analysis of the structure. Two of the methods are to use the stresses or moments at a certain distance from the connecting node or to use an average value of the stresses over a certain area.

According to Pacoste et al. (2012), a distance equal to half of the column width from the mid-point of the column is suitable when evaluating moments or stresses. If the column is not considered entirely rigid, a distance equal to 1/4 of the column width can be used instead. These recommendations are targeted at FE-analysis of concrete structures, but the same principle still applies for timber structures.

It is also possible to use average values in areas around points effected by singularity issues. Some commercial FE-software has built-in functions for average regions, but to avoid the "Black box problem" it is important to know how these programs treats the average regions. If an average region is applied, the program needs to know which variable that should be averaged with respect to which direction. If for example the resulting moments are averaged, the shear forces are later determined based on the averaged moments. If the shear forces are instead averaged, another moment and shear force distribution over the average region is achieved. It is also important to consider that different results converge differently fast when determining how fine the mesh should be.

Using a linear elastic material model increases the risk of stress concentrations. If compressive deformations perpendicular to the fibers in the timber are included in the analysis, this can contribute to a larger distribution of stresses.

4

Modeling CLT

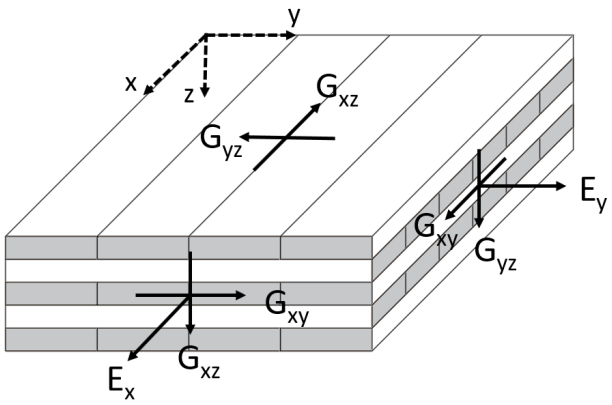

Figure 4.1: Convention of the different stiffness directions.

When modeling CLT shells in an FE-program, the parameters required for the analysis can be given in various ways. The two methods which are used in this thesis are: to create a new orthotropic (or isotropic) material which represents the properties of an entire CLT plate, or to define the stiffness matrix for each element directly. The add-on module *RF-LAMINATE* provided within the program *RFEM* can for example be used to generate stiffness matrixes for CLT shell elements, where the properties of each layer in the element is used as input. To create an orthotropic material, Mindlin plate theory should preferably be used to account for the shear deformations. (Aondio et al., 2020). This section addresses the theory behind the different modeling assumptions for CLT that are implemented in this thesis.

4.1 Equivalent orthotropic shell model

The equivalent orthotropic shell model is based on calculating the equivalent bending stiffness and shear stiffness. Orthotropic Mindlin shell elements require the inputs E_x, E_y, G_{xy}, G_{yz}, G_{xz}, ν_{xy} and ν_{yx} in order to assemble a stiffness matrix. The Poisson ratios ν_{xy} and ν_{yx} are usually assumed to be zero (Aondio et al., 2020), but the bending stiffnesses and shear stiffnesses needs to be determined in a way that correctly represents the mechanical properties of a CLT element.

4.1.1 Bending stiffness E_x and E_y

The bending stiffnesses E_x and E_y for an edge glued CLT element modeled as an orthotropic shell are commonly determined as an average of the elasticity moduli in the board layers. It is a simplification of the gamma method and shear analogy method, where the average is determined by the moment of inertia of each layer (Popovski et al., 2019). If the plate is not edge glued, the same procedure is used but the orthogonal layers are considered to have zero stiffness. The equations to determine E_x and E_y (defined in Figure 4.1) are:

$$E_x = \frac{\sum_{i=1,3,...}^{n} E_0 I_i + \sum_{j=2,4,...}^{n-1} E_{90} I_j}{I_{tot}} \tag{4.1}$$

$$E_y = \frac{\sum_{i=1,3,...}^{n} E_{90} I_i + \sum_{j=2,4,...}^{n-1} E_0 I_j}{I_{tot}} \tag{4.2}$$

Where:

E_x = Bending stiffness in the major direction
E_y = Bending stiffness in the minor direction
E_0 = Longitudinal elasticity modulus of boards
E_{90} = Transversal elasticity modulus of boards
i = Index of board layers in the major direction
j = Index of board layers in the minor direction
n = Number of board layers
I = Moment of inertia
I_{tot} = Total moment of inertia for CLT element

If the CLT element is expected to be loaded in its plane, as for example a shear wall, the membrane stiffness is instead preferably used when modeling the element as an orthotropic shell. The equation can be found in for example D'Arenzo et al. (2019), and it averages the stiffness over the area rather than the inertia. The equations to determine the membrane stiffnesses are:

$$E_x = \frac{\sum_{i=1,3,...}^{n} E_0 A_i + \sum_{j=2,4,...}^{n-1} E_{90} A_j}{A_{tot}} \tag{4.3}$$

$$E_y = \frac{\sum_{i=1,3,...}^{n} E_{90} A_i + \sum_{j=2,4,...}^{n-1} E_0 A_j}{A_{tot}} \tag{4.4}$$

E_x = Membrane stiffness in the major direction
E_y = Membrane stiffness in the minor direction
A = Cross section area
A_{tot} = Total cross section area for CLT element

4.1.2 In-plane shear stiffness G_{xy}

The in-plane shear stiffness G_{xy} can usually be taken as an average of the mean shear stiffness of the boards $G_{0,mean}$ (Gustafsson et al., 2019). However, imperfections like slits and splits in the CLT element, or if there is glue on the narrow sides needs to be considered by reduction factors for the in-plane shear stiffness.

Recommendations regarding reduction factors for G_{xy} differ based on if the element is loaded in torsional bending or in membrane shear. This has the consequence that there is no clear way to apply a single reduction factor to G_{xy}, since G_{xy} is used in both torsional bending and membrane shear. The effects of torsional bending and membrane shear are not coupled in the stiffness matrix (see eq. 4.21), meaning that it is possible to apply two different reductions if it is done in the stiffness matrix rather than on the material level.

4.1.2.1 Torsional bending stiffness reduction k_{33}

A reduction factor k_{33} (k_{cr}) determined in Silly (2010) treats the torsional bending. The reduction factor is recommended and proposed in Wallner-Novak et al. (2014) and Gustafsson et al. (2019), where the factor considers if there are slits or splits in the CLT boards. If there is no glue on the narrow sides of the boards, the element can usually be considered to have splits (Gustafsson et al., 2019). The reduction factor is defined as:

$$k_{33} = \begin{cases} 0.65 \text{ for CLT elements with slits or splits} \\ 0.8 \text{ for CLT elements without slits or splits} \end{cases} \tag{4.5}$$

Another reduction factor is used in DIN (2008) that is also proposed in Aondio et al. (2020). This reduction factor considers whether the CLT element is edge-glued or not and defined as:

$$k_{33} = \begin{cases} 1 \text{ for edge-glued CLT elements} \\ 0 \text{ for non edge-glued CLT elements} \end{cases} \tag{4.6}$$

The reduction factors in equations 4.5 and 4.6 should not be combined, but rather one should be chosen. There is no clear way of how this reduction factor should be chosen, but the torsional bending stiffness can often have a very small influence on an analysis, and in that case the reduction factor k_{33} is insignificant. If it is deemed that the torsional bending stiffness is significant (for example if the two-way action has a relatively large impact on the behaviour of the plate), more consideration needs to be put towards that reduction factor.

4.1.2.2 Membrane shear reduction k_{88}

Similarly as to k_{33}, a reduction factor k_{88} according to Silly (2010) is proposed in Wallner-Novak et al. (2014) and Gustafsson et al. (2019). This reduction factor is not dependant on any conditions and is defined as:

$$k_{88} = 0.75 \tag{4.7}$$

DIN (2008) and Aondio et al. (2020) also proposes a reduction factor that is defined as follows:

$$k_{88} = \begin{cases} 1 \text{ for edge-glued CLT elements} \\ 0.25 \text{ for non edge-glued CLT elements} \end{cases} \tag{4.8}$$

The various stiffness reduction factors regarding the membrane shear stiffness will be further investigated in the sensitivity study. This is due to their potentially large influence on horizontal deformation for taller buildings.

4.1.3 Shear stiffness G_{yz} and G_{xz}

The shear stiffnesses G_{yz} and G_{xz} are less agreed upon on how to determine due to the complexity of shear coupling of the differently oriented layers in the CLT element. This section will treat two different methods of determining the shear stiffnesses, where both methods will be analysed in the sensitivity study. Gustafsson et al. (2019) and Wallner-Novak et al. (2014) proposes the use of a laminate shear correction factor κ that considers coupling, while Aondio et al. (2020) uses the theory of virtual work in order to determine the shear moduluses.

4.1.3.1 Shear stiffness from shear correction factor

The shear correction factor κ is determined as (Gustafsson et al., 2019):

$$\kappa = \frac{\left(\sum (EI + EAa^2)\right)^2}{\sum G_i b t_i \cdot \int_h \frac{S^2(z) E^2(z)}{G(z) b(z)} \, dz} \tag{4.9}$$

Where:

κ = Shear correction factor for CLT element
E = Elasticity modulus of layer
I = Moment of inertia of layer
A = Area of layer
a = Distance between layer center and CLT element center
G = Shear modulus of layer
b = Width of CLT element
t = Thickness of layer
h = Height of CLT element
S = Static moment of layer

Due to the complexity of the analytical equation to determine the shear correction factor (eq. 4.9), different approximate values have been determined. Tables for shear correction factors for typical CLT-element also exist.

The approximate shear correction factors presented in Table 4.1 are valid for build-ups that are symmetrical, of equal laminate thicknesses, and a shear modulus ratio of $\frac{G_{90}}{G_0} = \frac{1}{10}$ (Wallner-Novak et al., 2014).

Table 4.1: Approximate shear reduction factors for symmetrical CLT-plates (Wallner-Novak et al., 2014).

Number of layers	1	3	5	7	9
κ	0.83 (5/6)	0.21	0.24	0.26	0.27

Besides the general approximations in Table 4.1, tables for specific build-ups also exists. In Gustafsson et al. (2019), shear correction factors for specific build-ups can be found. In Table 4.2, shear correction factors for build-ups with boards of strength class C24, $E_{0,mean} = 11$ GPa, $E_{90,mean} = 0$ GPa, $G_{090,mean} = 650$ MPa and $G_{9090,mean} = 50$ MPa are determined.

Table 4.2: Sample of shear correction factors for certain CLT build-ups from Gustafsson et al. (2019).

h_{CLT} [mm]	t_1 [mm]	t_2 [mm]	t_3 [mm]	t_4 [mm]	t_5 [mm]	κ_x [-]	κ_y [-]
60	20	20	20	-	-	0.163	0.722
80	30	20	30	-	-	0.178	0.677
100	40	20	40	-	-	0.196	0.637
100	20	20	20	20	20	0.194	0.152
120	20	20	40	20	20	0.234	0.157
120	30	20	20	20	30	0.188	0.147
140	40	20	20	20	40	0.189	0.142
160	40	20	40	20	40	0.219	0.147
180	40	30	40	30	40	0.199	0.146

With the use of shear correction factors, the shear moduli G_{yz} and G_{xz} can be determined as (Gustafsson et al., 2019):

$$G_{yz} = \kappa_y \frac{\sum_{i=1,3,...}^{n} G_0 t_i + \sum_{j=2,4,...}^{n-1} G_{90} t_j}{t_{tot}} \tag{4.10}$$

$$G_{xz} = \kappa_x \frac{\sum_{i=1,3,...}^{n} G_{90} t_i + \sum_{j=2,4,...}^{n-1} G_0 t_j}{t_{tot}} \tag{4.11}$$

4.1.3.2 Shear stiffness from virtual work

The shear stiffnesses can also be determined on the basis of virtual work (Aondio et al., 2020). For this method a linear shear flow is assumed and only the Steiner components of the boards are used for the overall flexural rigidity EI_B.

Equations 4.12 to 4.15 according to Aondio et al. (2020) are used to determine the shear modulus G_{xz}.

$$EI_{x,B} = \sum_{j=1}^{n} E_{0,j} t_j z_j^2 \tag{4.12}$$

$$c_{xz,i} = \frac{1}{EI_{x,B}} \sum_{j=1}^{i} E_{0,j} t_j z_j \tag{4.13}$$

$$\frac{1}{S_{xz}} = \sum_{i=1}^{n} \frac{1}{3G_{0,i}} \left(c_{xz,i-1}^2 + c_{xz,i-1} \cdot c_{xz,i} + c_{xz,i}^2 \right) \tag{4.14}$$

$$G_{xz} = \frac{S_{xz}}{t_{tot}} \tag{4.15}$$

Where:

$EI_{x,B}$ = Bending stiffness of CLT element in x-direction
z = Distance between layer center and CLT element center
c_{xz} = Shear average constant in xz-plane
S_{xz} = Static moment in xz-plane
G_{xz} = Shear modulus in xz-plane

The same principle is used to determine the shear modulus G_{yz}.

$$EI_{y,B} = \sum_{j=1}^{n} E_{90,j} t_j z_j^2 \tag{4.16}$$

$$c_{yz,i} = \frac{1}{EI_{y,B}} \sum_{j=1}^{i} E_{90,j} t_j z_j \tag{4.17}$$

$$\frac{1}{S_{yz}} = \sum_{i=1}^{n} \frac{1}{3G_{90,i}} \left(c_{yz,i-1}^2 + c_{yz,i-1} \cdot c_{yz,i} + c_{yz,i}^2 \right) \tag{4.18}$$

$$G_{yz} = \frac{S_{yz}}{t_{tot}} \tag{4.19}$$

Where:

$EI_{y,B}$ = Bending stiffness of CLT element in y-direction
c_{yz} = Shear average constant in yz-plane
S_{yz} = Static moment in yz-plane
G_{yz} = Shear modulus in yz-plane

A MATLAB-script that is used to determine the shear moduli on the basis of virtual work can be found in Appendix B.1, and the same calculation performed in Mathcad is found in Appendix A.2.1.

4.1.4 Implementation in FE-analysis

As previously mentioned, orthotropic CLT shells should be modeled using Mindlin plate theory (Aondio et al., 2020). Mindlin plate theory considers the out-of-plane shear deformations that can be relevant for CLT-plates.

A general stiffness matrix equation for a Mindlin plate is defined as:

$$\begin{bmatrix} m_x \\ m_y \\ m_{xy} \\ v_x \\ v_y \\ n_x \\ n_y \\ n_{xy} \end{bmatrix} = \begin{bmatrix} D_{11} & D_{12} & D_{13} & 0 & 0 & D_{16} & D_{17} & D_{18} \\ D_{12} & D_{22} & D_{23} & 0 & 0 & D_{17} & D_{27} & D_{28} \\ D_{13} & D_{23} & D_{33} & 0 & 0 & D_{18} & D_{28} & D_{38} \\ 0 & 0 & 0 & D_{44} & D_{45} & 0 & 0 & 0 \\ 0 & 0 & 0 & D_{45} & D_{55} & 0 & 0 & 0 \\ D_{16} & D_{17} & D_{18} & 0 & 0 & D_{66} & D_{67} & D_{68} \\ D_{17} & D_{27} & D_{28} & 0 & 0 & D_{67} & D_{77} & D_{78} \\ D_{18} & D_{28} & D_{38} & 0 & 0 & D_{68} & D_{78} & D_{88} \end{bmatrix} \begin{bmatrix} \kappa_x \\ \kappa_y \\ \kappa_{xy} \\ \gamma_{xz} \\ \gamma_{yz} \\ \varepsilon_x \\ \varepsilon_y \\ \gamma_{xy} \end{bmatrix} \tag{4.20}$$

Where:

$$\text{Bending} = \begin{Bmatrix} D_{11} & D_{12} & D_{13} \\ D_{12} & D_{22} & D_{23} \\ D_{13} & D_{23} & D_{33} \end{Bmatrix} \qquad \text{Shear} = \begin{Bmatrix} D_{44} & D_{45} \\ D_{45} & D_{55} \end{Bmatrix}$$

$$\text{Membrane} = \begin{Bmatrix} D_{66} & D_{67} & D_{68} \\ D_{67} & D_{77} & D_{78} \\ D_{68} & D_{78} & D_{88} \end{Bmatrix} \qquad \text{Eccentricity} = \begin{Bmatrix} D_{16} & D_{17} & D_{18} \\ D_{17} & D_{27} & D_{28} \\ D_{18} & D_{28} & D_{38} \end{Bmatrix}$$

Common properties of CLT elements are that the board layers only are arranged orthogonally to each other, and that the cross sections are symmetrical. These assumptions gives the more sparse stiffness matrix:

$$\mathbf{D} = \begin{bmatrix} D_{11} & D_{12} & 0 & 0 & 0 & 0 & 0 & 0 \\ D_{12} & D_{22} & 0 & 0 & 0 & 0 & 0 & 0 \\ 0 & 0 & D_{33} & 0 & 0 & 0 & 0 & 0 \\ 0 & 0 & 0 & D_{44} & 0 & 0 & 0 & 0 \\ 0 & 0 & 0 & 0 & D_{55} & 0 & 0 & 0 \\ 0 & 0 & 0 & 0 & 0 & D_{66} & D_{67} & 0 \\ 0 & 0 & 0 & 0 & 0 & D_{67} & D_{77} & 0 \\ 0 & 0 & 0 & 0 & 0 & 0 & 0 & D_{88} \end{bmatrix} \tag{4.21}$$

The Poisson ratio ν is commonly assumed to be 0 for CLT elements (Aondio et al., 2020), which results in the stiffness matrix elements D_{12} and D_{67} also to be equal to 0. The stiffness matrix elements and their associated planes are further illustrated in Figure 4.2.

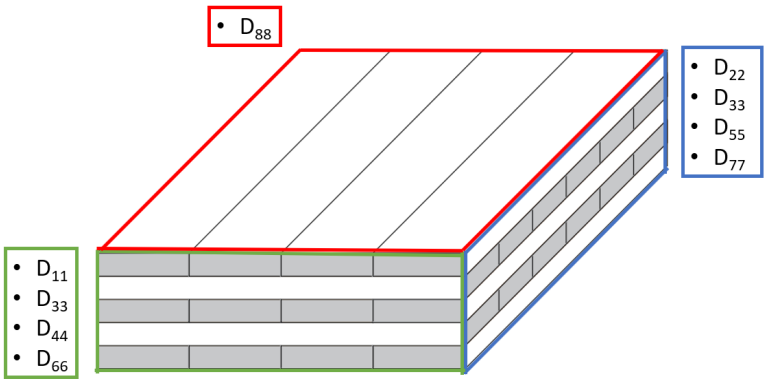

Figure 4.2: The planes and directions associated to each stiffness matrix element.

The stiffness matrix in Equation 4.21 is the stiffness matrix commonly used in FE-software when defining an orthotropic plate. The equations for the stiffness matrix elements may vary slightly, where for example the torsional stiffness reduction k_{33} could either be applied on the shear modulus or on the stiffness matrix element. Special consideration needs to be put on when this reduction should be applied. In an unfortunate case, a reduction factor could for example be applied twice (once by the program and once by the user) if it is unknown how the program treats the reduction factor. This is an example of the earlier mentioned "Black box problem".

The following equations are used by *RFEM* to determine the individual elements of the stiffness matrix of an orthotropic plate (Dlubal Software GmbH, 2016), if defined by stiffnesses:

$$D_{11} = \frac{E_x d^3}{12(1 - \nu_{xy}\nu_{yx})} \tag{4.22}$$

$$D_{22} = \frac{E_y d^3}{12(1 - \nu_{xy}\nu_{yx})} \tag{4.23}$$

$$D_{12} = \operatorname{sgn}(\nu_{xy})\sqrt{\nu_{xy}\nu_{yx}D_{11}D_{22}} \tag{4.24}$$

$$D_{33} = G_{xy}\frac{d^3}{12} \tag{4.25}$$

$$D_{44} = \frac{5}{6}G_{xz}d \tag{4.26}$$

$$D_{55} = \frac{5}{6}G_{yz}d \tag{4.27}$$

$$D_{66} = \frac{E_x d}{1 - \nu_{xy}\nu_{yx}} \tag{4.28}$$

$$D_{77} = \frac{E_y d}{1 - \nu_{xy}\nu_{yx}} \tag{4.29}$$

$$D_{67} = \text{sgn}(\nu_{xy})\sqrt{\nu_{xy}\nu_{yx} D_{66} D_{67}} \tag{4.30}$$

$$D_{88} = G_{xy} d \tag{4.31}$$

The laminate structure of CLT results in different stiffness when the plate is loaded in bending and in-plane action respectively. This becomes a problem when the program creates the matrix using equations 4.22 to 4.31, since the user defined input data is limited to two elastic stiffnesses, E_x and E_y. These stiffness values are applied in all equations for the matrix elements and a choice of whether to input the stiffness that corresponds to bending (according to equations 4.1 and 4.2) or the membrane stiffnesses (from equations 4.3 and 4.4) must be made. An orthotropic plate created with these equations by RFEM is thus not able to represent the general behaviour of the material correctly since the stiffness is dependent on the loading situation.

In equations 4.25 and 4.31, the reduction factor k_{cr} for D_{33} and D_{88} should be applied if they are not defined on a material level.

The equations for the out-of-plane stiffness matrix elements D_{44} and D_{55} (eq. 4.26 and eq. 4.27) considers the typical shear correction factor $\frac{5}{6}$ for homogeneous plates. In the case for the equivalent orthotropic shell element defined in this section, the shear correction factor is already considered within the shear moduli G_{yz} and G_{xz}. This means that for the case with *RFEM*, the shear moduli G_{yz} and G_{xz} should be multiplied with $\frac{6}{5}$ so that the shear correction factor is not accounted for twice.

4.2 Equivalent isotropic shell model

A further simplification for the CLT shell elements could also be accomplished by using isotropic material behaviour. This could in many cases be a poor assumption since it would overestimate the capacity of the plate if the plate is used as a two-way slab, and spanning in two directions is one of the advantages for CLT plates. However, if the plate is used as a one-way slab an isotropic material model might be accurate enough, and it will be furthered investigated in the sensitivity study.

4.2.1 Modulus of elasticity E

Since the main load transferring direction of the plate is the same as the direction with highest stiffness, it is suitable that the elasticity modulus E is defined as the modulus of the stronger direction of the CLT plate (according to eq. 4.1). A consequence of this is that the isotropic plate will have a too high stiffness in its secondary direction, and it is therefore suitable to only apply the isotropic shell model to one-way slabs.

4.2.2 Shear modulus G and Poisson ratio ν

A common recommendation for CLT slabs is that the Poisson ratio ν should be set to zero (Aondio et al., 2020). This does however become a problem for the isotropic shell model, since there is a fixed relationship between the elasticity modulus E, shear modulus G and Poisson ratio ν according to:

$$E = 2G(1 + \nu) \tag{4.32}$$

Common values for timber elasticity and shear stiffnesses are $E = 11$ GPa and $G = 690$ MPa. This would give the Poisson ratio $\nu = 6.97$, which is far outside of the recommended span of $0 \leq \nu \leq 0.5$ for FE analysis for plates in *RFEM*. If the Poisson ratio is on the other hand set to $\nu = 0$ and $E = 11$ GPa, the shear stiffness G would be highly overestimated.

An approach to circumvent this is to define the shell as orthotropic with the common isotropic relationships. That would be $E_x = E_y$ and $G_{xy} = G_{yz} = G_{xz}$, and also in this case $\nu = 0$. Even though this workaround somewhat deprive the advantages of the very much simplified method, it may be interesting to investigate whether the model is a good approximation.

4.3 Laminate action model

The laminate action model is incorporated into the *RFEM* add-on *RF-LAMINATE*. The model is based on plate theory, where the material stiffnesses are calculated by the program based on the per-layer geometry (Dlubal Software GmbH, 2016).

The model initially considers each separate layer as an orthotropic Kirchhoff plate according to:

$$\mathbf{d} = \frac{1}{1 - \nu^2 \dfrac{E_y}{E_x}} \begin{bmatrix} E_x & \nu \cdot E_y & 0 \\ \nu \cdot E_y & E_y & 0 \\ 0 & 0 & G_{xy} \end{bmatrix} \tag{4.33}$$

Where the different moduli of each layer is used.

The rotation of the cross layers is treated by transforming the local plate stiffness matrix by multiplying it with a transformation matrix.

The stiffness matrix used in the laminate action model is of the same size and function as the stiffness matrix previously defined in Equation 4.21. The methodology of calculating each element in the stiffness matrix is however different, where the laminate action model uses methods that are more adapted to numerical calculations. Bending and torsion elements are calculated as follows:

$$D_{ij} = \sum_{k=1}^{n} \frac{z_{max,k}^3 - z_{min,k}^3}{3} d_{ij,k} \tag{4.34}$$

Where:

i	= 1,2,3 (Stiffness matrix elements corresponding to bending and torsion action)
j	= 1,2 ($j = 2$ for Poisson contribution)
n	= Number of layers
z_{max}, z_{min}	= Max and min z-coordinates in the layer
d_{ij}	= Plate stiffness element ij from eq. 4.33

Membrane stiffness matrix elements are calculated in a similar way as the bending and torsion elements. The following equation determines the 6 membrane action elements in the reduced stiffness matrix:

$$D_{i+5,j+5} = \sum_{k=1}^{n} t_k \; d_{ij,k} \tag{4.35}$$

Where:

i	= 1,2,3 ($i + 5$ and $j + 5$ will give the membrane action contribution)
j	= 1,2 ($j = 2$ for Poisson contribution)
n	= Number of layers
t	= Thickness of the layer
d_{ij}	= Plate stiffness element ij from eq. 4.33

The shear stiffness elements D_{44} and D_{55} can be treated with or without consideration of shear coupling of the layers in the CLT element. The effects of whether shear coupling is considered or not can be seen in Figure 4.3. The top figure in Figure 4.3 illustrates the stress distribution if shear coupling is considered, and the bottom figure illustrates is shear coupling is not considered.

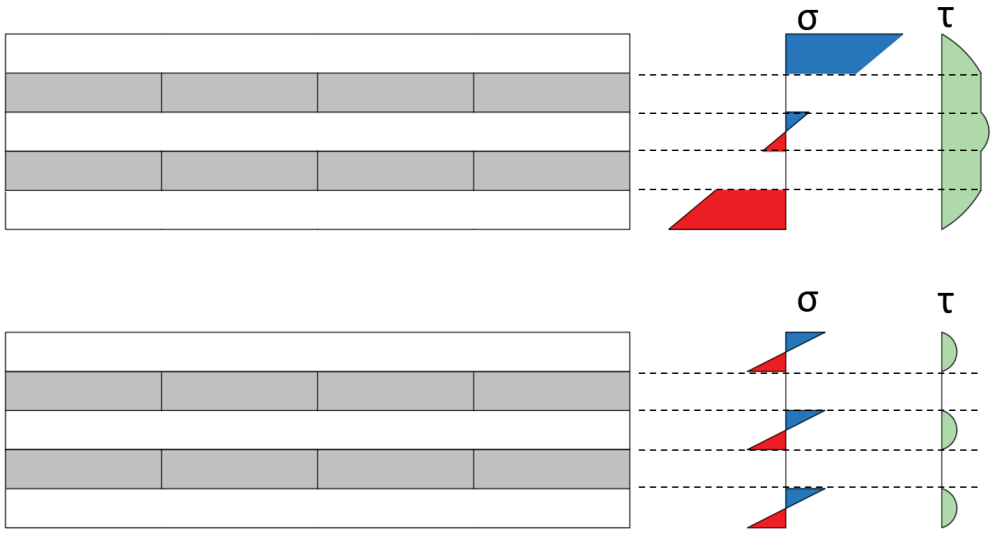

Figure 4.3: Difference between stresses if shear coupling is considered or not.

Shear coupling is relatively complicated to consider analytically as have been previously mentioned in section 4.1.3. *RF-LAMINATE* gives the option if shear coupling should be considered or not. Shear coupling should however generally be considered, since it is important for the behaviour of CLT elements.

If shear coupling is not considered, the methodology in *RF-LAMINATE* is similar to that of an orthotropic shell element. The stiffness matrix elements for shear are first calculated in its shear plane, and then modified for the global plane. The equations for the shear stiffness matrix elements in their shear plane are determined as:

$$D''_{44} = \frac{5}{6}\sum_{i=1}^{n} G''_{xz,i} t_i \tag{4.36}$$

$$D''_{55} = \frac{5}{6}\sum_{i=1}^{n} G''_{yz,i} t_i \tag{4.37}$$

Where:

$D''_{44},\ D''_{55}$ = Shear stiffness matrix elements in the local shear plane
$G''_{xz,i},\ G''_{yz,i}$ = Out of plane shear moduli in the local shear plane for layer i
t_i = Thickness of layer i

If shear coupling is instead considered, the calculation method becomes relatively more advanced. *RF-LAMINATE* considers the out-of-plane shear stiffnesses as the maximum value of an analytical derivation from the bending stiffnesses or a Grashoff integral. These expressions can be found in "RF-LAMINATE: Design of Laminate Surfaces" (Dlubal Software GmbH, 2016).

4.4 CLT Connections

To model the connections addressed in section 2.5, multiple approaches of various detail can be used. As previously mentioned, the moment rigidity between the floor elements could be modeled as stiff, hinged, and intermediate, or even with a non-linearity. The following model alternatives are identified for the connections between the floor elements:

1. Model the connections between the floor elements as entirely stiff. This is equivalent to modeling a plate without connections.
2. Model the connections between the floor elements as hinged.
3. Consider the hinges between the floor elements by reducing the stiffness of the plate in the transversal direction.
4. Model the connections between the floor elements as partly hinged with the use of a spring constant.
5. Model the connections between the floor elements with a non-linear plastic hinge.

This thesis will investigate model alternatives 1-3 in a small scale study to determine an efficient and well representative assumption for the connections between the floor elements. The different modeling assumptions for floor-to-floor connections will not be addressed in the sensitivity study.

5

Small scale studies

The small scale studies in this thesis are studies and analyses that are performed on an element level as opposed to the sensitivity study that is performed on a structure level. There are two main subjects treated in the small scale study chapter: the first one focuses on the the different stiffness assumptions discussed in chapter 4, while the second focuses on how the connection between the slab elements should be treated in the sensitivity study. In the small scale study addressing stiffness assumptions, the study is split into several parts regarding plates in bending, panels in in-plane shear and reduction factors.

The small scale studies serves a purpose in predicting and verifying the results from the sensitivity study. The conclusion from each part is summarized in a box in the end of each section. The conclusions can be helpful to distinguish if certain assumptions are too rough or too poor at an early stage. The small scale study regarding connections between floor elements serves a purpose in the design of the reference building.

5.1 The CLT panel used for small scale studies

The CLT panel used in the small scale studies is a 140-5s panel presented in Figure 5.1. The panel is included in a product sheet from Martinsons (Martinsons, 2019) where stiffnesses and strengths for different directions are presented. This enables a comparison between the calculated values in this thesis and the values provided by the manufacturer. The boards spanning in the panels' major direction are of grade C24, while the boards spanning in the minor direction are of grade C14.

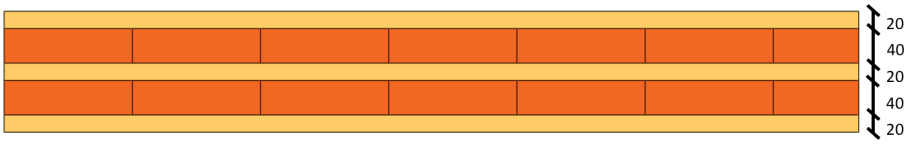

Figure 5.1: Martinssons 140-5s CLT elements. Dimensions are in mm.

5.2 Presentation of the modeling alternatives

Seven modelling assumptions are presented, of which four are orthotropic shell element, one is an isotropic shell element, one is a shell element defined using stiffnesses

from the product sheet by the manufacturer (Martinsons, 2019), and one is an element created by the plug-in program *RF-LAMINATE*. All seven alternatives are used to study the behavior in bending, but since some of the materials have very low in-plane shear stiffness, two modeling assumptions are excluded from the small scale study of in-plane shear deformations.

The elastic stiffnesses E_x and E_y are mostly identical for the plates within each study, as can be seen in the summary of the different methods in Table 5.1 and 5.2. This is due to that most plates uses the same equations for the elastic stiffness. For elastic stiffness when the plate is loaded in bending, all plates except *RF-LAMINATE* (which uses a direct assembly of the stiffness matrix) uses Equation 4.1 for calculation of the elasticity modulus in the strong direction of the plate, E_x. This equation calculates the mean elasticity modulus with respect to the moment of inertia of each layer around the center of the cross section. For calculation of E_y when the plate is loaded in bending, most plates uses Equation 4.2 which works in the same manner as the equation for E_x, and if this is not the case it is stated in the description of the method. A summary of the stiffness properties of each modeling assumption for shells loaded in bending is shown in Table 5.1.

When the shells are loaded with in-plane shear, the elastic stiffnesses E_x and E_y are instead determined by calculating an average stiffness using the thicknesses of the individual layers according to equations 4.3 and 4.4. For comparison purposes, a shell element with bending stiffnesses is also used in the in-plane shear study. The values used for the different materials are presented in Table 5.2.

As mentioned above, and as can be seen in tables 5.1 and 5.2, the elastic stiffnesses are similar for most materials while the shear stiffnesses varies to a higher extent. Therefore, more emphasis is put into the effects of the varying shear stiffness in the small scale and sensitivity studies.

5.2.1 Orthotropic plate - Shear correction factor

The methodology for obtaining the out-of-plane shear stiffness (G_{xz} and G_{yz}) for an orthotropic shell using a shear correction factor is explained in section 4.1.3.1 using equations 4.10 and 4.11. The approximate shear correction factor from Table 4.1 is only valid for CLT panels with equal thickness of all layers but it is used in this calculation as a simplification. This may however be a poor estimation. The shear stiffness in the plane of the shell, G_{xy}, is calculated by using the average stiffness considering the thickness and stiffness of each individual layer. The calculation of the input data for the orthotropic plate using shear correction factor is presented in Appendix A.2.2.

5.2.2 Orthotropic plate - Virtual work

The out-of-plane shear stiffnesses (G_{xz} and G_{yz}) for the orthotropic shell is calculated using the virtual work method is determined according to section 4.1.3.2. Similar to the shell designed using the shear correction factor, G_{xy} is calculated by using the

average stiffness considering the thickness and stiffness of each layer. The derivation of the input data is presented in Appendix A.2.1

5.2.3 Orthotropic plate - Simplified

This method applies several rough estimations. The purpose is to investigate if, from an engineering point of view, it is meaningful to spend time on more detailed calculations to obtain the stiffnesses for the material.

The value for G_{xy} is assumed to be the same as the shear stiffness for the strong boards in the CLT panel. G_{xz} and G_{yz} are assumed to be equal to the rolling shear of the material, which is commonly assumed to be 1/10 of the shear modulus of the boards $G_{0,mean}$.

5.2.4 Orthotropic plate - One-way stiffness

The orthotropic plate with stiffness in one direction is designed to act like a one-way slab even when it is supported on all four sides. This can be useful when one wants to achieve deformation continuity in connections to other elements on all sides but still aim to account for that the transition of out-of-plane forces and moment between the CLT elements is limited. Since connections between CLT slabs are mainly supposed to transfer in-plane shear forces to enable diaphragm action, the load transferred in the weak direction of the floors can be overestimated if the connections are not modeled. To avoid modeling each plate and connection separately, one solution may be to neglect the stiffness in the weak direction of the CLT elements and use them as one-way slabs.

This modelling assumption may be a possible way to generate a shell acting as a slab, but since the in-plane shear stiffness is negligible it cannot be used as a shear wall. Problems does also occur if the system is designed to use diaphragm action to transfer horizontal loads, since this requires the plate to transfer load in its minor direction, using the elastic stiffness E_y and the in plane shear stiffness G_{xy}.

For this element, E_y is set to zero and the plate is only loaded in bending. The shear stiffness G_{xz} is approximated to the rolling shear, while the other shear stiffnesses, G_{yz} and G_{xy} are assumed to be zero as well.

5.2.5 Isotropic plate

As described in section 4.2, the isotropic plate assumes the elastic modulus in the weak direction, E_y, to be equal to the elastic modulus in the strong direction, E_x. The model may not be used when the two-way load transferring has a large influence on the structural behavior of the plate, since it overestimates the stiffness in the weak direction. An isotropic material has the same shear stiffness in all directions, and in this case, G has been chosen to the value for rolling shear of the strong boards in the CLT element. This results in an unrealistically low value for the in-plane shear stiffness, G_{xy}, and thus the assumption is only used when the plate is loaded

in bending. The low in-plane shear stiffness G_{xy} can also be a problem if the plate is subjected to torsional bending.

5.2.6 Laminate structure - RF-LAMINATE

The laminate structure shell uses the *RFEM* plug-in *RF-LAMINATE* to determine the properties of the plate. The plug-in uses the geometry per-layer to assemble the properties directly into the stiffness matrix of the shell, and therefore no equivalent stiffnesses needs to be determined in advance.

5.2.7 Summary of material properties

The material properties differ based on if the slab is tested in bending or in-plane shear. In Table 5.1, the stiffness values for each panel included in the small scale study regarding bending are given. Similarly in Table 5.2, the stiffness values for each panel tested in the in-plane shear small scale study are given.

Table 5.1: Stiffnesses for the CLT panel 140-5s using different modeling alternatives in bending. All values are given in MPa.

Modeling alternative:	E_x	E_y	G_{yz}	G_{xz}	G_{xy}
Orthotropic plate - Shear corr. factor	7106	2767	119	93	547
Orthotropic plate - Virtual work	7106	2767	77	75	547
Orthotropic plate - Simplified	7106	2767	69	69	690
Orthotropic plate - One-way stiffness	7106	0	0	69	0
Isotropic plate	7106	7106	69	69	69
Laminate structure - *RF-LAMINATE*	- (*)	- (*)	- (*)	- (*)	- (*)
Orthotropic plate - Product sheet	7106	2767	133	73	547

(*) *RF-LAMINATE* assembles directly into the stiffness matrix, and no stiffness needs to be determined.

Table 5.2: Stiffnesses for the CLT panel 140-5s using different modeling alternatives in in-plane shear. All values are given in MPa.

Modeling alternative:	E_x	E_y	G_{yz}	G_{xz}	G_{xy}
Orthotropic plate - Shear corr. factor	4846	4159	119	93	547
Orthotropic plate - Virtual work	4846	4159	77	75	547
Orthotropic plate - Simplified	4846	4159	69	69	690
Laminate structure - *RF-LAMINATE*	- (*)	- (*)	- (*)	- (*)	- (*)
Orthotropic plate - Product sheet	4846	4159	133	73	547
Orthotropic plate - Bending stiffness	7106	2767	77	75	547

(*) *RF-LAMINATE* assembles directly into the stiffness matrix, and no stiffness needs to be determined.

5.3 Results for shell in bending

Three different slabs (one two-way, one large one-way and one small one-way) has been tested in bending using *RFEM* with the data from Table 5.1.

For the two one-way slabs, only the deflections are presented since the moments are identical for all modeling assumptions. In the two-way slab, the moments are also presented since the different modeling assumptions affects the moment distribution of a two-way slab.

5.3.1 One-way slabs of different sizes

The effects of different modeling assumptions are evaluated for two sizes of shells. Both shells have the same thickness, but the span lengths are either 2 or 5 m, which results in different relative thicknesses of the shells. The orthotropic plate created with the data from the product sheet is used as a reference, and a comparison of how much the other models deviates from this one is performed.

The deflections of a Mindlin shell consists of both bending deformations and shear deformations, and the proportional size of the shear deformations increases with an increasing thickness of the shell element. In tables 5.1 and 5.2 it can be seen that the bending stiffness for the modeling assumptions are very similar while the shear stiffnesses varies to a larger extent. Therefore, it is expected that the deflection of Mindlin modelled shells with a larger relative thickness are more affected by the different modeling assumptions than shells with a smaller relative thickness. To investigate if this hypothesis is valid, the relative difference compared to the deflection of the shell element modeled with the product sheet values are calculated for a plate that is 5 $\times$ 8 m and a plate that is 2 $\times$ 2 m. Both plates are Martinsons 140-5s panels.

5.3.1.1 Large one-way slab (5 $\times$ 8 m)

The geometry and load conditions of the larger one-way slab are presented in Figure 5.2. The slab is of similar size as the larger slabs in the reference building, and the load present is the typical imposed load of 2 kN/m^2 for domestic areas.

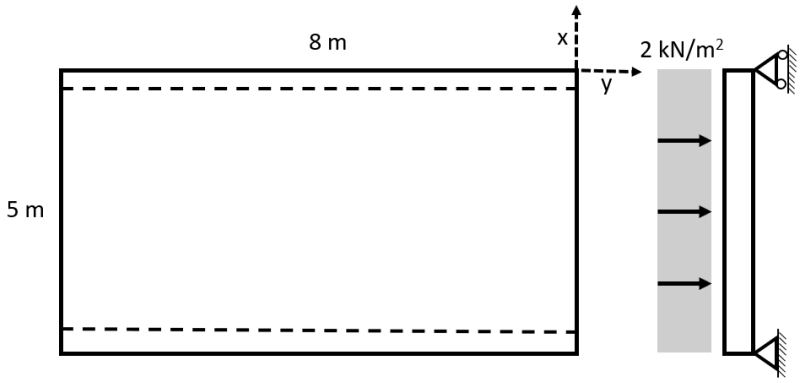

Figure 5.2: Geometry, boundary conditions and loading for the large shell analysed in one-way bending.

The resulting deflections in the slab for the different modelling assumptions is presented in Figure 5.3. Due to how similar the deflections are for the different modeling assumptions, a zoomed-in figure of the maximum deflections is also provided to more easily distinguish the differences of the results.

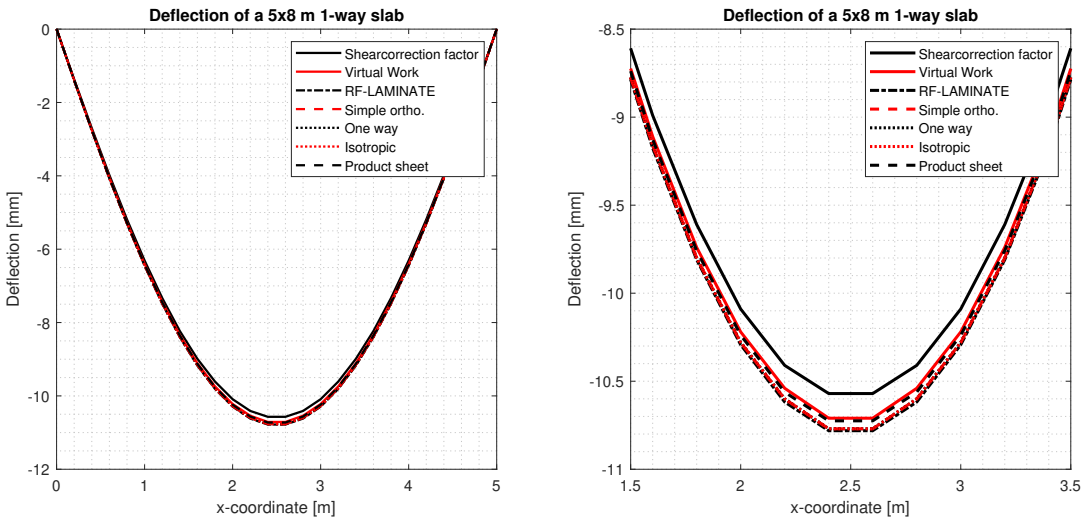

(a) Deflection of entire span. **(b)** Zoom-in over maximum deflections.

Figure 5.3: Deflections for a 5 × 8 m one-way slab in x-direction using different stiffness models.

The main conclusion of the deflections in the larger one-way slab is that the deflections generally are very similar for the different modeling assumptions. The outlier of approximately 0.5 mm is the shell model using a shear correction factor, and it might be an indication that the approximations for that model is too rough. The difference of 0.5 mm is however still very small.

5.3.1.2 Small one-way slab (2 × 2 m)

The geometry and load conditions of the smaller one-way slab is presented in Figure 5.4. A slab of this size is not present in the reference building, but the effects of shear deformations are larger for shells with a larger relative thickness, meaning that the modeling assumptions can differ more for smaller elements. The small one-way slab is loaded with an evenly distributed load of 10 kN/m^2 since smaller loads gives very small deflections.

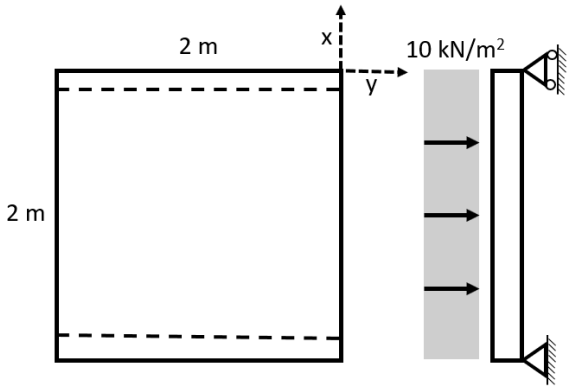

Figure 5.4: Geometry, boundary conditions and loading for the small shell analysed in one-way bending.

The resulting deflections in the slab for the different modelling assumptions are presented in Figure 5.5.

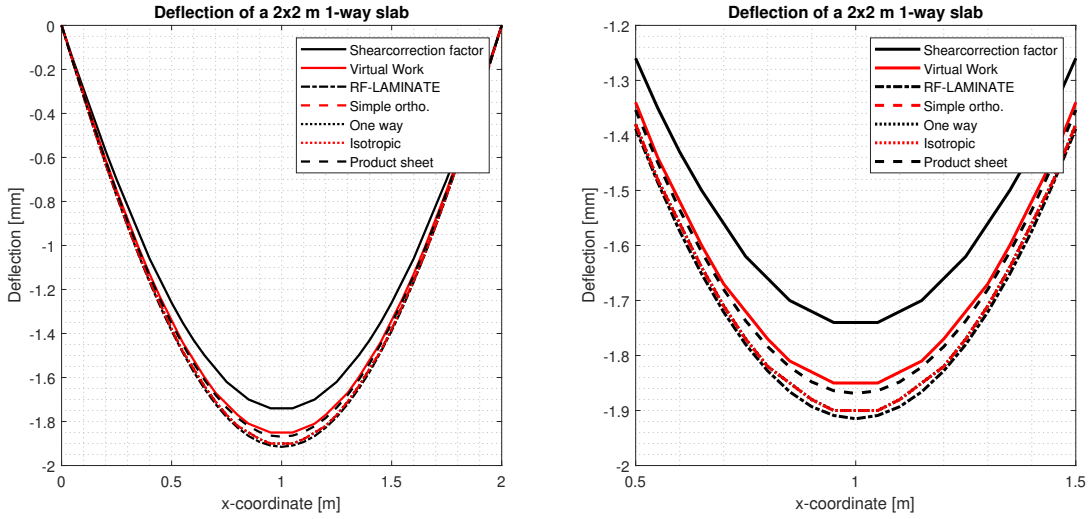

(a) Deflection of entire span. **(b)** Zoom-in over maximum deflections.

Figure 5.5: Deflections for a 2 × 2 m one-way slab in x-direction using different stiffness models.

The deflections for the different modeling assumption applied on the small plate shows the same pattern as the study of the large plate. As seen in Figure 5.5, the shear correction factor method results in the smallest deflections while *RF-LAMINATE* yields the largest deflections, and the difference between these two maximum values are as small as 0.18 mm.

5.3.1.3 Comparison of deflections with respect to shell sizes

The deflection difference for the different modeling assumptions is noticeable between the large slab and the small slab, as can be seen by comparing Figure 5.3 and 5.5. The relative difference in deflection compared to the product sheet element for each slab size is presented in Figure 5.6.

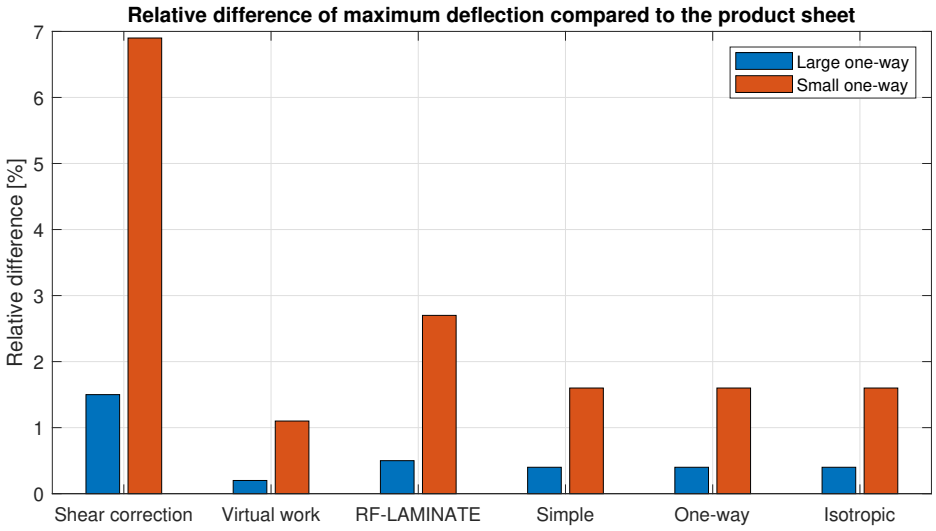

Figure 5.6: Comparison of the relative difference to the product sheet shell for all other modeling assumptions.

The effect of shear deformation for different slab sizes is clearly seen in Figure 5.6, where the smaller slab has relatively larger differences in deflections. The importance of a reasonable shear stiffness model is seen to be especially important for smaller slabs, but if the modeling of shear stiffness is poor (as the Shear correction model) it also has a non-negligible effect of larger slabs.

The relative differences in deflection are also tabulated in Table 5.3. The difference in deflection is approximately 4-5 times greater for the small slab compared to the large slab, regardless of modeling assumption.

Table 5.3: Resulting deflections for the larger and smaller one-way slabs.

	Deflection [mm]		Relative difference [%]		$\frac{\Delta u_{2x2}}{\Delta u_{5x8}}$
Modeling assumption	u_{5x8}	u_{2x2}	Δu_{5x8}	Δu_{2x2}	
Shear correction	10.57	1.74	-1.5	-6.9	4.6
Virtual work	10.71	1.85	-0.2	-1.1	5.5
RF-LAMINATE	10.78	1.92	-0.5	2.7	5.4
Simple orthotropic	10.77	1.90	-0.4	1.6	4
One way	10.77	1.90	-0.4	1.6	4
Isotropic	10.77	1.90	-0.4	1.6	4
Product sheet	10.73	1.87	0	0	0

5.3.2 Two-way slab

In the two-way slab, load can be transferred over both the short and the long span. Unlike the one-way slab, the moment distribution in the two-way slab is dependent on the stiffness properties of the slab, and the moment distribution will therefore be investigated for the two-way slab. The geometry and load conditions of the two-way slab are presented in Figure 5.7.

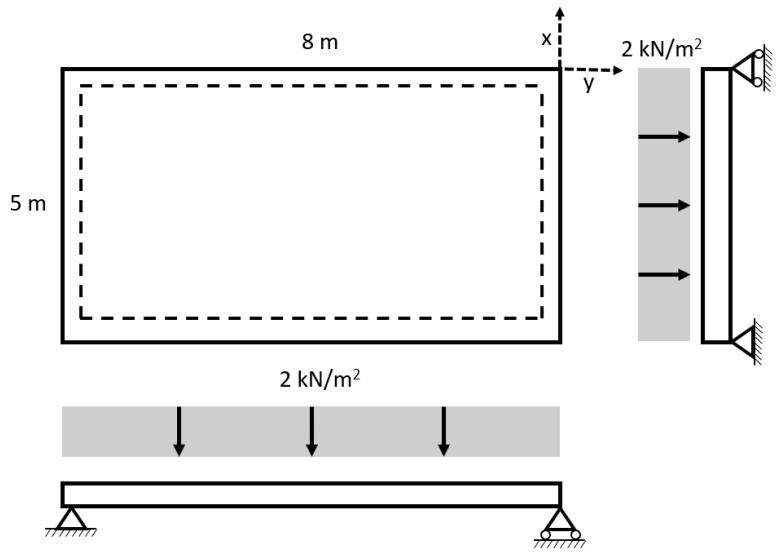

Figure 5.7: Geometry, boundary conditions and loading for the shell analysed in two-way bending.

The resulting deflections for the two-way slab in both x and y-direction are presented in Figure 5.8 and 5.9.

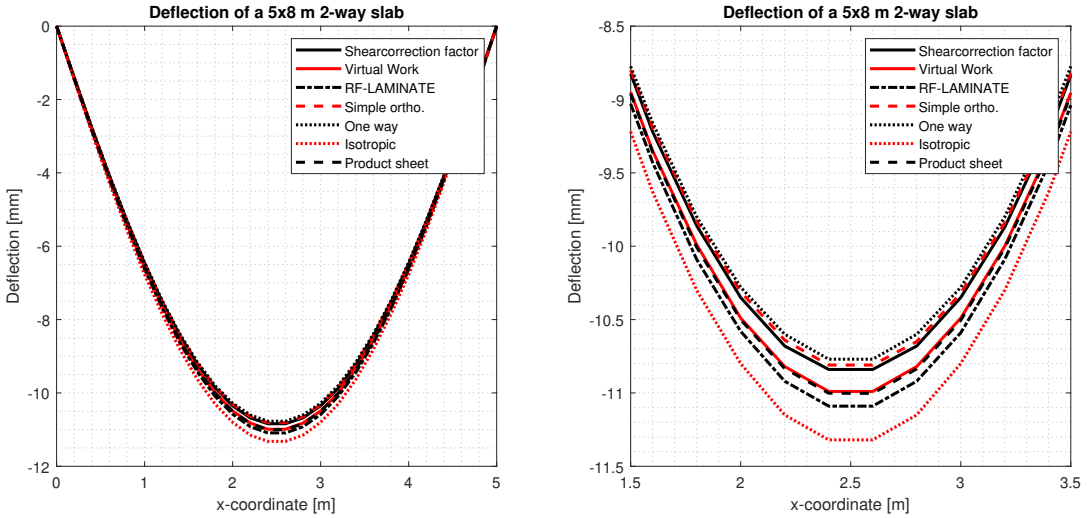

(a) Deflection of entire span. **(b)** Zoom-in over maximum deflections.

Figure 5.8: Deflections for a 5 × 8 m two-way slab in x-direction using different stiffness models.

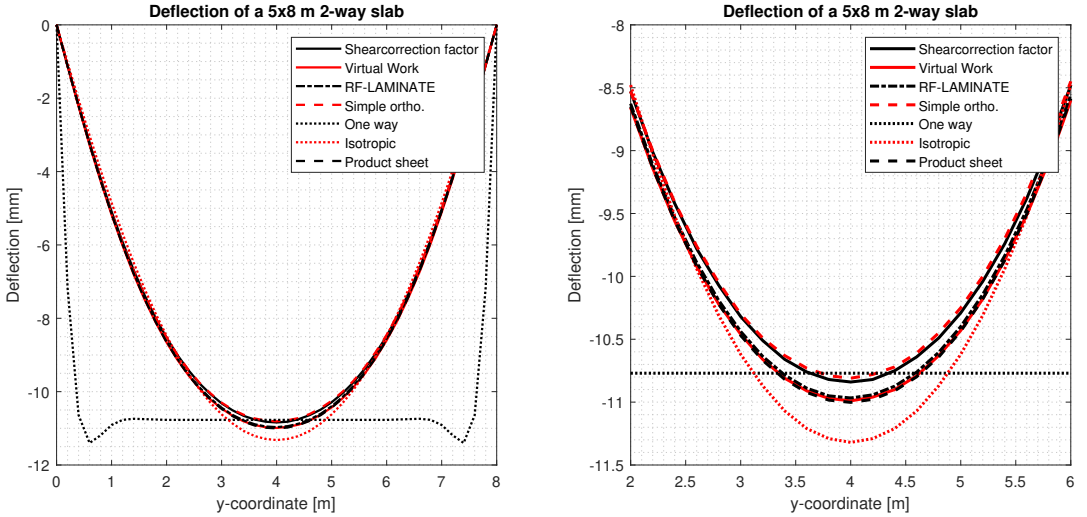

(a) Deflection of entire span. **(b)** Zoom-in over maximum deflections.

Figure 5.9: Deflections for a 5 × 8 m two-way slab in y-direction using different stiffness models.

It can be seen from figures 5.8 and 5.9 that the deflections from the isotropic shell element is larger than the other deflections. This is not the case for the one-way slab, where the *RF-LAMINATE* shell has the largest deflections (although by a very small margin). The reason for why the isotropic shell has the largest deflections in two-way bending is due to its low in-plane shear stiffness G_{xy}. G_{xy} affects the torsional bending that is present in two-way slabs, while one-way slabs are not affected by

torsional bending. One conclusion that could be made from this is that the in-plane shear stiffness needs consideration for two-way CLT slabs in bending, while it is not as important for one-way slabs.

Another comparison that could be made is between the maximum deflections for the one-way slab and the two-way slab. The slabs have, as previously stated, the same geometry and they are subjected to the same loads. The maximum deflections are illustrated in Figure 5.10.

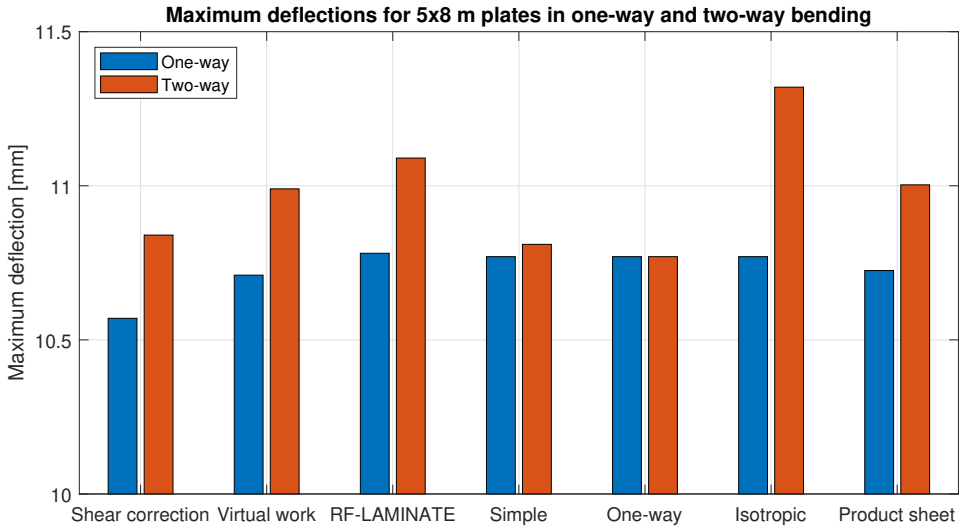

Figure 5.10: Comparison of total deflection for the 5 × 8 m shell elements.

Several observations can be made in Figure 5.10. The maximum deflections are higher for the two-way slab than for the one-way slab, for all modeling assumptions. This is not common, as one-way slabs usually has the higher deflection. The reason for the unusual behaviour of why the two-way slab has higher deflections is due to a number of rather specific conditions discussed in the following paragraphs.

Firstly, the slab is rectangular with its long side parallel to its minor direction. If the same analysis is performed for a square slab, or a slab with its major direction longer than its minor direction, the deflections for the two-way slab would be less than the deflections for the one-way slab. Secondly, the slab's relatively low in-plane shear stiffness G_{xy} corresponds to a low torsional bending stiffness for the two-way slab. A torsional bending stiffness approximately 7 times higher than what is used in the analysis would give similar maximum deflections for the two slabs. For simply supported slabs under uniform load, the torsional bending stiffness usually has a negligible effect. Its effect here is still small, but it is partly a reason for why the two-way slab shows higher deflections than the one-way slab.

In general, the one-way deflections in Figure 5.10 are rather similar with the exception of the shear correction factor slab which slightly underestimates the deflection. Furthermore, the deflection of the isotropic two-way slab is overestimated compared to the other results.

The resulting moments for the two-way slab in both x and y-direction are presented in Figure 5.11 and 5.12.

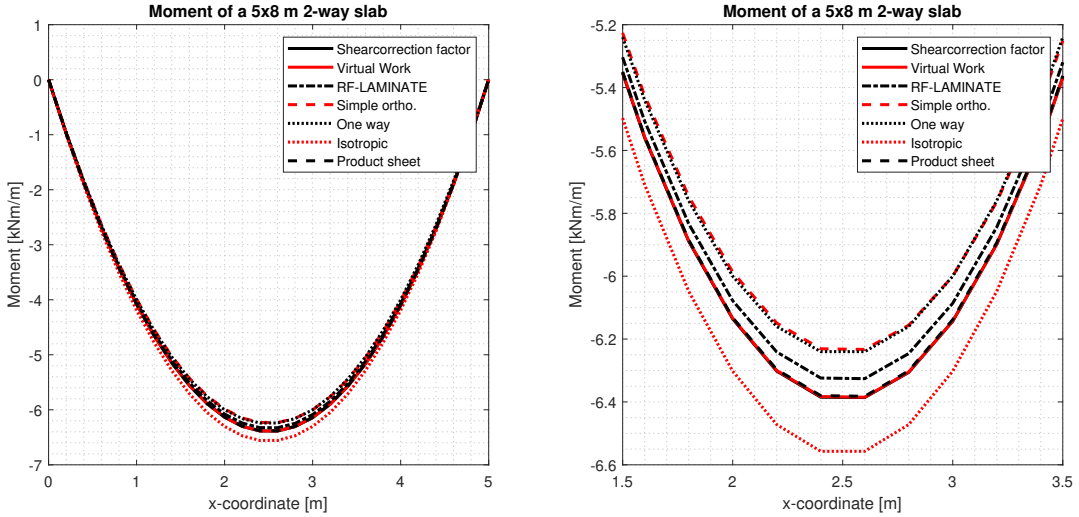

(a) Moments of entire span. **(b)** Zoom-in over maximum moments.

Figure 5.11: Moments for a 5 × 8 m two-way slab in x-direction using different stiffness models.

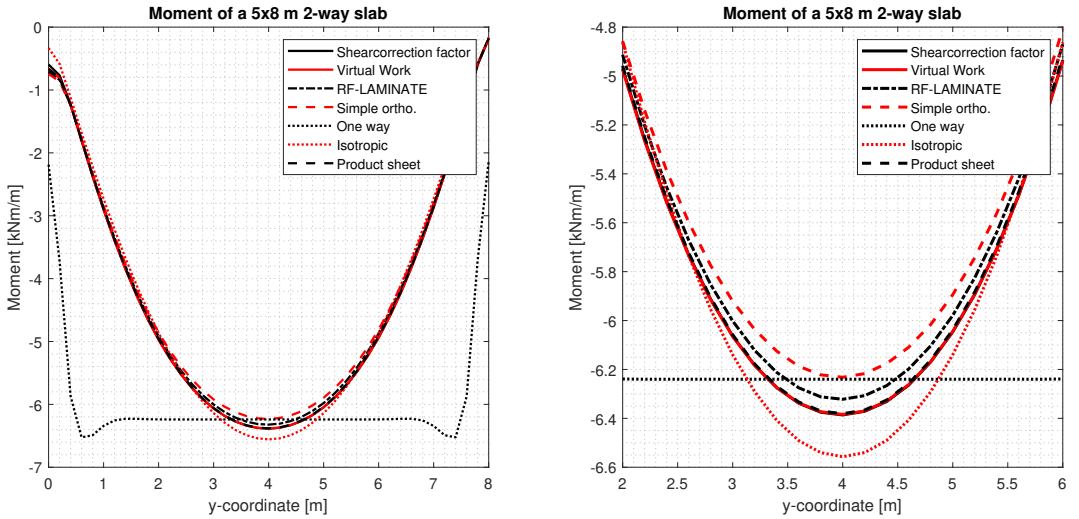

(a) Moments of entire span. **(b)** Zoom-in over maximum moments.

Figure 5.12: Moments for a 5 × 8 m two-way slab in y-direction using different stiffness models.

The resulting moments correlate well with the deflections, which is expected since the slabs are simply supported. The resulting moments does therefore not contribute to any new understandings or conclusions.

5.3.3 Conclusion and summary for bending study

A summary of the deflections and their relative difference compared to the product sheet values is presented in Table 5.4 and Figure 5.13. The relative differences are compared to the product sheet modeling assumption.

Table 5.4: Deflections and relative difference for all modeling assumptions in bending. All numbers are given in mm.

Modeling assumption	$u_{1way,large}$	$u_{1way,small}$	u_{2way}	$\Delta u_{1way,large}$	$\Delta u_{1way,small}$	Δu_{2way}
Shear correction	10.57	1.74	10.84	-1.5	-6.9	-1.5
Virtual work	10.71	1.85	10.99	-0.2	-1.1	-0.1
RF-LAMINATE	10.78	1.92	11.09	-0.5	2.7	0.8
Simple ortho	10.77	1.90	10.81	-0.4	1.6	-1.7
One way	10.77	1.90	10.77	-0.4	1.6	-2.1
Isotropic	10.77	1.90	11.32	-0.4	1.6	2.9
Product sheet	10.73	1.87	11.00	0	0	0

The relative differences from Table 5.4 are also illustrated in Figure 5.13.

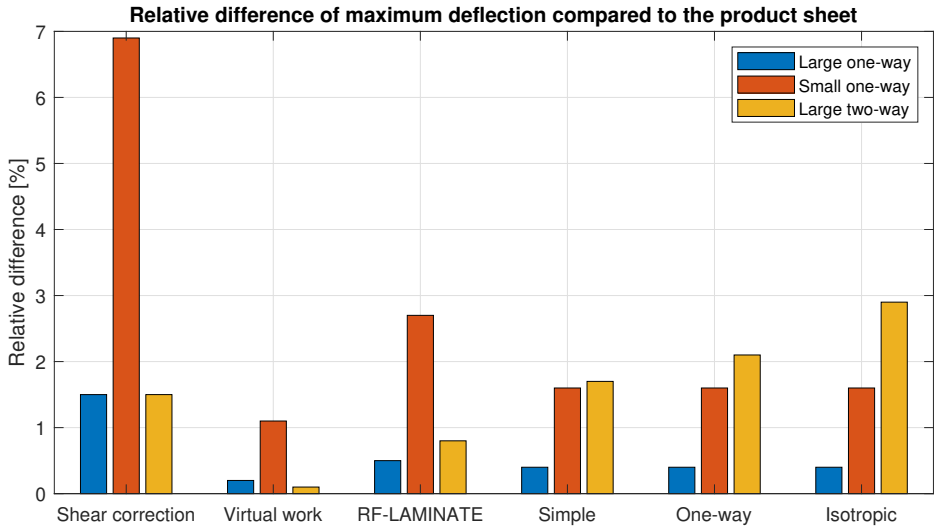

Figure 5.13: Comparison of the relative difference to the product sheet shell for all other model assumptions.

Figure 5.13 summarizes the results and also shows possible conclusions for the small-scale study regarding bending. It can be seen that for the three more thoroughly defined modeling assumptions (*Shear correction, Virtual work* and *RF-LAMINATE*) that the small slab shows the largest differences compared to the product sheet slab. Since it is the size of the slab that differs, it is probable that the shear deformations in Mindlin plates are the reason for the larger difference. In the other three more simplified and approximate modeling assumption (*Simple orthotropic, One-way stiffness* and *Isotropic*), it is instead the two-way slab that shows the

largest difference compared to the product sheet slab. This is an indication that the bending stiffness distribution causes the difference in deflection.

Conclusions from the **bending small-scale study**:

- The relative deflection difference between the modeling alternatives is proportional to the relative thickness of the plate.
- For smaller plates, correct out-of-plane shear stiffnesses G_{xz} and G_{yz} are essential to correctly estimate the deformations.
- Unexpected behaviours where two-way action is not beneficial for the deformations may occur in CLT plates due to certain geometric conditions in combination with low torsional stiffness.
- For more simplified modeling alternatives, one-way action may be sufficiently represented, even though the modeling alternatives are not an appropriate representation of a two-way plate.

5.4 Shell loaded in in-plane shear

Only one slab has been tested in in-plane shear, but two different analyses are made. One analysis is focused on the different modeling assumptions from Table 5.2, while the other analysis is focused on the different membrane shear reduction factors that are presented in section 4.1.2.2. The geometry and loading conditions of the plate are as follows:

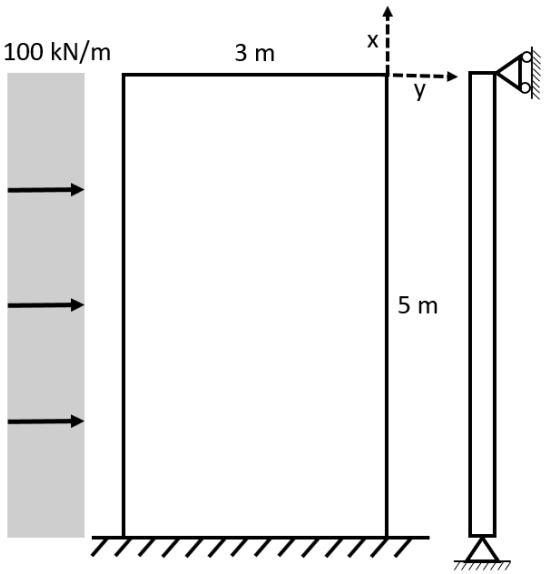

Figure 5.14: Geometry, boundary conditions and loading for the shell analysed in in-plane shear.

5.4.1 Comparison between modeling alternatives

The data from Table 5.2 is used when comparing the different modeling assumptions. Modeling assumptions that are tested in bending that has low in-plane shear stiffness G_{xy} (*One-way stiffness* and *Isotropic plate*) are not tested in in-plane shear. This is due to the unreasonably large deformations that are consequences of very low in-plane shear stiffnesses. An alternative modeling assumption called *Bending stiffness* is added and addresses the difference caused by entering the elastic stiffnesses associated with bending instead of the stiffnesses associated with in-plane forces. The deformation results of the in-plane loading can be seen in Figure 5.15.

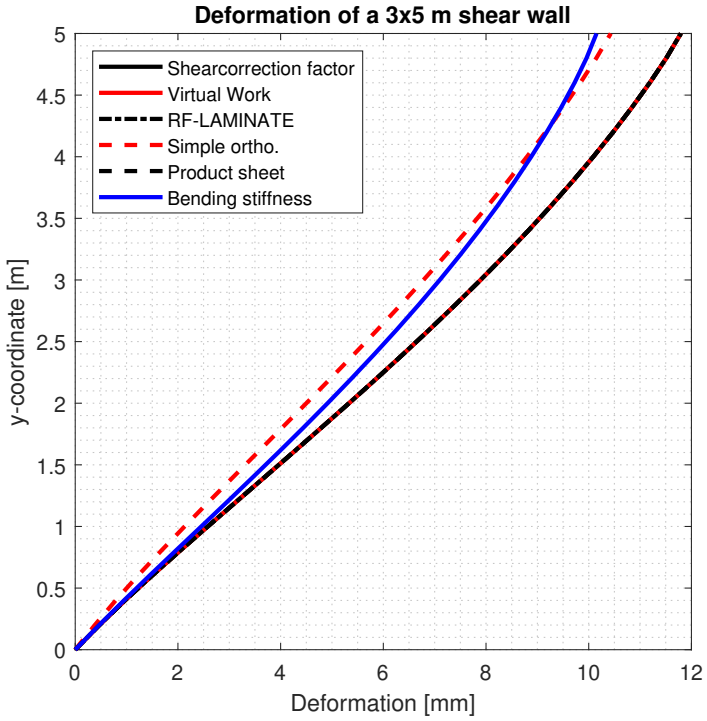

Figure 5.15: Horizontal deformation in the shell element.

Several of the tested shell elements have identical deformations and are thus plotted on top of each other in Figure 5.15. The fact that many results are identical is expected since they have identical E_x, E_y and G_{xy}. The results from *RF-LAMINATE* also identically follows the orthotropic shells with identical stiffnesses. The simple orthotropic shell has smaller deformations due to its slightly overestimated G_{xy} compared to the other shells, while the shell that is defined with bending stiffnesses has smaller deformations due to the difference in E_x and E_y. This is further discussed in section 5.5.

5.4.2 Comparison for membrane shear reduction factor

The membrane shear reduction factor k_{88} that is previously mentioned in section 4.1.2.2 is tested in a small scale study with the same geometry and load conditions as Figure 5.14. The various recommendations of $k_{88} = 1$, $k_{88} = 0.75$ or $k_{88} = 0.25$ is tested as well as an intermediate value of $k_{88} = 0.5$. For the comparison of different values of the reduction factor k_{88}, the *Orthotropic plate - Virtual work* plate from Table 5.2 has been used for all tests. The results of the small scale study regarding the reduction factor k_{88} are presented in Figure 5.16.

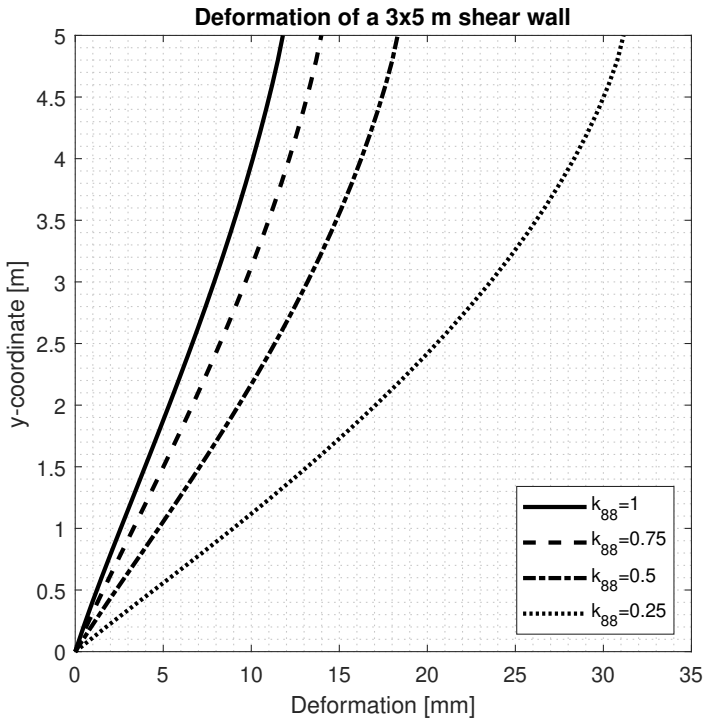

Figure 5.16: Deformation for different values of the reduction factor k_{88}.

The influence of the reduction factor k_{88} is significant in the small scale study as can be seen in Figure 5.16. The two different recommendations of either $k_{88} = 0.75$ (Silly, 2010) or $k_{88} = 0.25$ (DIN (2008)) differ significantly for the deformations, where the reduction factor $k_{88} = 0.75$ yields a deformation of approximately 14 mm while the reduction factor $k_{88} = 0.25$ yields a deformation of approximately 31 mm. This difference is substantial, and a large difference can be expected for the sensitivity study of the reference building as well.

5.4.3 Conclusions from in-plane small scale study

The study of k_{88} yields a much wider spread of results than the study of the modeling assumptions varying the stiffness parameters. This is probably caused by the difference in how much the parameters such as G_{xy}, E_x and E_y varies compared to

the relatively much larger variation of the reduction factor k_{88}, and thus it is not possible to deem one parameter more important than the other on the basis of this small scale study.

Conclusions from **in-plane shear small-scale study**:

- The two most important parameters for performance of the material in in-plane shear is the in-plane shear stiffness G_{xy} and the membrane shear reduction factor k_{88}.
- When an orthotropic shell is expected to act primarily in its plane, membrane stiffness should be used as E_x and E_y according to equations 4.3 and 4.4.

5.5 Orthotropic shells defined by a stiffness matrixes

As seen from Figure 5.15, similar deflections using bending stiffnesses and membrane stiffnesses cannot be expected for a shell loaded in-plane. The same is true for a shell loaded in bending, where the deflections would be very large if membrane stiffnesses were used instead of bending stiffnesses. When defining a CLT element as an orthotropic shell where the in-data is entered as stiffnesses, it is impossible to expect the shell to behave correctly in both bending and in-plane shear.

Several sources (Aondio et al. (2020) and Gustafsson et al. (2019)) suggest that a CLT element should be modeled directly by a stiffness matrix. This is a similar approach as to how *RF-LAMINATE* treats the CLT element. Defining the shell by stiffnesses is still however very possible if the element is expected to behave mainly in bending or in membrane loading. For example, a CLT floor structure should be modeled with bending stiffnesses while a shear wall should be modeled with membrane stiffnesses.

A comparison of different stiffness matrixes is done below, where the general stiffness matrix from Equation 4.21 is used. The stiffness matrix can be further reduced if ν_{xy} is assumed to be zero, resulting in the stiffness matrix in Equation 5.1. A comparison between four different stiffness matrixes is made in Table 5.5, where the first matrix is generated by *RF-LAMINATE*, the second matrix is user-defined using the theory of virtual work (Aondio et al., 2020), and the third and fourth are generated by *RFEM* using equations 4.22 - 4.31 when the stiffnesses are either defined as bending stiffnesses or membrane stiffnesses. A Martinssons 140-5s CLT element is modeled by stiffness matrixes and presented in Table 5.5. The row marked *Bending stiff.* is used for slabs and *Membrane stiff.* is used for shear walls. *User defined* is neither used in the small-scale studies nor in the sensitivity study but is a more accurate stiffness matrix which should (similarly to the matrix defined by *RF-LAMINATE*) be able to resemble the behaviour both when the CLT element is loaded in bending and in-plane shear.

$$\begin{bmatrix} m_x \\ m_y \\ m_{xy} \\ v_x \\ v_y \\ n_x \\ n_y \\ n_{xy} \end{bmatrix} = \begin{bmatrix} D_{11} & 0 & 0 & 0 & 0 & 0 & 0 & 0 \\ 0 & D_{22} & 0 & 0 & 0 & 0 & 0 & 0 \\ 0 & 0 & D_{33} & 0 & 0 & 0 & 0 & 0 \\ 0 & 0 & 0 & D_{44} & 0 & 0 & 0 & 0 \\ 0 & 0 & 0 & 0 & D_{55} & 0 & 0 & 0 \\ 0 & 0 & 0 & 0 & 0 & D_{66} & 0 & 0 \\ 0 & 0 & 0 & 0 & 0 & 0 & D_{77} & 0 \\ 0 & 0 & 0 & 0 & 0 & 0 & 0 & D_{88} \end{bmatrix} \begin{bmatrix} \kappa_x \\ \kappa_y \\ \kappa_{xy} \\ \gamma_{xz} \\ \gamma_{yz} \\ \varepsilon_x \\ \varepsilon_y \\ \gamma_{xy} \end{bmatrix} \tag{5.1}$$

Table 5.5: Resulting stiffness matrix elements from the different methodologies of defining the stiffness matrix. *Membrane stiff.* is not used in the sensitivity study but is in theory a more accurate way to model the stiffness. All values are $\cdot 10^6$ and of varying units.

	D_{11}	D_{22}	D_{33}	D_{44}	D_{55}	D_{66}	D_{77}	D_{88}
RF-LAMINATE	1.63	0.63	0.14	7.90	13.6	678	582	76.6
Virtual work - *User defined*	1.63	0.63	0.27	8.78	9.00	678	582	76.6
Virtual work - *Bending stiff.*	1.63	0.63	0.13	8.78	9.00	995	387	76.6
Virtual work - *Membrane stiff.*	1.11	0.95	0.13	8.78	9.00	678	582	76.6

The stiffness matrixes generated by *RF-LAMINATE* and the user-defined stiffness matrix are relatively similar. This can be somehow expected since both matrixes are defined as stiffness matrixes using similar theories. The differences in the stiffness matrixes from *bending stiff.* and *membrane stiff.* compared to the user-defined stiffness matrix are quite large. Either the bending elements D_{11} and D_{22} agree, or the membrane elements D_{66} and D_{77} agree, but they can never agree simultaneously if the shell is defined using stiffnesses. This is however, as previously stated, generally only a problem if an element is loaded in-plane and in bending at the same time. The small scale studies regarding both bending and in-plane loads show that the differences in deformation between the different modeling assumptions generally are small if the element is loaded in only in-plane or bending.

Conclusions from the **stiffness and stiffness matrix comparison**:

- Determining a shell's stiffness properties is most accurately done by directly defining its stiffness matrix. This option is however relatively time consuming.
- If the shell is expected to be loaded almost exclusively in bending or almost exclusively in its plane, defining the shell by its stiffness properties is sufficient.
- If a plug-in such as *RF-LAMINATE* is available, the shell can be expected to behave correctly both in bending and in in-plane shear.

5.6 Hinged connections or rigid plate

CLT slabs are usually connected on site using single or double splines, which results in connections that resists small or close to no moments. To accurately represent the behavior of the entire floor the CLT members and their connections should be modeled individually, but since this is time consuming a small scale study is conducted in *RFEM* to evaluate the difference of the results, depending on if the floor is modeled as rigid or with hinges.

The setup of the model is presented in Figure 5.17. A section is running in the long direction through the middle of each plate (marked with black dashed lines and arrows). These sections are used in figures 5.21 - 5.25, where the resulting deflections are presented.

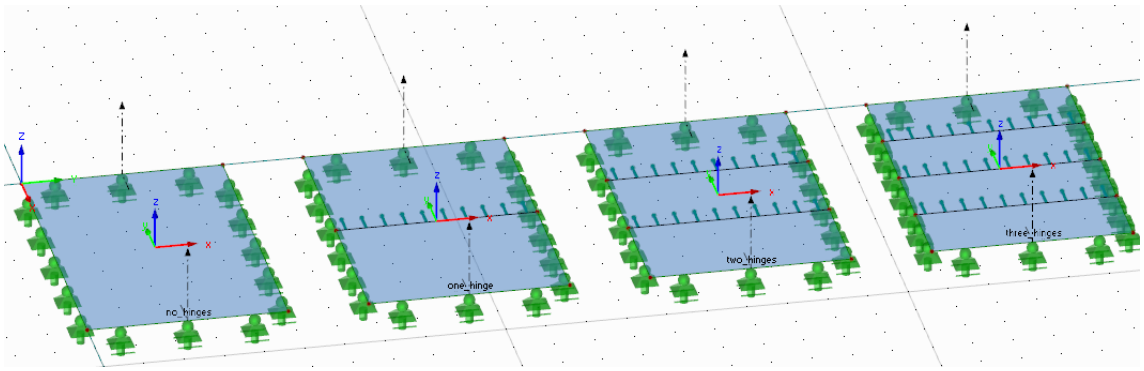

Figure 5.17: Setup for small scale study addressing hinges between CLT elements.

The main direction of the CLT element is spanning in the short direction of the plate, which is 5 m. Commonly, the slabs are only supported with beams or walls on their short side which results in a one-way behavior in parts of the slab. How efficiently the weak direction of the slabs can be used for carrying loads, depends on how large the capacity of the spline orthogonal to its direction is, which in turn is affected by the slip and plasticity of the connection. These effects are not included in the sensitivity study, but are certainly interesting subjects for further investigations.

The influence of the hinges is highly dependent on the geometry of the plate. If the plate is relatively long in its minor direction, it has the consequence that the plate behaves in one-way in the center of the long direction of the slab. The conclusions in this section are only valid when the span of the weak direction is significantly larger than the span in the strong direction.

Each plate in the study has the dimensions 8×5 m, where the strong direction of the plate spans 5 m. The plates are divided by zero, one, two or three hinges, which means that the widths of the sections between the hinges varies in the range 2 m to 8 m.

5.6.1 Results and conclusions

As can be seen in Figure 5.18 and 5.19, the deformations and the maximum moment in x-direction are similar for the four cases. The distribution on the contrary, is affected significantly of the introduced hinges. The hinges contributes to a one-way behaviour in the slabs of the plate which are not connected to the supports on the short sides. This also affects the moments in y-direction which can be seen in Figure 5.20, even though the moments in this direction are generally small.

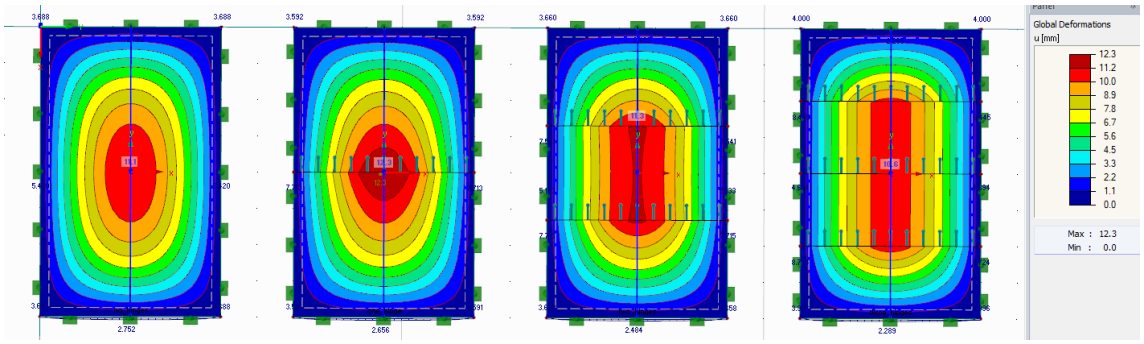

Figure 5.18: Deflections of CLT element loaded with evenly distributed load.

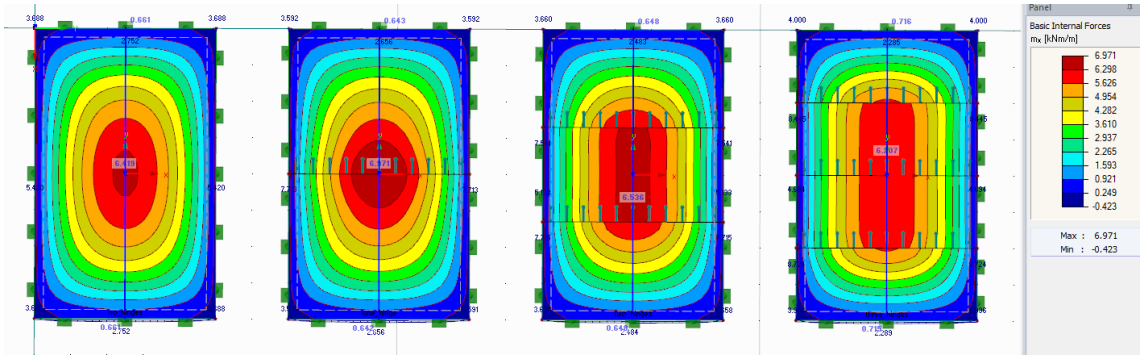

Figure 5.19: Distribution of moments in x-direction (strong direction) under evenly distributed load.

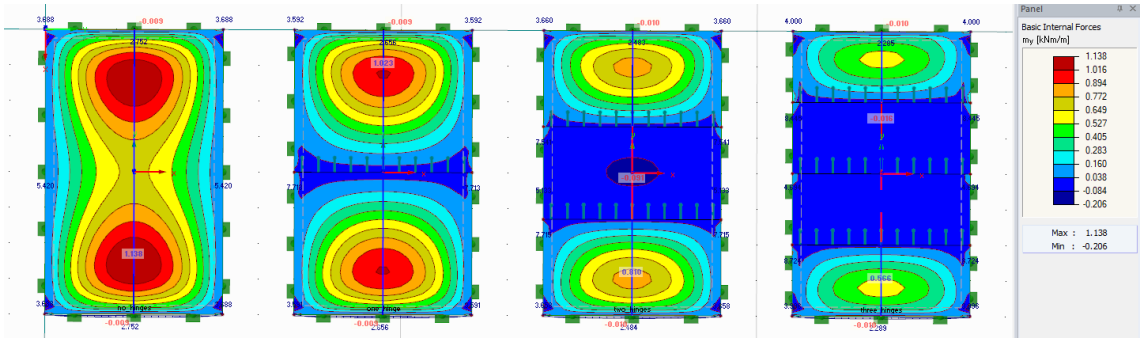

Figure 5.20: Distribution of moments in y-direction (weak direction) under evenly distributed load.

The maximum values of moments in the strong direction of the plate is similar for all four slabs (see Figure 5.22a), independently of the number of hinges. The maximum deflection is also approximately the same in all four cases (see Figure 5.21). This means that if the slabs are designed using hand calculations and a one-way slab model, which in this case yields a maximum deflection of 10.3 mm (see Appendix A.1.2), three of the models will correlate quite well with the design values, and the one-hinge model will differ about 1.5 mm.

When observing the graph showing the moments in y-direction (see Figure 5.22b), the model without hinges differs to a relatively large extent compared to the other models. Since the plate is not designed by the moments in y-direction when the design is made by hand, this does not affect the dimensions of the plate obtained by the design calculations. The moments in y-directions can thus be considered of less importance than the other results. However, the reason for the relatively large deviation of the curve is a result of that there are no hinges with zero moment along the plate.

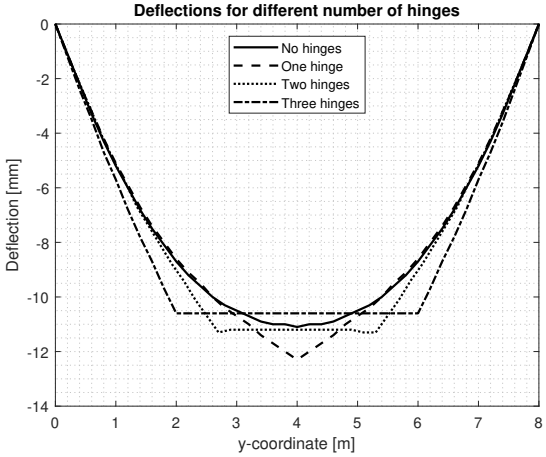

Figure 5.21: Deflections for a 5 × 8 m two-way slab along the y-direction.

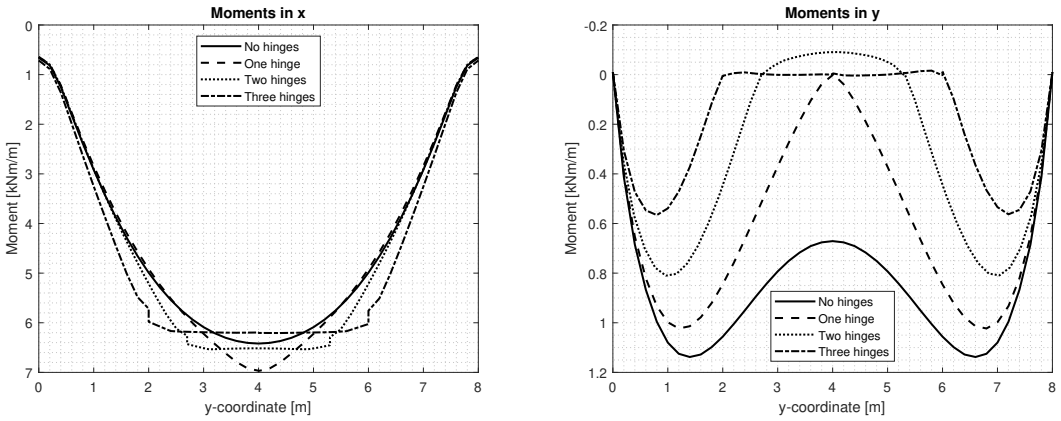

(a) Moments in x-direction. **(b)** Moments in y-direction.

Figure 5.22: Moments for a CLT slab from the sections in Figure 5.17.

From Figure 5.23 the conclusion can be drawn that the effect from the number of hinges is small considering the amount of load that is transferred in the strong respectively in the weak direction. However, the amount of load that is transferred in the weak direction of the plates is reduced when the number of hinges is increased. This is due to a more pronounced one-way behaviour in the plates that include hinges compared to the rigid plate. The redistribution of load to the different supports is relatively small which means that for other members than the slabs themselves within a structural system, modeling the floors with or without hinges will have an effect but it is likely to be relatively small.

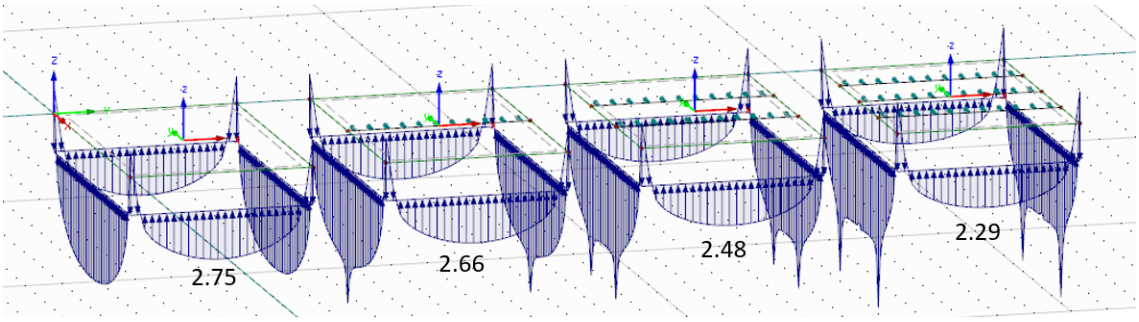

Figure 5.23: Reaction forces for slab with zero hinges to the left and three hinges to the right. The value for maximum force on the short edge of the slab is given in kN/m.

5.6.2 Representing hinges by reduced stiffness in y-direction

Conclusions that can be drawn from figures 5.18 to 5.20 is that the more hinges that are introduced, the more pronounced the one-way behaviour becomes. To avoid the time consuming and computationally expensive process of modelling each CLT-element separately, the behaviour of a plate with hinges can be represented by a plate with reduced stiffness perpendicular to the hinges.

The two different materials used in the comparison in Figure 5.24 and 5.25 are presented in Table 5.6, where the orthotropic material derived by the theory of virtual work is used for the regular plate without hinges and the plate with three hinges, while the material with reduced E_y is used for the newly introduced plate with a reduced stiffness in its weak direction to compensate for the hinges that are assumed to exist in the real plate.

Table 5.6: Stiffness values for the material with reduced E_y compared with the original stiffness values for the orthotropic plate designed using the method virtual work for bending. All numbers are given in MPa.

	Virtual work	Reduced E_y
E_x	7 106	7 106
E_y	**2 767**	**300**
G_{xy}	547	547
G_{xz}	75	75
G_{yz}	77	77

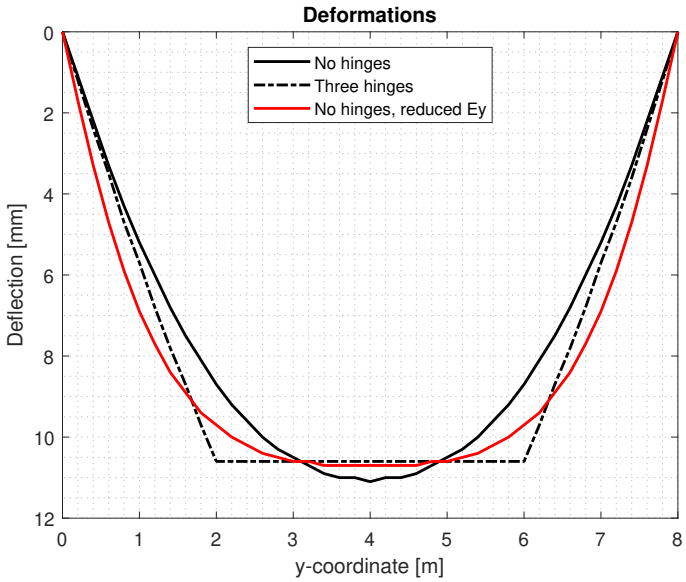

Figure 5.24: Deformations for a 5 × 8 m two-way slab along the y-direction.

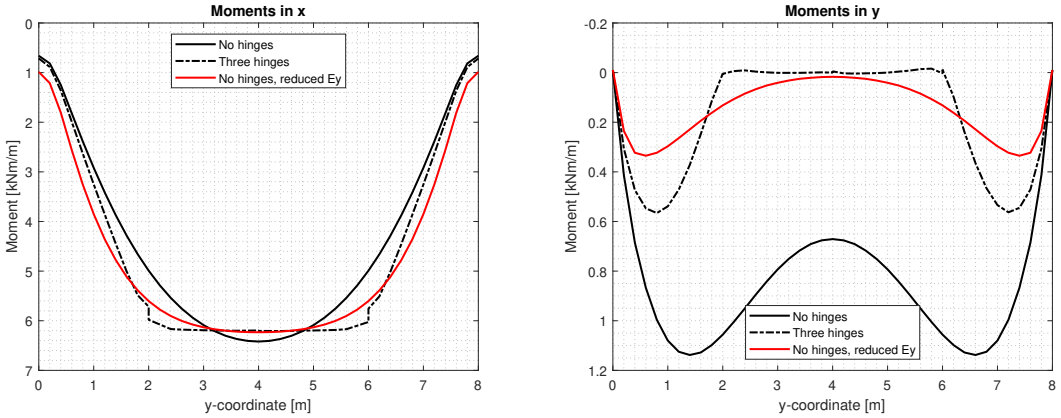

(a) Moments in x-direction. **(b)** Moments in y-direction.

Figure 5.25: Moments for a CLT slab from the sections shown in Figure 5.17.

The behaviour of the plate with reduced E_y is significantly more similar to the plate with three hinges than the original plate without hinges. From this point of view, it can be considered reasonable to reduce the stiffness in the weak direction of the CLT elements.

Since the reduction of E_y makes a reasonably good estimation of the behaviour of the plate, the sensitivity study uses plates without hinges. The variation of the Virtual work orthotropic plate where E_y is reduced, is used as an additional modeling assumption in the sensitivity study.

5.6.3 Conclusions of the hinged connections small scale study

Depending on what the FE-model is to be used for, the importance of including hinges between plate elements is varying. A study focusing on the global behaviour of a building does not necessarily need to consider the hinges, while a study of the behaviour of the slabs may benefit from considering the hinges, either by modeling them or by reducing the stiffness of the floor slabs to obtain more realistic patterns of deflections and moments in the slabs.

Conclusions from the **hinged connections small-scale study**:

- The maximum values of deflection and moments in the major direction of the plate are affected by the hinges to a relatively small extent.
- The load distribution between the supports is affected by the hinges to a relatively small extent.
- The bending stiffness in the minor direction E_y can be reduced to relatively accurately represent hinges in the plate.

6

Design of reference building

The reference building is used in the sensitivity study in order to determine the differences caused by CLT modeling assumptions for a system-level analysis. The design of the building is decided considering several criteria, chosen in order for the building to yield relevant and trustworthy results when conducting the sensitivity analysis.

The design of the reference building is done on the basis of hand-calculations. Relevant stresses and deformations from the FE-analysis is verified against hand calculations in order to confirm that the FE-analysis is correctly performed. Figure 6.1 illustrates the final design of the reference building.

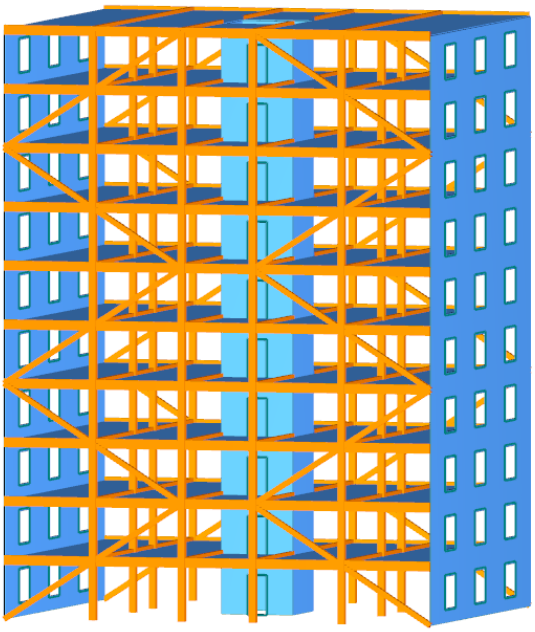

Figure 6.1: Final design of the reference building.

6.1 Building geometry

One of the main purposes and aims in the design of the reference building is that it should represent and resemble a real building. The building *Treet* in Bergen, Norway was a major inspiration in the design of the building. *Treet* is an approximately 45 m tall timber building (Abrahamsen & Malo, 2014) that uses glulam truss bracing and a CLT core as stabilising elements. The reference building also utilizes a core and glulam trusses as a stabilizing units, but in addition it also has CLT shear walls in the facade. CLT shear walls are used so that the behaviour of CLT in horizontal shear using different modeling assumptions can be studied in the reference building.

Figure 6.2: Photograph of the building *Treet*. "Treet" by Andrew M Butler is licensed under CC BY-NC 2.0.

The building should not have dynamic effects as a designing load case, since static loads and response are analysed in the studies. In a study conducted by Bezabeh et al. (2020), it was concluded that a specific 34 m tall massive timber building with the footprint 30 × 42 m did not have any problems related to dynamic wind loads. However, the dynamic effects from wind load rapidly increases with an increasing height.

To be able to analyse the effects of the modeling assumptions on the horizontal stability for a high-rise timber building, while still delimiting the project to address static loads, a height of 32 m is chosen. The assumption of neglecting the dynamic effects is also supported by the conclusions made in Edskär (2018), where it is stated that timber buildings of ten stories and the ratio 1.5 between the height and the base of the building has small or no problems with dynamic loads.

Non-rectangular slabs and non-orthogonal angles are common in real buildings, but when modeling a building with more complex geometry, effects such as singular points and complicated load paths are more common. Since the purpose of the reference building is to compare different modeling assumptions, the building's geometry should be relatively simple in order to minimize matters that does not contribute to the understanding of the effects of the modeling assumptions. The geometry of the reference building is presented in Figure 6.3.

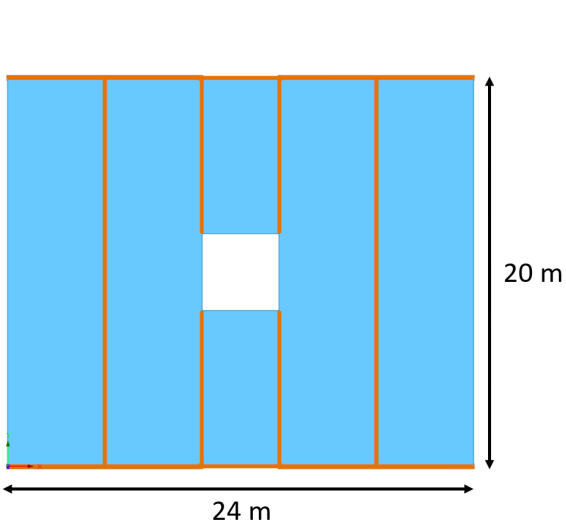

(a) Seen from above in xy-plane.

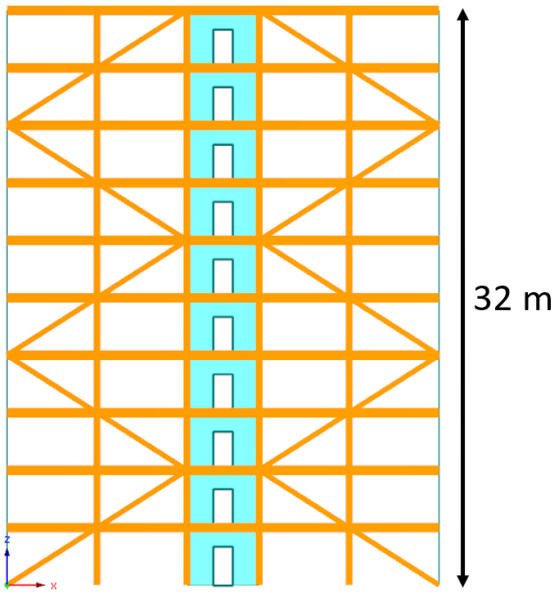

(b) Seen from the side in xz-plane.

Figure 6.3: Geometry of the reference building.

The CLT panels are limited in size by production and transportation factors. One example of how the panels can be placed is given in Figure 6.4. In an actual building, it is likely that the length of the CLT panels (which is not as limited as the width) would be used to make the floors continuous over the supporting beams. This would decrease the deflections of the floors but it may also have consequences for e.g. the acoustic performance. The widths of the CLT elements are not addressed in the sensitivity study, but the material with reduced E_y is composed to approximately represent the CLT dimensions in Figure 6.4. The lengths of the CLT elements are considered by introducing hinges at the connections between slabs, as described in Figure 6.8.

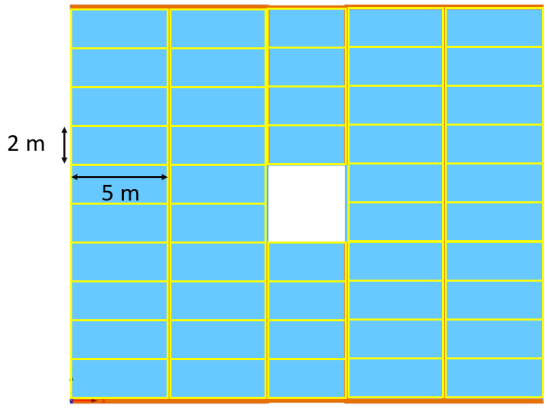

Figure 6.4: Example of how the CLT panels can be distributed over the floor.

6.2 Member sizing

The members chosen for design of the reference building are presented in Figure 6.5. No design calculations are conducted for the core of the building, but the assumption that the same dimensions can be used for the core as for the shear walls is made. This assumption is verified using the results from the FE-analysis. The same procedure is used for the diagonal bracing units which was originally assumed to have the same dimensions as the horizontal beams. The capacity of the bracing units is checked against the design forces from the FE model to ensure a sufficient capacity. When calculating the design loads for the walls and columns, it is done for the bottom floor of the building.

The boundary conditions, element geometry, cross sections, capacities and utilization ratios as well as a reference to the calculations in the appendix are presented in Table 6.1. The reference numbers are used to correlate Table 6.1 with Figure 6.5.

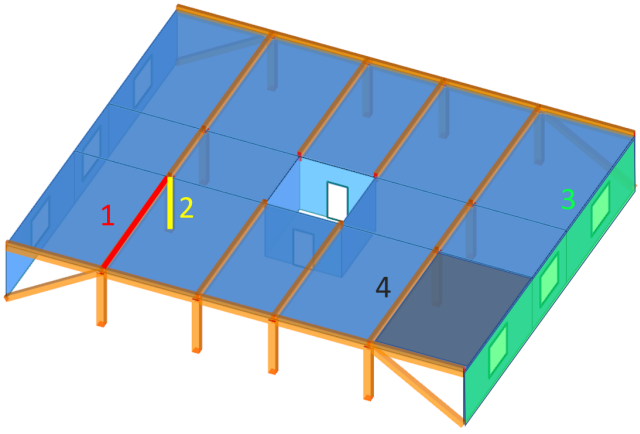

Figure 6.5: The members chosen for design of the reference building. The numbering correlates to the reference numbers in Table 6.1.

Table 6.1: Design of members based on hand calculations.

Member type	Ref. Number	Boundary condition & Element geometry	Cross section	Designing force/moment	Capacity	Utilization	Appendix
Beam GL30c	1	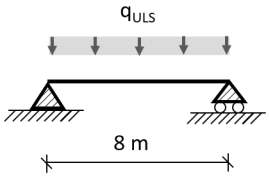	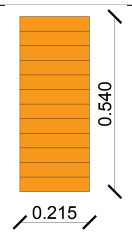	161 kNm	201 kNm	80 %	A.1.1
Column GL30c	2	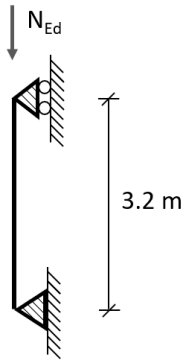	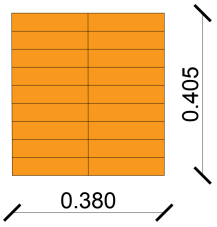	1200 kN	2370 kN	51 %	A.1.4
Wall 100-5s	3	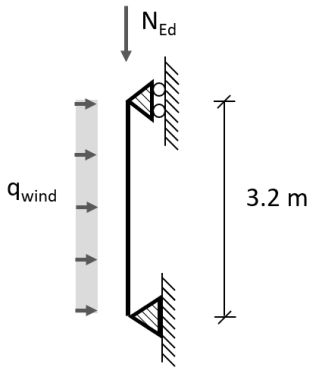	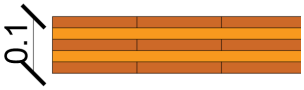	0.51 kNm & 167 kN	23 kNm & 292 kN	60 %	A.1.3
Floor slab 140-5s	4	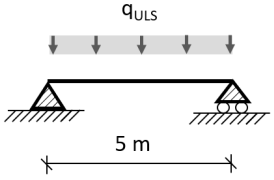	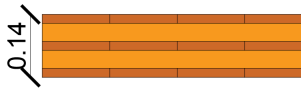	12.1 kNm	36.8 kNm	33 %	A.1.2

6.3 Boundary conditions and connections

The reference building is supported by line supports along all CLT elements in the bottom of the structure. The elements are free to rotate but restraint from translation in all directions. The columns are pinned in the bottom.

The general approach used when constructing the model of the reference building was to connect elements with pinned connections in the largest extent possible. Considering deformations, this is a conservative assumption.

In Figure 6.6, the column-beam system of the first floor can be seen. All beams are free to rotate around their y-axis (local coordinate system according to Figure 6.7) and the columns are free to rotate around both their y-axis and their z-axis.

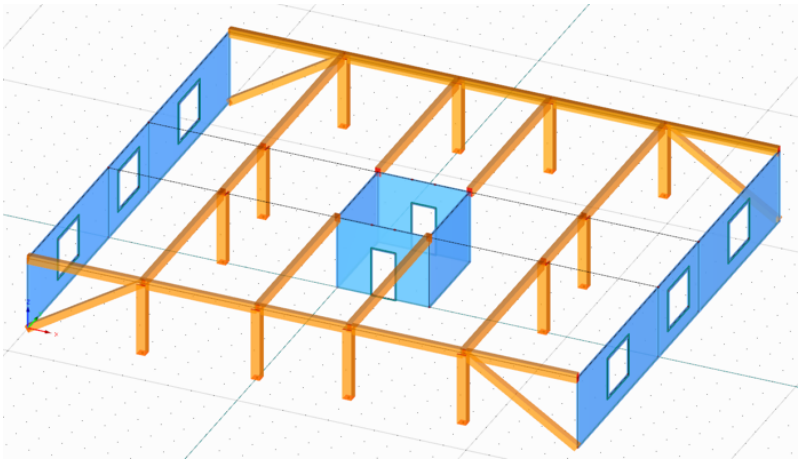

Figure 6.6: Beam and column system of the first floor.

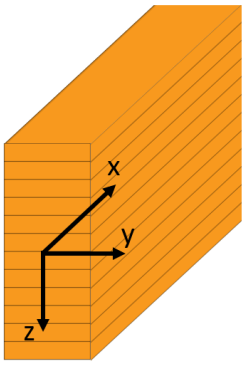

Figure 6.7: Local coordinate system for beams and columns.

Where the CLT plates rests on beams or walls, they are modeled as hinged in the connection to other CLT elements since this has a large effect on the size of the deflections and cannot be neglected. The connections between CLT elements that transfers forces in the weak direction of the plates are not modeled, and thus the

CLT plates acts as if they has full interaction. This connection differs to the hinged connection applied between plates when the plates are supported by a beam. This choice was made in accordance with the conclusions drawn in the small scale study in section 5.6 and the connections between plates are shown in Figure 6.8. An additional material with reduced E_y is included in the sensitivity study to consider the effects of the hinges transferring forces in the weak direction of the CLT elements. The material with reduced E_y is the same that is used in the small scale study.

The core of the reference building is modeled as completely hinged in all connections, so that the elements are only continuous over the height of one floor. The CLT elements thus becomes 4 m (the width of the core) times 3.2 m (the height of one floor). This is not a reasonable element size considering transportation logistics, and furthermore, the stabilizing properties of the core would probably benefit from a continuity over several floors. Since the essence of this thesis not is to investigate how to efficiently construct a core structure, the core has not been modified since the original design, assuming that the structure approximately can represent an arbitrary core.

The locations of the hinges between CLT elements in slabs, walls and core are presented in Figure 6.8.

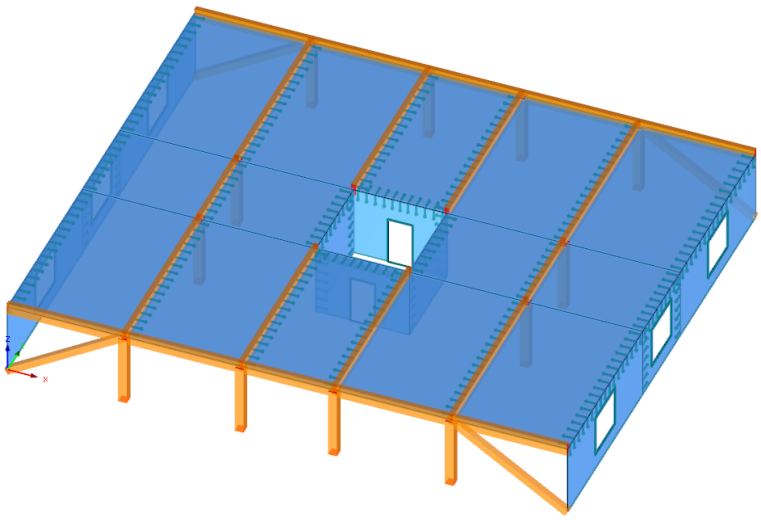

Figure 6.8: First floor of reference building with marked line hinges for the CLT elements.

6.4 Loads

As mentioned in the introduction of the thesis, the loading of the structure is simplified to make it easier to distinguish the effects from the modeling choices. Table 6.2 presents the magnitudes of all loads included in the analysis. Calculations of the wind loads are found in Appendix A.1.5, imposed loads are applied according to EKS 11 (Boverket, 2019). Wind loads are applied either in the global x-direction or y-direction. Several other loads that are usually present in real buildings such as snow loads and loads from non-load bearing walls are not considered in the reference building. Since the reference building is only used for comparison purposes, the neglect of certain loads does not affect the conclusions that can be made based on the results of the sensitivity study.

Table 6.2: Loads applied on the reference building.

Type:	Size:	Acts on:
Self weight	4.75 kN/m^3	Timber members
Imposed load	2 kN/m^2	Floors (Residential)
Wind load	0.97 kN/m^2	Facade, Pressure on upper parts of building
Wind load	0.88 kN/m^2	Facade, Pressure on lower parts of building
Wind load	-0.63 kN/m^2	Facade, Suction on higher parts of building
Wind load	-0.58 kN/m^2	Facade, Suction on lower parts of building

6.5 Load combinations

The ultimate limit state (ULS) load combination is composed according to SS-EN 1990 (SIS, 2010) while the serviceability limit state (SLS) load combinations are simplified versions of the regulations in the same document. For design of slabs, walls, beams and columns the ULS and the SLS (imp. main) load combinations are used. The SLS load combinations including wind are used to check horizontal deformations of the entire system.

Table 6.3: Factors applied on the loads when they are assembled in to the simplified load combinations.

Load combination:	Applied coefficients for each load:			
	Self weight	Imposed load	Wind (x)	Wind (y)
ULS (Imp. main)	1.35	1.5	$1.5 \cdot 0.3$	0
SLS (Imp. main)	1.0	1.0	0	0
SLS (Wind x main)	1.0	0	1.0	0
SLS (Wind y main)	1.0	0	0	1.0

7

Sensitivity study

In the sensitivity study, the modeling assumptions for CLT are applied to the reference building to observe how they affect the deformations. The resulting deformations are extracted at three sections, two along the slab addressing the vertical deflections and one along the core to observe the horizontal deformations along the height of the building.

7.1 Input data

The reference building uses Martinsons 140-5s elements as floor slabs and Martinsons 100-5s elements as shear walls and core walls based on the design in chapter 6. The different modeling assumptions for the slabs and walls are presented in Table 7.1.

Table 7.1: The different modeling assumptions used in the sensitivity study of the reference building. All numbers are in MPa.

	Slab 140-5s					Wall 100-5s				
Modeling assumption	E_x	E_y	G_{yz}	G_{xz}	G_{xy}	E_x	E_y	G_{yz}	G_{xz}	G_{xy}
Ortho. plate - Shear corr. factor	7106	2767	119	93	547	6692	3022	88	125	590
Ortho. plate - Virtual work	7106	2767	77	75	547	6692	3022	55	92	590
Ortho. plate - Simplified	7106	2767	69	69	690	6692	3022	69	69	690
Ortho. plate - Reduced E_y (*)	7106	300	77	75	547	-	-	-	-	-
Isotropic plate (*)	7106	7106	69	69	69	-	-	-	-	-
RF-LAMINATE (**)	-	-	-	-	-	-	-	-	-	-
Ortho. plate - Product sheet	7106	2767	133	73	547	6692	3022	104	100	590

(*) Uses the element created with product sheet as walls.

(**) *RF-LAMINATE* assembles directly into the stiffness matrix, and no stiffness needs to be determined.

Since the floors are utilized almost exclusively in bending, the bending stiffnesses are used for E_x and E_y when modeling the slabs. The membrane stiffnesses for E_x and E_y are used for the walls which are primarily loaded in compression.

The isotropic plate is not used as walls due to its low in-plane shear modulus G_{xy}. If it was used, the horizontal deformations would be unrealistically large. When the slabs are modeled using the isotropic plate, the walls are modeled using the stiffness properties from the product sheet (Martinsons, 2019).

The orthotropic plate with reduced E_y is used to simulate the effect of hinges between the slabs, and it is therefore not meaningful to model the walls using the same assumption. When the slabs are modeled using the orthotropic plate with reduced E_y, the walls are modeled using the stiffness properties from the product sheet (Martinsons, 2019).

No reduction factors are used in the analysis regarding stiffness assumptions. The CLT elements are also considered to have glue on the narrow sides, meaning that the stiffnesses of the cross layers are included when evaluating the bending stiffness of the orthotropic shell elements. Although it is usually assumed that there is no glue on the narrow sides, the CLT panels in the sensitivity study are considered having glue on their narrow sides since that assumption yields less reduction factors and more influence from the cross layers, which can be favorable for comparison purposes.

The influence of the membrane shear reduction factor k_{88} is analysed in a separate part of the sensitivity study of the reference building. The same reduction factors as in the small scale study in section 5.4.2 are used.

7.2 Stiffness study - Results

The results are presented along three different sections in the reference building. The first two sections span along multiple floor slabs on the first floor of the building in either x or y-direction. The third section spans along one of the core walls along the height of the building. The first two sections are used to study floor deflections and the third section is used to study global horizontal deformations of the building. The sections and their naming conventions are presented in Figure 7.1. The floor slabs have their major direction parallel to section (1).

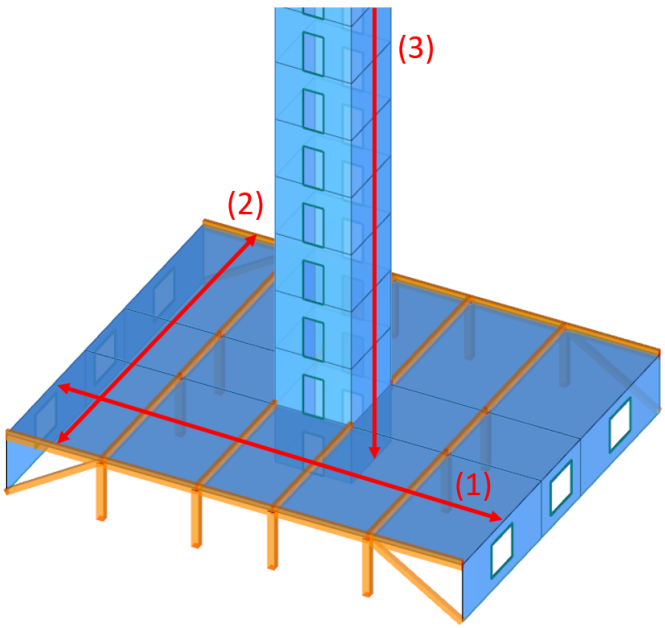

Figure 7.1: Sections and their naming convention for the results of the analysis.

7.2.1 Deflections along section (1)

Section (1) spans along the global x-direction of the building on the first floor. It is composed of five simply supported floor spans of either 4 or 5 m. The resulting deflections are presented in Figure 7.2.

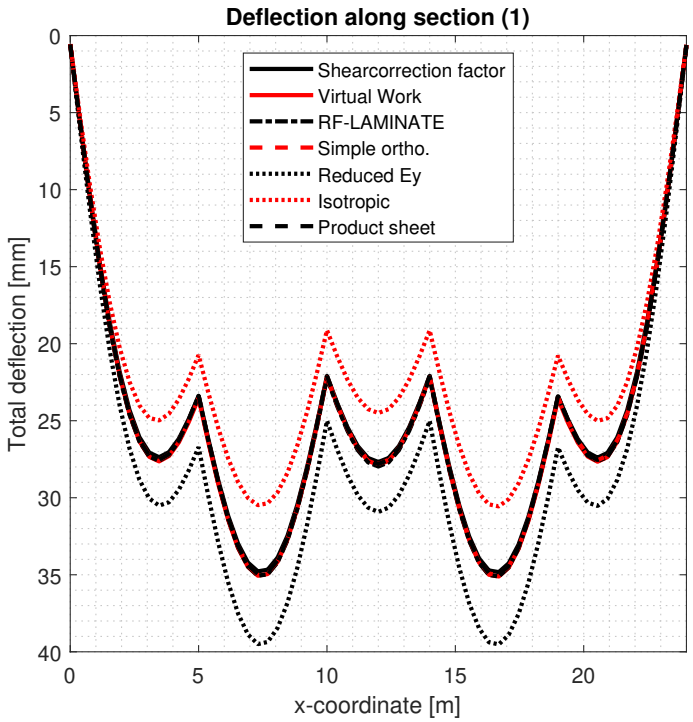

Figure 7.2: Deflection along section (1) for different modeling assumptions.

Compared to the small scale study in section 5.3, there is a larger spread in results for some of the modeling assumptions. Figure 7.2 illustrates the global deflections which includes the deflections of the beams at the supports. An interesting observation that can be made is that the beams on which the slabs are resting deforms differently for the modeling assumptions. The two outliers when it comes to beam deflection are the isotropic and reduced E_y model. This is due to the relation between stiffness in x-direction and in y-direction. The isotropic plate which has a significantly larger stiffness in y-direction compared to the majority of the plates, transfers a larger part of the load in y-direction and less load in the x-direction. The loading on the beam is therefore smaller and thus the deformation of the beam becomes smaller. The same reasoning is valid for the plate with reduced E_y, which has a lower E_y compared to the majority of the plates and therefore transfers more load in x-direction and yields larger deflections of the beam.

As mentioned above, in the sensitivity study the differences in deflection between the modeling assumptions partly depends on the effects of the deflection of the supports. Even if the support deflections are neglected, differences in deflection between the modeling assumptions are still larger compared to the small scale studies. This is

illustrated in Figure 7.3 where the maximum deflections of the slab along section (1) with neglected beam deflections are plotted together with the maximum deflections from the small scale study of a one-way slab with the same span length.

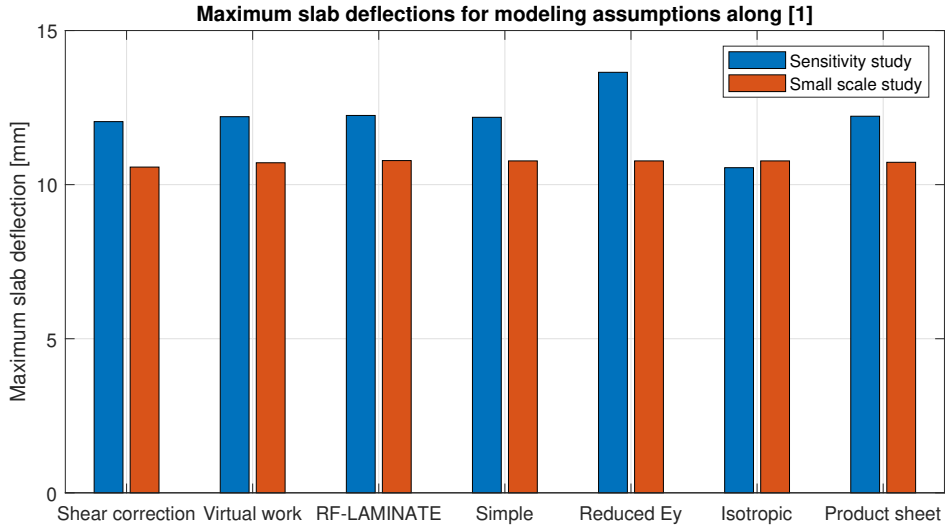

Figure 7.3: Comparison of maximum deflections of the plates for the sensitivity study and the small scale study. Deformations from the sensitivity study are viewed excluding the deformations of the supporting beams.

The largest difference between conclusions from the small scale study and the sensitivity study is for the isotropic plate, which in section (1) of the sensitivity study for the reference building has the smallest deflections as can be seen in Figure 7.2 and Figure 7.3. In the small scale study, it instead had an intermediate deflection for the one-way slab (as presented in Figure 7.3) and the largest deflection for the two-way slab (see Figure 5.10).

A conclusion that can be made is that the influence of stiffness parameters is different in section (1) compared to the small scale studies. The isotropic plate has relatively high bending stiffnesses and relatively low shear stiffnesses compared to the other modeling assumptions. This means that the bending stiffnesses are more significant in section (1) compared to the small scale study, and the bending stiffness E_y can therefore be concluded to have a reasonably large influence on the deflections along (1).

The orthotropic plate with reduced E_y has the largest deflections along (1). This is another indication of the large influence of the bending stiffness E_y. A conclusion that can be made is that influence of hinges is rather significant, assuming that the way of representing slabs from the small scale study is a good approximation. The assumption could be verified by implementing individual slabs with hinges in the reference building, but that is delimited in this analysis.

The remaining modeling assumptions have very similar deflections. The difference between these modeling assumptions are the out-of-plane shear stiffnesses G_{yz} and G_{xz}, meaning that the influence from shear deformations are small for section (1).

7.2.2 Moment and shear along section (1)

The resulting moments and shear are presented in Figure 7.4.

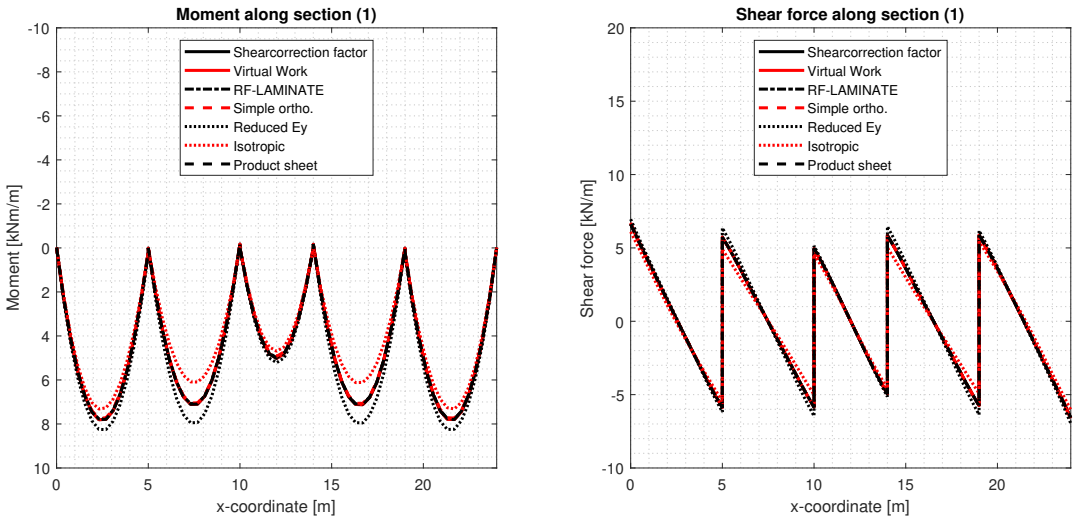

(a) Moments along (1). **(b)** Shear along (1).

Figure 7.4: Moments and shear along section (1) for different modeling assumptions.

The moments and shear results behaves similarly as to the deflections in Figure 7.2, which is expected since the slabs are simply supported and thus the correlation between deflection, moments and shear is rather definite. This is however not the case if more complex geometries are analysed, such as if the slabs are continuous over the supports or if the boundary conditions of the slabs results in a statically indeterminate problem. In that case, there is a possibility that the moments and shear are more uncoupled from the deflections.

Due to the rather simple geometry of the reference building addressed in the rest of the sensitivity study, only the deformations of the remaining sections are considered.

7.2.3 Deflections along section (2)

Section (2) spans along the global y-direction of the building on the first floor according to Figure 7.1. The resulting deflections are presented in Figure 7.5.

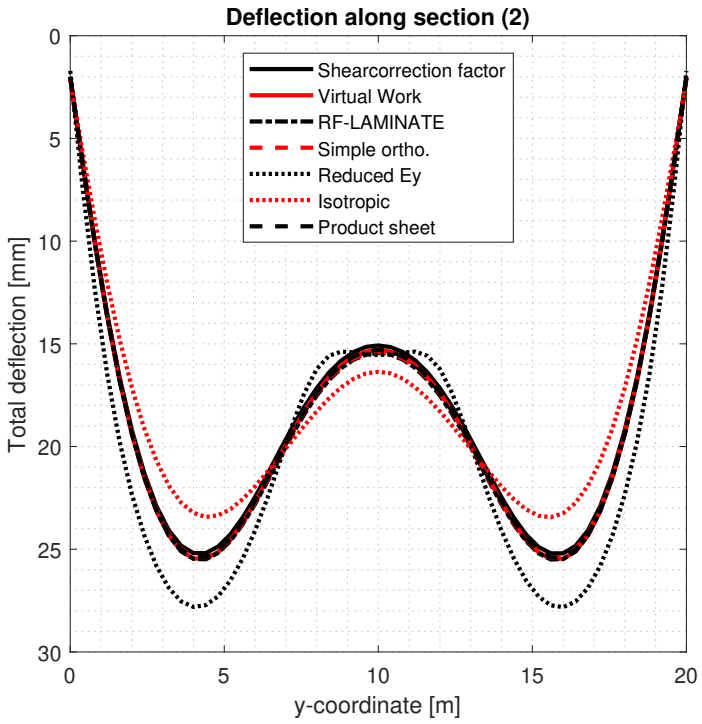

Figure 7.5: Deflection along section (2) for different modeling assumptions.

Just like the deflections along the strong direction of the slabs, the deflection in y-direction is more or less identical for the majority of the modeling assumptions. The deviating curves are the isotropic plate and the plate with reduced E_y, where the isotropic plate has a more pronounced two-way action while the slab with reduced E_y acts more like a one-way slab. When the plate works like a two-way slab, the deformations are more even across the weak direction of the slab. The local variations in deflection due to weaker or stiffer supports becomes less significant since load is efficiently transferred in both directions. The one-way slab to the contrary, is very sensitive to local variation in support stiffness and will deflect significantly more where the supports are weaker than where the supports are more stiff. In this case, the supports of the slab are more stiff in the center of the y-direction, since the beam in this area has the same dimensions but spans a shorter distance.

7.2.4 Horizontal deformations

Section (3) spans vertically along the core of the reference building in its z-direction. The section is 10 floors and 32 m. The horizontal deformations for wind in the x-direction are presented in Figure 7.6 and the horizontal deformations for wind in the y-direction in Figure 7.7.

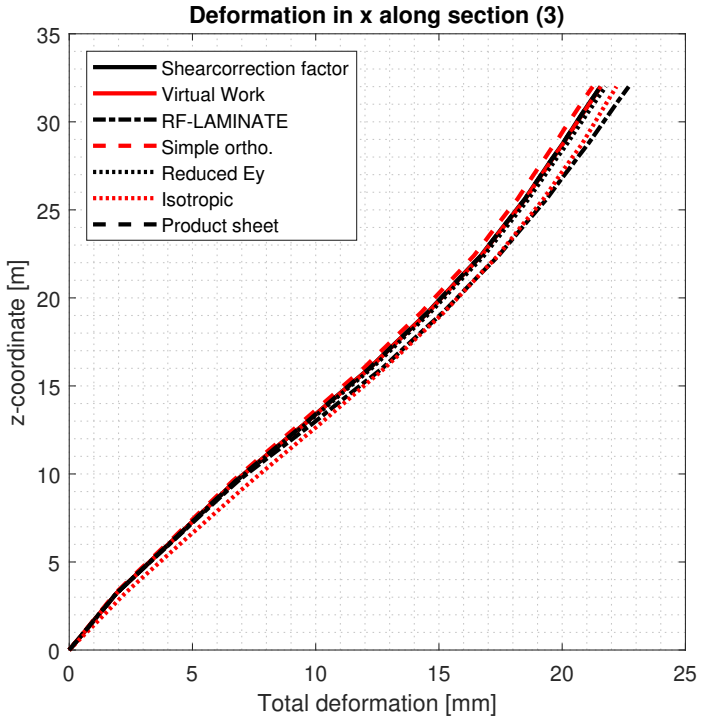

Figure 7.6: Deformation along section (3) in x-direction for different modeling assumptions.

Wind-load in the x-direction of the reference building is resisted mainly by the glulam truss bracing, but the CLT core is also providing slight stability in the x-direction.

The difference in deformation for the modeling assumptions is relatively small as can be seen in Figure 7.6. The *RF-LAMINATE* model has the largest deformation while the simplified orthotropic model has the smallest, but the difference is only approximately 2 mm.

If the deformations in Figure 7.6 are compared to the small scale study deformations seen in Figure 5.15, some differences can be observed. The most notable difference is that most of the modeling assumptions had identical deformations in the small scale study, while the deformations vary slightly in the sensitivity study. The small difference can be a consequence of the more advanced model, where several effects and geometry interact. Diaphragm action could for example vary between the modeling assumptions, meaning that different amounts of load is transferred to the core

and thus resulting in different deformations along section (3). Another reason is the small difference in in-plane shear stiffness G_{xy} for several of the modeling assumptions.

The horizontal deformations in y-direction along section (3) is presented in Figure 7.7.

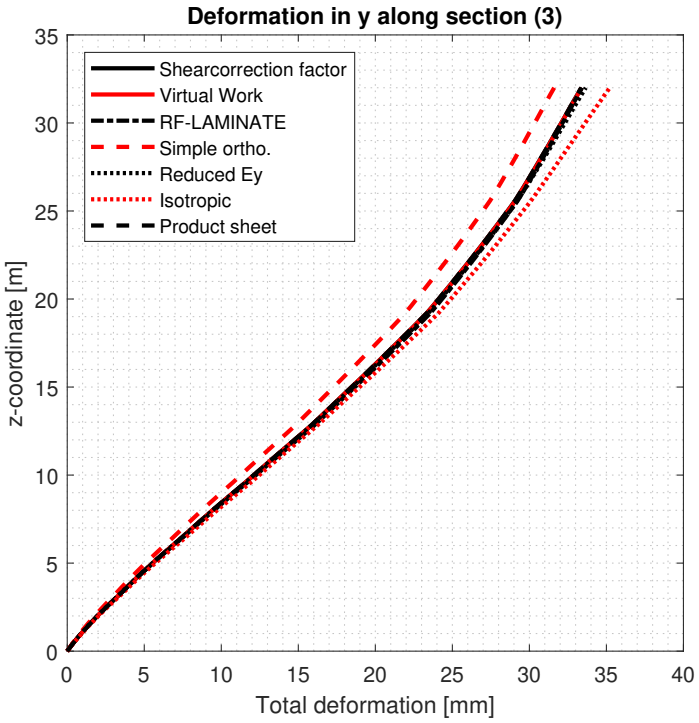

Figure 7.7: Deformation along section (3) in y-direction for different modeling assumptions.

Wind-load in the y-direction of the reference building is resisted exclusively by CLT shear wall elements, either in the facade or in the core. The effect of the CLT modeling assumptions will therefore be greater compared to when wind load is acting in the x-direction.

The difference in deformation in Figure 7.7 is greater than in Figure 7.6, as is expected, but the difference is still relatively small with a maximum of 4 mm. An interesting phenomena is that the largest deformation when the wind acts in the global x-direction (Figure 7.6) and the largest deformation when the wind acts in global y-direction (Figure 7.7) derives from different modeling assumptions. In Figure 7.7 where the horizontal loads are taken by shear walls, the largest deformation is for the isotropic model while it is the *RF-LAMINATE* model that has the largest deformations when the wind load is taken mainly by the glulam truss in Figure 7.6.

One reason for the difference could be that the diaphragm stiffness varies depending on which direction the wind load is applied. Since the floor elements are modeled with bending stiffnesses, they don't have correctly modeled membrane stiffnesses

when modeled as orthotropic plates, resulting in a larger disparity between the in-plane stiffness in x and y-direction. This disparity affects how the load is transferred through the floor and it could be a reason for why the isotropic model yields larger deformations when wind load is applied in the y-direction.

The simple orthotropic modeling assumption has the lowest horizontal deformation. This is due to its high in-plane shear stiffness of 690 MPa, where the other modeling assumptions have an in-plane shear stiffness of 590 MPa for the wall panels.

7.3 Membrane shear reduction study - Results

The horizontal deformation for wind in the y-direction using different membrane shear reduction factors k_{88} is presented in Figure 7.8. The reduction factors are only applied on the wall elements.

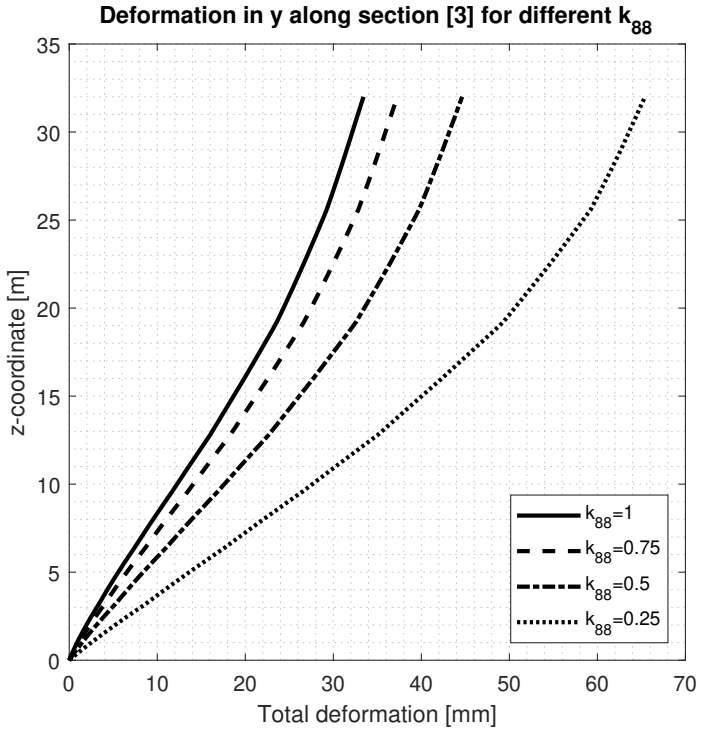

Figure 7.8: Deformation along section (3) in y-direction for different reduction factors k_{88}.

The resulting deformation for different reduction factors closely reassemble the results from the small scale study in section 5.4.2. This can be expected since the loading conditions are similar, where in the reference building the wind loads in y-direction are taken entirely by shear wall elements. The reduction factor is affecting all stabilising wall elements in both the small scale study and in the sensitivity study, but since the reduction factor is not applied to the slabs in the sensitivity study the diaphragm action is not affected. If the reduction factor would be applied

to the slabs as well, the similarities between the small scale study and the sensitivity study might become smaller.

The influence of the reduction factor is substantial for the horizontal deformations. The fact that the recommendations for the reduction factor k_{88} are so widely spread, is an indicator of uncertainties which may lead to over or underestimations of the stiffness. In a design situation, the assumption $k_{88} = 0.25$ could be very much on the safe side while the assumption $k_{88} = 0.75$ could be on the unsafe side based on the spread of the results, but due to the limited amount of research done in the field no certain conclusions can be drawn. The older German standards use the reduction factor $k_{88} = 0.25$ since it is conservative, and it was also established at a time when even less research had been done regarding the topic. Newer research (Silly, 2010) suggests a higher and less conservative reduction factor, but it is still uncertain of how it should be applied in contrast to the older factor, and the need for standardisation is evident.

7.4 Verifying the results using hand calculations

The load paths of the reference building are compared for the hand calculations and the FE-analysis comparing the maximum stresses, forces or deformations within individual members in the model. The members used for comparison are the same ones as used in design of the structure, as seen in Table 6.1. The stresses from the FE-model are calculated using the maximum moment and/or section force for a member. The stiffness of the structure is verified by comparing deflections at different points of the structure, such as in a beam on the first floor or horizontal deformation in the top of the core.

As seen in Table 7.2, the hand calculations and the FE-model correlates reasonably well, and all values are within the maximum allowed values for the structure considering both SLS and ULS. However, it can be seen that the hand calculations are generally more conservative than the FE calculations. The comparison is carried out using *Orthotropic plate - Product sheet* in both slabs and walls.

Table 7.2: Comparison between hand calculations and FE analysis (*Product sheet*) together with limiting values.

Structural part	Results hand calc.	Results FEM	Max allowed value
Slab def. (SLS)	13.7 mm	10.0 mm	16.7 mm
Slab stress (ULS)	5.81 MPa	4.97 MPa	17.7 MPa
Beam (8 m span) def.	20.1 mm	18.3 mm	26.7 mm
Beam (8 m span) stress	15.4 MPa	11.9 MPa	19.2 MPa
Column normal force	1200 kN	1050 kN	2370 kN
Wall compression	167 kN/m	142.0 kN/m	907 kN/m
Global horizontal deformation	43.3 mm	33.4 mm	64 mm

A difference that can be observed in Table 7.2 is for example the amount of load transferred to the column, where the hand calculations yield a larger design load

than the FE-analysis. This depends on the difference in stiffness between the wall elements and the columns. In contrast to the FE-analysis, the stiffness of the members is not considered when distributing the load in the hand calculations. While the hand calculations assume an even split of the load, the FE-analysis considers that the columns has a lower stiffness than the walls and thus less load is transferred to the columns.

Comparing the designing loads in the walls is more challenging, since the load distribution is affected by the window openings and the material characteristics of the panels. In the hand calculation, all loads are distributed on the efficient length of the wall, that is, the length of the wall that does not have any window openings. In the FE-analysis, the load is able to be distributed on a larger part of the wall, since the load can partly spread around the openings and utilize the stiffness of the wall in both directions.

8

Conclusion

The aims and objectives of this thesis are stated in the introduction, where one of the main objectives was to develop a number of recommendations regarding modeling choices and assumptions for CLT in FE-analysis.

Although CLT modeling in FE-analysis is a broad topic, several conclusions can be drawn from the sensitivity study. These conclusions are presented in two different ways, where the first part addresses recommendations which can be made on the basis of the study of this thesis, while the second part summarizes the areas of the subject where further research remains in order to reach reliable recommendations.

8.1 Recommendations for modeling CLT

A general conclusion and framing of question that is always relevant when using FE-analysis is what the model should be used for. Whether the model is used for verification or design determines for example the level of detail that is appropriate when modeling the stiffnesses. In an earlier design situation, rougher estimates for the stiffness could be used, which may be inappropriate in a situation where a structure is to be analysed in detail. The purpose of the model should always be considered and in many cases it is a partly determining factor regarding the modeling choices. For some types of structures, it is important to consider if the model is to be used for assessing the structure in ULS or SLS, as these two cases might require different types of models. However, in the reference building of this thesis most elements are simply supported, which causes the maximum moments and deflections to be obtained from the same conditions and thus the same model can be used for both limiting states. For the remainder of this chapter, more material specific effects to consider when constructing an FE model of a CLT structure are addressed rather than loading conditions.

8.1.1 Defining CLT surfaces

Two main methods of defining a CLT surface have been discussed and evaluated in this thesis. The first method is to define a surface by its orthotropic stiffnesses and the other method is to define the stiffness matrix by using the plugin *RF-LAMINATE*. The stiffness matrix can also be directly defined into the FE-software without the use of a plugin, but that option has not been explored in this thesis.

The script in Appendix B.1 provides the output D which is the stiffness matrix of the analysed element, if such an option were to be analysed.

The main conclusion and recommendation is that to obtain the most precise results, surfaces should preferably be defined using stiffness-matrixes, in which case both the bending and membrane stiffness matrix elements are correctly represented. *RF-LAMINATE* provides this option, but with plenty of hidden reduction factors and corrections that could be a problem if they are not noticed or if they are unknown. If the user is comfortable in *RF-LAMINATE*, it is a powerful tool for analysing CLT slabs.

Several of the modeling assumptions has been analysed when defined with stiffnesses to varying results. In general, defining a surface using stiffnesses is also a sufficiently good option, as long as the distinction between bending stiffness and membrane stiffness is clear and that the surface is modeled with the correct stiffnesses regarding bending or in-plane loads. This could however have small disadvantages in a case where an element is loaded in a way that it is not designed for. A slab could for example be loaded in its plane by diaphragm action, and in that case its in-plane stiffness is not correctly defined, but this difference should in general be small.

8.1.2 Out-of-plane shear stiffness

Modeling assumptions regarding out-of-plane shear stiffness has been investigated relatively thoroughly in this thesis, as it is the main difference for many of the modeling assumptions. The out-of-plane shear stiffnesses are defined by similar methods regardless if the surface is defined through stiffnesses or through a stiffness matrix, meaning that the differences for the out-of-plane shear stiffness assumptions applies regardless of how the surface is modeled.

Determining which modeling assumption is most advantageous regarding the out-of-plane shear stiffness is difficult since there is no reference to what is correct in neither the small scale studies nor in the sensitivity study, only mutual comparison between the models is possible. The differences in results between the modeling assumptions could be compared, where the modeling assumptions without larger deviations are deemed better. In that case, the modeling assumptions *Virtual work*, *Product sheet* and *RF-LAMINATE* are deemed more suitable. There is however no guarantee that this conclusion is correct due to the lack of a correct reference.

8.1.3 Reduction factors

The influence of the reduction factor k_{88} has in this thesis been studied, and its impact on horizontal deflections has been deemed considerable. This makes a distinct recommendation difficult since the various factors gives very different results, and there is currently no standardization regarding these reduction factors. The most conservative approach is to assign $k_{88} = 0.25$, which should always be on the safe side. Another option is to run an analysis for both $k_{88} = 0.25$ and $k_{88} = 0.75$, and then observe the difference and based on the results make an educated decision of

which reduction factor to use. As previously stated, the need for standardization is evident and especially regarding the reduction factors.

When the application of reduction factors are more evident, such as reduction factors considering that the narrow sides of the boards are not glued or the shear deformation of the element, it is essential that caution is given to where the factors are applied. How the factors should be applied is fully dependent on the FE software and a fundamental understanding is crucial for applying the reduction factors correctly. Two things to be particularly observant of is if a reduction factor of 5/6 is applied to orthotropic surfaces, and if assumptions regarding the in-plane shear stiffness G_{xy} are made by the software.

8.2 Further work

This thesis started out with a very broad approach, and with the intention to investigate which subjects would be of interest with respect to the results of a FE-analysis for a timber building. As a not very surprising realisation, the interesting topics turned out to be more numerous and extensive than what could be fitted in to a master's thesis. This chapter aims to summarize and present topics related to the thesis which has been excluded due to the time limitation, with the hope and objective that further investigations can be carried out in future projects.

8.2.1 Verification of small scale studies with experiments

To be able to determine which of the modeling choices yields the best approximation of the behaviour of CLT elements, the results from the small scale study would need to be compared with experimental results. These results may consist either of newly conducted experiments or by experiments from earlier investigations that contains results which are suitable for the comparison with the elements of the small scale study. The small scale studies could for example be re-calibrated to represent an already existing four-point bending test for a CLT-slab, in which case verification of the different modeling assumptions is possible.

8.2.2 Slip between CLT elements

The slip within connections, for example between CLT elements, is a highly interesting subject considering the investigations and conclusions which has been made in this report. It can be questioned how large the effect of the material deformations are in relation to the deformation of the structure due to slip in the connections, and if the effect of the material parameters are relatively small, it might be suitable to adjust the level of detail when modeling the material accordingly.

Slip occurs to some extent in all connections. In the reference building of this project, it would be of particular interest to investigate the effect on the horizontal deformations due to slip orthogonal to the direction of the connections in the shear walls. Furthermore, the slip in the fasteners that restraints uplift of the structure from the concrete foundation would be of interest. The modeling of the core is one

of the possible weak point of the reference design, since it does not take the slip into account. The stiffness of the core is overestimated when the four CLT walls are fully restraint from moving in relation to one another. Slip may also affect the diaphragm action of the CLT slabs.

8.2.3 Effective stiffness of CLT

To take into account the limited moment resistance in the connections between the CLT slab elements, the stiffness E_y can be reduced. The small scale study in section 5.6 supports the theory that a reduction of stiffness orthogonal to the hinges yields a result closer to the actual situation. This is also common practice in other fields of the industry, such as when hollow core concrete slabs are designed. How much the stiffness is to be reduced for different geometries and materials is an interesting topic for future research.

Another effect that needs to be studied regarding the reduction of stiffness in the weak direction of the slab is how load is transferred around openings of slabs. A low stiffness in the weak direction of the slab contributes to a one way action of the elements, which is not compatible with openings in the slabs. It could be interesting to investigate how the openings in slabs affect the choice of modeling assumptions for CLT.

8.2.4 Reduction factor k_{33}

Similarly as for the reduction factor k_{88}, multiple recommendations exist without standardization. The influence from the reduction factor k_{88} was deemed large in both the small scale study and in the sensitivity study, but the influence of the reduction factor k_{33} is not studied in this thesis, although different recommendations are stated in section 4.1.2.1. The reduction factor k_{33} is more or less relevant in different situations, and it could be interesting to identify in which situations it is influential and how influential it is. One example is the unexpected behavior of the slabs in the small scale study, where the factor k_{33} is one of the parts contributing to that the two-way slabs generally have larger deflections than the one-way slabs.

8.2.5 Continuous slabs

In a real design, the floor slabs are probably designed as continuous over at least one beam support due to the more favourable deflections. The reference building only used simply supported slabs due to their simplicity for comparison purposes. If continuous slabs are used, other interesting phenomena to investigate could arise.

8.2.6 Material non-linearity

Even though the linear-elastic material model is usually a suitable model for timber, more complex material models can be used to more accurately represent the response of timber and CLT. A linear-elastic model with a brittle failure could for example be used for tension, while a different elasticity modulus could be used for

compression. Hardening and softening could also be included in the material model. The magnitude of the differences between the modeling assumptions in the studies could be different if a non-linear material model is used, where plastic deformation and stress-redistribution influences the results.

8.2.7 Core

Due to the limited time frame for this project, the core has not been thoroughly investigated even though this was the initial intention. The behaviour of the core is highly dependent on the interaction between the four core walls and effects such as for example slip, since this determines if the core acts as four separate shear walls or more like a box girder with full interaction between the walls of the core. After having constructed a reasonable model for interaction between the elements, it could be of interest to investigate how the modeling assumptions addressed in this project affects the stabilizing properties of the core and how the load distribution within the structure is affected by different stiffness assumptions.

8.3 Concluding remarks

The literature study, calculations and FE analyses that have been performed in this thesis has given a plethora of results and conclusions. Many conclusions and recommendations can be rather useful for a practicing engineer, especially in projects with a relatively simple geometry, while some of the conclusions could be deemed to have a more narrow application.

The most important observation, and also the reason for why this thesis exists at all, is that CLT design and FE application for timber structures lacks standardization. Both of these areas are currently being heavily developed, and the standardization for both CLT design and FE analysis of timber structures might soon catch up with the explosive demand for CLT construction. In the future, CLT construction with the aid of FE analysis will hopefully be implemented in the Eurocode, so that use of the sustainable and high-performing material CLT is encouraged, and available to as many designing engineers as possible.

Bibliography

Abrahamsen, R. B., & Malo, K. A. (2014). *STRUCTURAL DESIGN AND ASSEMBLY OF "TREET"-A 14-STOREY TIMBER RESIDENTIAL BUILDING IN NORWAY* (tech. rep.). www.swecogroup.com

Al-Emrani, M. (2019). Eurokodfamiljen för stål utökas. *Tidningen Stålbyggnad*, (2). https://www.stalbyggnad.se/konstruktion/eurokodfamiljen-for-stal-utokas/

Aondio, P., Glaser, P., & Kreuzinger, H. (2020). FE calculation of glued cross laminated timber – part 1: Theory. *Bauingenieur*, *95*(1), 22–25.

Asselstine, J., Lam, F., & Zhang, C. (2021). New edge connection technology for cross laminated timber (CLT) floor slabs promoting two-way action. *Engineering Structures*, *233*, 111777. https://doi.org/10.1016/j.engstruct.2020.111777

Bezabeh, M. A., Bitsuamlak, G. T., Popovski, M., & Tesfamariam, S. (2020). Dynamic Response of Tall Mass-Timber Buildings to Wind Excitation. *Journal of Structural Engineering*, *146*(10), 04020199. https://doi.org/10.1061/(asce)st.1943-541x.0002746

Boverket. (2019). *Boverkets konstruktionsregler EKS 11*. www.boverket.se/publikationer

Crocetti, R., Kliger, R., Johansson, M., & Mårtensson, A. (2016). *Design of timber structures Volume 1, Structural aspects of timber construction* (E. Borgström, Ed.; 2:2016). Swedish Wood. https://www.swedishwood.com/publications/list_of_swedish_woods_publications/design-of-timber-structures/

D'Arenzo, G., Casagrande, D., Reynolds, T., & Fossetti, M. (2019). In-plane elastic flexibility of cross laminated timber floor diaphragms. *Construction and Building Materials*, *209*, 709–724. https://doi.org/10.1016/j.conbuildmat.2019.03.060

DIN. (2008). *DIN 1052: Entwurf, Berechnung und Bemessung von Holzbauwerken - Allgemeine Bemessungsregeln und Bemessungsregeln für den Hochbau*. Deutsches Institut für Normung DIN.

Dlubal Software GmbH. (2016). RF-LAMINATE: Design of Laminate Surfaces. https://www.dlubal.com/-/media/Files/website/documents/manuals/rfem-and-rstab-add-on-modules/others/rf-laminate/rf-laminate-manual-en.pdf?mlid=A1793038DDBA4F60A129F84FD9B33209

Edskär, I. (2018). *Modal Analysis, Dynamic Properties and Horizontal Stabilisation of Timber Buildings* (Doctoral dissertation). Luleå University of Technology. Luleå. www.ltu.se

Fitzgerald, D., Sinha, A., Miller, T. H., & Nairn, J. A. (2021). Axial slip-friction connections for cross-laminated timber. *Engineering Structures*, *228*, 111478. https://doi.org/10.1016/j.engstruct.2020.111478

Gustafsson, A., Crocetti, R., Just, A., Landel, P., Olsson, J., Pousette, A., Silfverhielm, M., & Östman, B. (2019). *The CLT Handbook* (E. Borgström & J. Fröbel, Eds.). Swedish Wood.

Johansson, M. (2016). Chapter 2 Structural properties of sawn timber and engineered wood products. In E. Borgström (Ed.), *Design of timber structures volume 1, structural aspects of timber construction* (2:2016, pp. 28–66). Swedish Wood.

Larsson, F., & Runesson, K. (2014). *INTRODUCTION TO FINITE ELEMENT ANALYSIS OF PLATES*. (n.p).

Liu, G. R., & Quek, S. S. (2013). *The Finite Element Method: A Practical Course: Second Edition*. Elsevier Ltd. https://doi.org/10.1016/C2012-0-00779-X

Lukacs, I., Björnfot, A., & Tomasi, R. (2019). Strength and stiffness of cross-laminated timber (CLT) shear walls: State-of-the-art of analytical approaches. *Engineering Structures*, *178*, 136–147. https://doi.org/10.1016/j.engstruct.2018.05.126

Martinsons. (2019). KL-trä Konstruktionsfakta. https://martinsons.se/byggnader-i-tra/limtra-och-kl-tra-for-byggnadsobjekt/kl-tra/konstruktionsfakta/

Mohammad, M., Ni, C., & Munoz, W. (2019). Chapter 5 Connections in cross-laminated timber buildings. In E. Karacabeyli & S. Gagnon (Eds.), *Canadian cross laminated timber handbook: 2019 edition*. FPInnovations.

Ottosen, N. S., & Petersson, H. (1992). *Introduction to the finite element method*. Prentice-Hall.

Pacoste, C., Plos, M., & Johansson, M. (2012). *Recommendations for finite element analysis for the design of reinforced concrete slabs* (tech. rep.). Stockholm.

Popovski, M., Gagnon, S., Mohammad, M., & Chen, Z. (2019). *Canadian Cross Laminated Timber Handbook: 2019 Edition* (E. Karacabeyli & S. Gagnon, Eds.). FPInnovations.

Silly, G. (2010). *Numerische Studien zur Drill-und Schubsteifigkeit von Brettsperrholz (BSP)* (tech. rep.). Institut für Holzbau und Holztechnologie, Technische Universität Graz. Graz.

SIS. (2010). *SS-EN 1990: Eurocode - Basis of structural design*. Swedish Standards Institute SIS.

Voulpiotis, K., Köhler, J., Jockwer, R., & Frangi, A. (2021). A holistic framework for designing for structural robustness in tall timber buildings. *Engineering Structures*, *227*, 111432. https://doi.org/10.1016/j.engstruct.2020.111432

Wallner-Novak, M., Koppelhuber, J., & Pock, K. (2014). *Cross-Laminated Timber Structural Design*. proHolz Austria. www.proholz.at

A

Calculations

A.1 Design calculations

A.1.1 Beam

8 meter beam in one span

Geometry:

$l := 8\ m$

$b := 0.215\ m$ *Beam geometry*

$h := 0.54\ m$

$t_{CLT} := 0.14\ m$ *Approx. CLT thickness*

$l_{CLT} := 5\ m$ *Loading width*

Material & factors:

GL30c:

$\rho := 475\ \frac{kg}{m^3}$

$f_{mk} := 30\ MPa$

$E_{005} := 10.8\ GPa$

$E_{mean} := 13\ GPa$

$k_{mod} := 0.8$ *Service class 1, medium load duration*

$\gamma_M := 1.25$

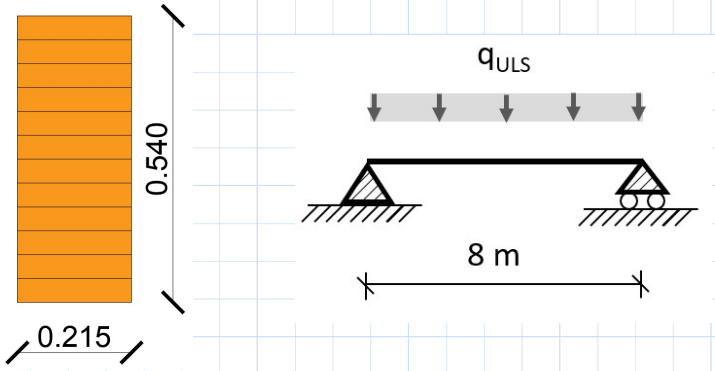

Loads:

$q_{imp\_m2} := 2\ \frac{kN}{m^2}$ *Imposed load (area load)*

$q_{self} := b \cdot h \cdot \rho \cdot g = 0.541\ \frac{kN}{m}$ *Self weight from beam*

$q_{CLT} := l_{CLT} \cdot t_{CLT} \cdot \rho \cdot g = 3.261\ \frac{kN}{m}$ *Self weight from CLT-plate (line load)*

$q_{imp} := q_{imp\_m2} \cdot l_{CLT} = 10\ \frac{kN}{m}$ *Imposed load (line load)*

$q_{ULS} := 1.35 \cdot (q_{self} + q_{CLT}) + 1.5 \cdot q_{imp} = 20.132\ \frac{kN}{m}$

$q_{SLS} := 1.0 \cdot (q_{self} + q_{CLT}) + 1.0 \cdot q_{imp} = 13.802\ \frac{kN}{m}$

Design moment:

$M_{Ed} := \frac{q_{ULS} \cdot l^2}{8} = 161.056\ kN \cdot m$ *Design moment*

Capacity: (GL30c)

$f_{md} := k_{mod} \cdot \frac{f_{mk}}{\gamma_M} = 19.2\ MPa$ *Design capacity of timber when loaded in bending*

$W := \frac{b \cdot h^2}{6} = 0.01\ m^3$

$M_{Rd} := f_{md} \cdot W = 200.621\ kN \cdot m$ *Moment recistance of beam*

$I := \frac{b \cdot h^3}{12} = \left(2.821 \cdot 10^9\right)\ mm^4$

$\sigma_{top} := \frac{M_{Ed}}{I} \cdot \frac{h}{2} = 15.414\ MPa$ *Stress in utmost fiber of beam, caused ULS-load case*

Lateral stability

$E_{005} = 10.8\ GPa$

$\sigma_{m\_crit} := \frac{0.78 \cdot b^2}{h \cdot l} \cdot E_{005} = 90.139\ MPa$

$\lambda_{rel} := \sqrt{\frac{f_{mk}}{\sigma_{m\_crit}}} = 0.577$ < 1 ok!

Deflections:

$E_{mean} = 13\ GPa$

$k_{def} := 0.6$ Service class 1

$w_{inst\_G} := \frac{5 \cdot \left(q_{self} + q_{CLT}\right) \cdot l^4}{384 \cdot E_{mean} \cdot \frac{b \cdot h^3}{12}} = 5.528\ mm$

$\psi_0 := 0.3$
$\psi_{2\_imp} := 0.3$
$\psi_{2\_wind} := 0$

$w_{fin\_G} := w_{inst\_G} \cdot \left(1 + k_{def}\right) = 8.845\ mm$

$w_{inst\_imp} := \frac{5 \cdot q_{imp} \cdot l^4}{384 \cdot E_{mean} \cdot \frac{b \cdot h^3}{12}} = 14.542\ mm$

$w_{inst} := w_{inst\_G} + w_{inst\_imp} = 20.07\ mm$

$w_{fin\_imp} := w_{inst\_imp} \cdot \left(1 + \psi_{2\_imp} \cdot k_{def}\right) = 17.159\ mm$

$w_{fin} := w_{fin\_G} + w_{fin\_imp} = 26.004\ mm$

Allowed values for deflections:

$\frac{l}{300} = 26.667\ mm$ > $w_{inst} = 20.07\ mm$ > $\frac{l}{500} = 16\ mm$

$\frac{l}{150} = 53.333\ mm$ > $w_{fin} = 26.004\ mm$ < $\frac{l}{300} = 26.667\ mm$

Both the instant and the final deflections are ok!

Shear:

$V_{Ed} := \frac{q_{ULS}}{2} \cdot l = 80.528\ kN$

$f_{vk} := 3.5\ MPa$

$f_{vd} := k_{mod} \cdot \frac{f_{vk}}{\gamma_M} = 2.24\ MPa$

$k_{cr} := min\left(\frac{3\ MPa}{f_{vk}}, 1\right) = 0.857$

$b_{eff} := k_{cr} \cdot b = 0.184\ m$

$V_{Rd} := \frac{b_{eff} \cdot h \cdot f_{vd}}{1.5} = 148.608\ kN$ Ok!

A.1.2 CLT slab

Design of slab (span 5 m)

Martinsons 140-5s

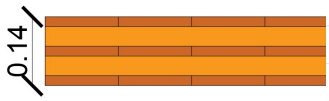

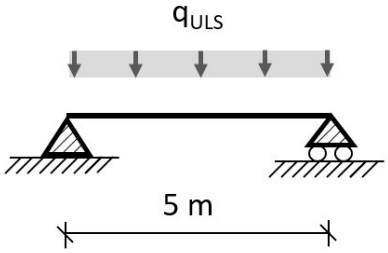

Geometry:

$t_1 := 20\ mm$ $\quad b := 1\ m$

$t_2 := 40\ mm$

$t_3 := 20\ mm$ $\quad \rho := 475\ \frac{kg}{m^3}$

$t_4 := 40\ mm$

$t_5 := 20\ mm$ $\quad h := t_1 + t_2 + t_3 + t_4 + t_5 = 0.14\ m$

Calculating effective cross section (Gamma method):

$E_0 := 11.6\ GPa$ $\quad G_{9090} := 50\ MPa$ $\quad l_{ref} := 5\ m$

$$\gamma_1 := \frac{1}{1 + \frac{\pi^2 \cdot E_0 \cdot t_1}{l_{ref}^2} \cdot \frac{t_2}{G_{9090}}} = 0.932$$

$\gamma_3 := 1$

$$\gamma_5 := \frac{1}{1 + \frac{\pi^2 \cdot E_0 \cdot t_5}{l_{ref}^2} \cdot \frac{t_4}{G_{9090}}} = 0.932$$

$$a_1 := \frac{t_1}{2} + t_2 + \frac{t_3}{2} = 60\ mm$$

$a_5 := a_1 = 60\ mm$

$$I_{x\_ef} := \frac{b \cdot t_1^3}{12} + \gamma_1 \cdot b \cdot t_1 \cdot a_1^2 + \frac{b \cdot t_3^3}{12} + \frac{b \cdot t_5^3}{12} + \gamma_5 \cdot b \cdot t_5 \cdot a_5^2 = \left(1.362 \cdot 10^8\right)\ mm^4$$

$$W_{x\_ef} := \frac{I_{x\_ef}}{0.5 \cdot h} = \left(1.945 \cdot 10^6\right)\ mm^3$$

Calculating net cross section

$$I_{x\_net} := \frac{b \cdot t_3^3}{12} + \frac{b \cdot t_1^3}{12} + b \cdot t_1 \cdot \left(\frac{t_1}{2} + t_2 + \frac{t_3}{2}\right)^2 + \frac{b \cdot t_5^3}{12} + b \cdot t_5 \cdot \left(\frac{t_5}{2} + t_4 + \frac{t_3}{2}\right)^2 = \left(1.46 \cdot 10^8\right)\ mm^4$$

$$W_{x\_net} := \frac{I_{x\_net}}{0.5 \cdot h} = \left(2.086 \cdot 10^6\right)\ mm^3$$

Design load

$q_{imp} := 2 \ \frac{kN}{m}$

$q_{self} := h \cdot \rho \cdot g \cdot b = 0.652 \ \frac{kN}{m}$

$q_{ULS} := 1.35 \cdot q_{self} + 1.5 \cdot q_{imp} = 3.88 \ \frac{kN}{m}$ $q_{SLS} := 1.0 \cdot q_{self} + 1.0 \cdot q_{imp} = 2.652 \ \frac{kN}{m}$

$l_{span} := 5 \ m$

$M_{Ed} := \frac{q_{ULS} \cdot l_{span}^{2}}{8} = 12.126 \ kN \cdot m$

$\sigma_{myd} := \frac{M_{Ed}}{W_{x\_net}} = 5.814 \ MPa$

Capacity

$f_{mk} := 24 \ MPa$

$k_{mod} := 0.8$

$\gamma_M := 1.25$

$k_{sys} := 1.15$

$f_{md} := k_{sys} \cdot k_{mod} \cdot \frac{f_{mk}}{\gamma_M} = 17.664 \ MPa$

$\sigma_{myd} = 5.814 \ MPa$ < $f_{md} = 17.664 \ MPa$

Deflections:

$w_{inst} := \frac{5 \cdot q_{SLS} \cdot l_{ref}^{4}}{384 \cdot E_0 \cdot I_{x\_ef}} = 13.664 \ mm$ Max allowed deflection: $\frac{l_{ref}}{300} = 16.667 \ mm$

$k_{def} := 0.6$

$w_{creep} := k_{def} \cdot w_{inst} = 8.198 \ mm$

$w_{fin} := w_{inst} + w_{creep} = 21.862 \ mm$ Max allowed deflection: $\frac{l_{ref}}{150} = 33.333 \ mm$

A.1.3 CLT wall

Walls in combined compression and bending

Martinsons 100-5s

Geometry:

$t_{slab} := 140\ mm$
$t_{wall} := 100\ mm$
$h_{wall} := 3.2\ m$

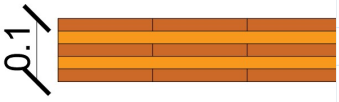

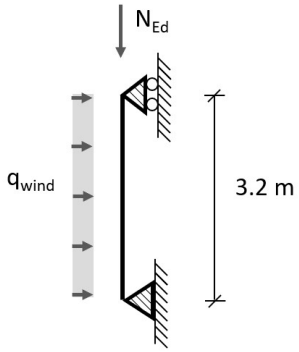

Loads:

$l_{span} := 2.5\ m$ *Width of the loading transferred to the wall from the slab*

$b := 1\ m$

$\rho := 475\ \frac{kg}{m^3}$

$q_{imp} := 2\ \frac{kN}{m^2} \cdot l_{span} = 5\ \frac{kN}{m}$

$q_{slab} := \rho \cdot g \cdot l_{span} \cdot t_{slab} = 1.63\ \frac{kN}{m}$

$q_{self} := \rho \cdot h_{wall} \cdot g \cdot t_{wall} = 1.491\ \frac{kN}{m}$

$q_{ULS} := 10 \cdot 1.35 \cdot \left(q_{slab} + q_{self}\right) + 10 \cdot 1.5 \cdot q_{imp} = 117.133\ \frac{kN}{m}$

$q_{wind} := 0.88\ \frac{kN}{m^2}$ $q_{wind\_ULS} := q_{wind} \cdot 1.5 \cdot 0.3 \cdot b = 0.396\ \frac{kN}{m}$

Material characteristics:

$f_{mk} := 24\ MPa$

$f_{c0k} := 21\ MPa$

$\gamma_M := 1.25$

$k_{mod} := 0.9$

$f_{md} := k_{mod} \cdot \frac{f_{mk}}{\gamma_M} = 17.28\ MPa$

$f_{c0d} := k_{mod} \cdot \frac{f_{c0k}}{\gamma_M} = 15.12\ MPa$

Cross section constants:

$t_1 := 20\ mm$ $t_2 := 20\ mm$ $t_3 := t_1$ $t_4 := t_2$ $t_5 := t_1$

$t_{wall} := t_1 + t_2 + t_3 + t_4 + t_5 = 100\ mm$

$z_s := \frac{t_{wall}}{2} = 50\ mm$

$A_{x\_net} := b \cdot (t_1 + t_3 + t_5) = (6 \cdot 10^4)\ mm^2$

$I_{x\_net} := b \cdot \left(\frac{{t_1}^3}{12} + t_1 \cdot \left(\frac{t_1}{2} + t_2 + \frac{t_3}{2} \right)^2 + \frac{{t_3}^3}{12} + \frac{{t_5}^3}{12} + t_5 \cdot \left(\frac{t_5}{2} + t_4 + \frac{t_3}{2} \right)^2 \right) = (6.6 \cdot 10^7)\ mm^4$

$W_{x\_net} := \frac{I_{x\_net}}{z_s} = (1.32 \cdot 10^6)\ mm^3$

Gamma method inertia (I_ef)

$E_0 := 11\ GPa$ $G_{9090} := 50\ MPa$ $E_{005} := 7.4\ GPa$

$\gamma_1 := \frac{1}{1 + \frac{\pi^2 \cdot E_0 \cdot t_1}{{h_{wall}}^2} \cdot \frac{t_2}{G_{9090}}} = 0.922$

$\gamma_3 := 1$

$\gamma_5 := \frac{1}{1 + \frac{\pi^2 \cdot E_0 \cdot t_5}{{h_{wall}}^2} \cdot \frac{t_4}{G_{9090}}} = 0.922$

$I_{x\_ef} := b \cdot \left(\frac{{t_1}^3}{12} + \gamma_1 \cdot t_1 \cdot \left(\frac{t_1}{2} + t_2 + \frac{t_3}{2} \right)^2 + \frac{{t_3}^3}{12} + \frac{{t_5}^3}{12} + \gamma_5 \cdot t_5 \cdot \left(\frac{t_5}{2} + t_4 + \frac{t_3}{2} \right)^2 \right) = (6.1 \cdot 10^7)\ mm^4$

Check buckling:

$i_{x\_ef} := \sqrt{\frac{I_{x\_ef}}{A_{x\_net}}} = 31.884\ mm$

$\lambda_y := \frac{h_{wall}}{i_{x\_ef}} = 100.363$

$\lambda_{rel\_y} := \frac{\lambda_y}{\pi} \cdot \sqrt{\frac{f_{c0k}}{E_{005}}} = 1.702$

$$k_y := 0.5 \cdot \left(1 + 0.1 \cdot \left(\lambda_{rel\_y} - 0.3\right) + \lambda_{rel\_y}^{\ 2}\right) = 2.018$$

$$k_{c\_y} := \frac{1}{k_y + \sqrt{k_y^{\ 2} - \lambda_{rel\_y}^{\ 2}}} = 0.322$$

Concider 30 % window area:

$b_0 := 20\ m$ $\qquad$ $b_{ef} := b_0 - 0.3 \cdot b_0 = 14\ m$

$$f_b := \frac{b_0}{b_{ef}} = 1.429$$

Check capacities:

$$N_d := b \cdot f_b \cdot q_{ULS} = 167.333\ kN$$

$$M_d := \frac{q_{wind\_ULS} \cdot h_{wall}^{\ 2}}{8} = 0.507\ kN \cdot m$$

$$\frac{N_d}{k_{c\_y} \cdot A_{x\_net} \cdot f_{c0d}} + \frac{M_d}{W_{x\_net} \cdot f_{md}} = 0.595$$

Utilization ratio of 60 %
Ok!

Horizontal deformation of shear wall caused by wind pressure:

Input data:

Assumes wind pressure for upper part of the building over the whole wall (conservative assumption)

$q_{wind} := 1.6 \ \frac{kN}{m^2}$

$h := 32 \ m$
$t := 100 \ mm$
$b_{ef} := 14 \ m$
$d := 24 \ m$

$G_{mean} := 590 \ MPa$ *(from Product sheet)*
$E_{x\_mean} := 6.6 \ GPa$ *(from Product sheet)*

Horizontal load:

$F_d := q_{wind} \cdot h \cdot \frac{d}{2} = 614.4 \ kN$

Shear deformation:

$\delta_{shear} := F_d \cdot \frac{h}{b_{ef} \cdot t \cdot G_{mean}} = 23.802 \ mm$

Geometry:

$t_{ef} := 60 \ mm$ $b_1 := 3 \ m$ $b_2 := 4 \ m$ $b_{window} := 2 \ m$

Inertia of wall element:

$$I_{net} := 2 \cdot \frac{t \cdot {b_1}^3}{12} + 2 \cdot \frac{t \cdot {b_2}^3}{12} + 2 \cdot b_1 \cdot t \cdot \left(b_{window} \cdot 1.5 + b_2 + \frac{b_1}{2} \right)^2 + 2 \cdot b_2 \cdot t \cdot \left(\frac{b_{window}}{2} + \frac{b_2}{2} \right)^2 = 52.067 \ m^4$$

Bending deformation of shear wall:

$\delta_{bend} := F_d \cdot \frac{h^3}{3 \cdot E_{x\_mean} \cdot I_{net}} = 19.529 \ mm$

Total deformation:

$\delta_{shear} + \delta_{bend} = 43.331 \ mm$

Maximum deflection:

$\frac{h}{500} = 64 \ mm$ Ok!

A.1.4 Column

Column

Indata:

CLT:

$t := 0.140\ m$

$\rho := 475\ \frac{kg}{m^3}$

Column:

$b := 0.405\ m$

$h := 0.380\ m$

$l := 3.2\ m$

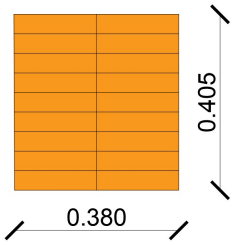

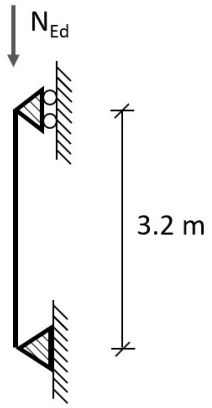

Loads:

$A_{load} := 5\ m \cdot 6\ m = 30\ m^2$

$n := 10$ *Number of floors*

$q_{imp} := 2\ \frac{kN}{m^2}$

$N_{imp} := q_{imp} \cdot n \cdot A_{load} = 600\ kN$

$q_{CLT\_m2} := t \cdot \rho \cdot g = 0.652\ \frac{kN}{m^2}$

$N_{CLT} := q_{CLT\_m2} \cdot n \cdot A_{load} = 195.643\ kN$

$N_{1floor} := b \cdot h \cdot l \cdot \rho \cdot g = 2.294\ kN$

$N_{column} := n \cdot N_{1floor} = 22.941\ kN$

$N_{Ed} := 1.35 \cdot \left(N_{CLT} + N_{column}\right) + 1.5 \cdot N_{imp} = \left(1.195 \cdot 10^3\right)\ kN$

Capacity:

$f_{c0k} := 24.5\ MPa$

$E_{005} := 10.8\ GPa$

$I := \frac{b \cdot h^3}{12} = 0.002\ m^4$

$A := b \cdot h = 0.154\ m^2$

$i := \sqrt{\frac{I}{A}} = 0.11\ m$

$\lambda := \frac{l}{i} = 29.171$

$\lambda_{rel} := \frac{\lambda}{\pi} \cdot \sqrt{\frac{f_{c0k}}{E_{005}}} = 0.442$

$\beta_c := 0.1$

$k := 0.5 \cdot \left(1 + \beta_c \cdot \left(\lambda_{rel} - 0.3\right) + {\lambda_{rel}}^2\right) = 0.605$

$k_c := \frac{1}{k + \sqrt{k^2 - {\lambda_{rel}}^2}} = 0.983$

$k_{mod} := 0.8$ $\gamma_M := 1.25$

$f_{c0d} := k_{mod} \cdot \frac{f_{c0k}}{\gamma_M} = 15.68\ \textbf{\textit{MPa}}$

$N_{Rd} := f_{c0d} \cdot A \cdot k_c = \left(2.371 \cdot 10^3\right)\ \textbf{\textit{kN}}$ $N_{Ed} = \left(1.195 \cdot 10^3\right)\ \textbf{\textit{kN}}$

$\eta := \frac{N_{Ed}}{N_{Rd}} = 0.504$ ok!

A.1.5 Wind loads

Wind loads:

Calculation according to: SS-EN 1991-1-4

Geometry:

$h := 30\ m$

$b := 24\ m$

$d := 20\ m$

Reference velocity:

$v_b := 25\ \frac{m}{s}$

$q_b := \frac{{v_b}^2}{2} \cdot 1.25\ \frac{kg}{m^3} = 0.391\ \frac{kN}{m^2}$

$k_r := 0.19$ Assume terrain category II

$z_{min} := 2\ m$

$z_0 := 0.05\ m$

$c_e(z) := \left(k_r \cdot \ln\left(\frac{z}{z_0}\right)\right)^2 \cdot \left(1 + \frac{7}{\ln\left(\frac{z}{z_0}\right)}\right)$

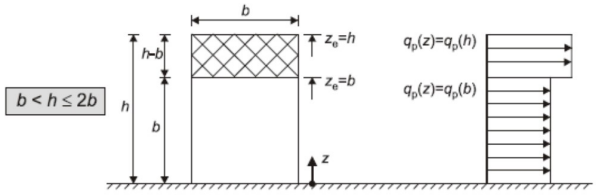

$q_p(z) := c_e(z) \cdot q_b$

$q_{p20m} := q_p(20\ m) = 1.098\ \frac{kN}{m^2}$ Wind pressure at the height 20 m

$q_{p30m} := q_p(30\ m) = 1.208\ \frac{kN}{m^2}$ Wind pressure at the height 30 m

$\frac{h}{d} = 1.5$

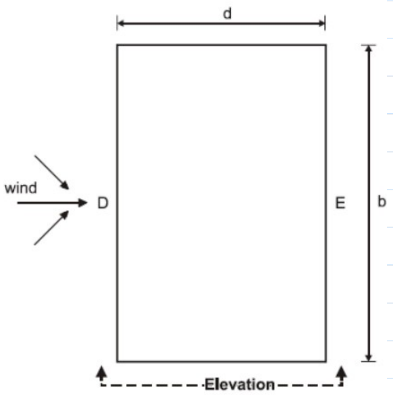

$$c_{pe\_10D} := 0.8$$

$$c_{pe\_10E} := \frac{-0.7-(-0.5)}{5-1}\cdot 0.5+(-0.5) = -0.525$$

$$w_{eD20} := q_{p20m}\cdot c_{pe\_10D} = 0.878\ \frac{kN}{m^2}$$

$$w_{eD30} := q_{p30m}\cdot c_{pe\_10D} = 0.967\ \frac{kN}{m^2}$$

$$w_{eE20} := q_{p20m}\cdot c_{pe\_10E} = -0.576\ \frac{kN}{m^2}$$

$$w_{eE30} := q_{p30m}\cdot c_{pe\_10E} = -0.634\ \frac{kN}{m^2}$$

A.2 Stiffness calculations

A.2.1 Equivalent stiffness using virtual work

Virtual Work 140-5s

indata:

$t := [20 \;\; 40 \;\; 20 \;\; 40 \;\; 20]\ mm$ $\qquad$ $b := 1\ m$

$$t := \begin{bmatrix} 20 \\ 40 \\ 20 \\ 40 \\ 20 \end{bmatrix} mm \qquad E_{xx} := \begin{bmatrix} 11 \\ 0.23 \\ 11 \\ 0.23 \\ 11 \end{bmatrix} GPa \qquad E_{yy} := \begin{bmatrix} 0.37 \\ 7 \\ 0.37 \\ 7 \\ 0.37 \end{bmatrix} GPa$$

$$G_{xz} := \begin{bmatrix} 690 \\ 50 \\ 690 \\ 50 \\ 690 \end{bmatrix} MPa \qquad G_{yz} := \begin{bmatrix} 50 \\ 690 \\ 50 \\ 690 \\ 50 \end{bmatrix} MPa \qquad G_{xy} := \begin{bmatrix} 690 \\ 440 \\ 690 \\ 440 \\ 690 \end{bmatrix} MPa$$

Calculations:

$$z_{gross} := \frac{\sum t}{2} = 0.07\ m$$

$$t_{cs} := \begin{bmatrix} \sum_{i=0}^{0} t(i) \\ \sum_{i=0}^{1} t(i) \\ \sum_{i=0}^{2} t(i) \\ \sum_{i=0}^{3} t(i) \\ \sum_{i=0}^{4} t(i) \end{bmatrix} = \begin{bmatrix} 0.02 \\ 0.06 \\ 0.08 \\ 0.12 \\ 0.14 \end{bmatrix} m$$ Cumulative sum of t

$$z := t_{cs} - \frac{t}{2} = \begin{bmatrix} 0.01 \\ 0.04 \\ 0.07 \\ 0.1 \\ 0.13 \end{bmatrix} m$$ Center of gravity of each layer (from top)

$$I := \frac{b \cdot t^3}{12} + b \cdot t \cdot \overrightarrow{\left(z_{gross} - z\right)^2} = \begin{bmatrix} 7.267 \cdot 10^{-5} \\ 4.133 \cdot 10^{-5} \\ 6.667 \cdot 10^{-7} \\ 4.133 \cdot 10^{-5} \\ 7.267 \cdot 10^{-5} \end{bmatrix} m^4$$

Inertia of each layer

$$B_{xi} := \overrightarrow{E_{xx} \cdot t \cdot \left(z - z_{gross}\right)^2} + \frac{\overrightarrow{E_{xx} \cdot t^3}}{12} = \begin{bmatrix} 7.993 \cdot 10^5 \\ 9.507 \cdot 10^3 \\ 7.333 \cdot 10^3 \\ 9.507 \cdot 10^3 \\ 7.993 \cdot 10^5 \end{bmatrix} J$$

$$B_x := \sum B_{xi} = \left(1.625 \cdot 10^6\right) J$$

Stiffness matrix element for bending in x-direction

$$B_{yi} := \overrightarrow{E_{yy} \cdot t \cdot \left(z - z_{gross}\right)^2} + \frac{\overrightarrow{E_{yy} \cdot t^3}}{12} = \begin{bmatrix} 2.689 \cdot 10^4 \\ 2.893 \cdot 10^5 \\ 246.667 \\ 2.893 \cdot 10^5 \\ 2.689 \cdot 10^4 \end{bmatrix} J$$

$$B_y := \sum B_{yi} = \left(6.327 \cdot 10^5\right) J$$

Stiffness matrix element for bending in y-direction

$$B_{xy} := \sum \left(\overrightarrow{2 \cdot G_{xy} \cdot t \cdot \left(z - z_{gross}\right)^2} + \frac{\overrightarrow{G_{xy} \cdot t^3}}{6} \right) = \left(2.742 \cdot 10^5\right) J$$

Stiffness matrix element for torsion

$$D_x := \sum \left(\overrightarrow{E_{xx} \cdot t}\right) = \left(6.784 \cdot 10^8\right) \frac{kg}{s^2}$$

Stiffness matrix element for membrane action in x-direction

$$D_y := \sum \left(\overrightarrow{E_{yy} \cdot t}\right) = \left(5.822 \cdot 10^8\right) \frac{kg}{s^2}$$

Stiffness matrix element for membrane action in y-direction

$$D_{xy} := \sum \left(\overrightarrow{G_{xy} \cdot t}\right) = \left(7.66 \cdot 10^7\right) \frac{kg}{s^2}$$

Stiffness matrix element for in plane shear

$$EI_x := \sum \overrightarrow{E_{xx} \cdot t \cdot \left(z - z_{gross}\right)^2} = \left(1.601 \cdot 10^6\right)\ \boldsymbol{J}$$ Flexural rigidity in x

$$c_{xz} := \frac{1}{EI_x} \begin{bmatrix} \sum_{i=0}^{0} \left(E_{xx}(i) \cdot t(i) \cdot \left(z(i) - z_{gross}\right)\right) \\ \sum_{i=0}^{1} \left(E_{xx}(i) \cdot t(i) \cdot \left(z(i) - z_{gross}\right)\right) \\ \sum_{i=0}^{2} \left(E_{xx}(i) \cdot t(i) \cdot \left(z(i) - z_{gross}\right)\right) \\ \sum_{i=0}^{3} \left(E_{xx}(i) \cdot t(i) \cdot \left(z(i) - z_{gross}\right)\right) \\ \sum_{i=0}^{4} \left(E_{xx}(i) \cdot t(i) \cdot \left(z(i) - z_{gross}\right)\right) \end{bmatrix} = \begin{bmatrix} -8.247 \\ -8.42 \\ -8.42 \\ -8.247 \\ 1.164 \cdot 10^{-15} \end{bmatrix} \frac{1}{\boldsymbol{m}}$$ c-constant

$$S_{xz\_inv} := \sum_{i=1}^{4} \frac{t(i)}{3 \cdot G_{xz}(i)} \cdot \left(c_{xz}(i-1)^2 + c_{xz}(i-1) \cdot c_{xz}(i) + c_{xz}(i)^2\right) = \left(1.138 \cdot 10^{-7}\right) \frac{\boldsymbol{s}^2}{\boldsymbol{kg}}$$

$$S_{xz} := \frac{1}{S_{xz\_inv}} = \left(8.785 \cdot 10^6\right) \frac{\boldsymbol{kg}}{\boldsymbol{s}^2}$$ Shear stiffness in xz

$$EI_y := \sum \overrightarrow{E_{yy} \cdot t \cdot \left(z - z_{gross}\right)^2} = \left(5.573 \cdot 10^5\right)\ \boldsymbol{J}$$ Flexural rigidity in y

$$c_{yz} := \frac{1}{EI_y} \begin{bmatrix} \sum_{i=0}^{0} \left(E_{yy}(i) \cdot t(i) \cdot \left(z(i) - z_{gross}\right)\right) \\ \sum_{i=0}^{1} \left(E_{yy}(i) \cdot t(i) \cdot \left(z(i) - z_{gross}\right)\right) \\ \sum_{i=0}^{2} \left(E_{yy}(i) \cdot t(i) \cdot \left(z(i) - z_{gross}\right)\right) \\ \sum_{i=0}^{3} \left(E_{yy}(i) \cdot t(i) \cdot \left(z(i) - z_{gross}\right)\right) \\ \sum_{i=0}^{4} \left(E_{yy}(i) \cdot t(i) \cdot \left(z(i) - z_{gross}\right)\right) \end{bmatrix} = \begin{bmatrix} -0.797 \\ -15.87 \\ -15.87 \\ -0.797 \\ -2.089 \cdot 10^{-16} \end{bmatrix} \frac{1}{\boldsymbol{m}}$$ c-constant

$$S_{yz\_inv} := \sum_{i=1}^{4} \frac{t(i)}{3 \cdot G_{yz}(i)} \cdot \left(c_{yz}(i-1)^2 + c_{yz}(i-1) \cdot c_{yz}(i) + c_{yz}(i)^2\right) = \left(1.111 \cdot 10^{-7}\right) \frac{\boldsymbol{s}^2}{\boldsymbol{kg}}$$

$$S_{yz} := \frac{1}{S_{yz\_inv}} = \left(9.003 \cdot 10^6\right) \frac{\boldsymbol{kg}}{\boldsymbol{s}^2}$$ Shear stiffness in yz

Input parameters for orthotropic shell in RFEM:

$$E_{x\_eq} := \frac{12 \cdot B_x}{\left(\sum t\right)^3} = 7.106 \ \textit{GPa}$$

$$E_{y\_eq} := \frac{12 \cdot B_y}{\left(\sum t\right)^3} = 2.767 \ \textit{GPa}$$

$$G_{xz\_eq} := \frac{6}{5} \cdot \frac{S_{xz}}{\sum t} = 75.302 \ \textit{MPa}$$

$$G_{yz\_eq} := \frac{6}{5} \cdot \frac{S_{yz}}{\sum t} = 77.169 \ \textit{MPa}$$

$$G_{xy\_eq} := \frac{D_{xy}}{\sum t} = 547.143 \ \textit{MPa}$$

A.2.2 Equivalent stiffness using shear correction factor

Shear correction factor 140-5s

Input data:

$t := [20 \;\; 40 \;\; 20 \;\; 40 \;\; 20]\ mm$ $\qquad$ $b := 1\ m$

$$t := \begin{bmatrix} 20 \\ 40 \\ 20 \\ 40 \\ 20 \end{bmatrix} mm \qquad E_{xx} := \begin{bmatrix} 11 \\ 0.23 \\ 11 \\ 0.23 \\ 11 \end{bmatrix} GPa \qquad E_{yy} := \begin{bmatrix} 0.37 \\ 7 \\ 0.37 \\ 7 \\ 0.37 \end{bmatrix} GPa$$

$$G_{xz} := \begin{bmatrix} 690 \\ 50 \\ 690 \\ 50 \\ 690 \end{bmatrix} MPa \qquad G_{yz} := \begin{bmatrix} 50 \\ 690 \\ 50 \\ 690 \\ 50 \end{bmatrix} MPa \qquad G_{xy} := \begin{bmatrix} 690 \\ 440 \\ 690 \\ 440 \\ 690 \end{bmatrix} MPa$$

Shear reduction factor:

$\kappa := 0.24$

Caluclations:

$$z_{gross} := \frac{\sum t}{2} = 0.07\ m$$

$$t_{cs} := \begin{bmatrix} \sum_{i=0}^{0} t(i) \\ \sum_{i=0}^{1} t(i) \\ \sum_{i=0}^{2} t(i) \\ \sum_{i=0}^{3} t(i) \\ \sum_{i=0}^{4} t(i) \end{bmatrix} = \begin{bmatrix} 0.02 \\ 0.06 \\ 0.08 \\ 0.12 \\ 0.14 \end{bmatrix} m$$

Cumulative sum of t

$$z := t_{cs} - \frac{t}{2} = \begin{bmatrix} 0.01 \\ 0.04 \\ 0.07 \\ 0.1 \\ 0.13 \end{bmatrix} m$$

Center of gravity of each layer (from top)

$$I := \frac{b \cdot t^3}{12} + b \cdot t \cdot \overrightarrow{\left(z_{gross} - z\right)^2} = \begin{bmatrix} 7.267 \cdot 10^{-5} \\ 4.133 \cdot 10^{-5} \\ 6.667 \cdot 10^{-7} \\ 4.133 \cdot 10^{-5} \\ 7.267 \cdot 10^{-5} \end{bmatrix} m^4$$ Inertia of each layer

Input parameters for orthotropic shell in RFEM:

$$E_{x\_eq} := \frac{\sum \left(\overrightarrow{E_{xx} \cdot I}\right)}{\sum I} = 7.106 \ GPa$$

$$E_{y\_eq} := \frac{\sum \left(\overrightarrow{E_{yy} \cdot I}\right)}{\sum I} = 2.767 \ GPa$$

$$G_{xz\_eq} := \frac{6}{5} \cdot \kappa \ \frac{\sum \left(\overrightarrow{G_{xz} \cdot t}\right)}{\sum t} = 93.394 \ MPa$$

$$G_{yz\_eq} := \frac{6}{5} \cdot \kappa \ \frac{\sum \left(\overrightarrow{G_{yz} \cdot t}\right)}{\sum t} = 119.726 \ MPa$$

$$G_{xy\_eq} := \frac{\sum \left(\overrightarrow{G_{xy} \cdot t}\right)}{\sum t} = 547.143 \ MPa$$

B

MATLAB Code

B.1 Equivalent stiffness using virtual work

```
function [Ex_eq,Ey_eq,Gxy_eq,Gyz_eq,Gxz_eq,D] =
   CLT_plate_VW(t,Exx,Eyy,Gxy,Gxz,Gyz,glue)
% Script calculating the eq. orthotropic stiffnesses of a
    CLT plate
% based on the paper "FE-Berechnung von geklebtem
   Brettspe" by Aondio
% (2020). Indata should be but in in an alternating way
   like the example
% below.

% Example of indata
% t = [21 21 21 21 21 21 21]*1e-3;
% Exx = [11 0.37 11 0.37 11 0.37 11]*1e9;
% Eyy = [0.37 11 0.37 11 0.37 11 0.37]*1e9;
% Gxz = [690 69 690 69 690 69 690]*1e6;
% Gyz = [69 690 69 690 69 690 69]*1e6;
% Gxy = [690 690 690 690 690 690 690]*1e6;


% Main program

% Reduction factors regarding if glue on narrow side is
   considered or not.
if glue == 1
    Bxy_glue = 1;
    Dxy_glue = 1;
end
if glue == 0
    Bxy_glue = 0;
    Dxy_glue = 1/4;
end

% Gross centre of gravity
```

```
z_gross = sum(t)/2;

% Distances from top
cumsum_t = cumsum(t);

%Centres and inertias of each layer
for i=1:length(t)
z(i) = cumsum_t(i)-t(i)/2;
I(i) = 1*t(i)^3/12 + 1*t(i)*(z_gross-z(i))^2;
end

%Bending stiffness elements in x and y
Bxi = Exx.*t.*(z-z_gross).^2+Exx.*t.^3./12;
Bx = sum(Bxi);

Byi = Eyy.*t.*(z-z_gross).^2+Eyy.*t.^3./12;
By = sum(Byi);

% Torsional bending stiffness
Bxyi = 2*Gxy.*t.*(z-z_gross).^2+Gxy.*t.^3./6;
Bxy = Bxy_glue*sum(Bxyi);

% Membrane stiffnesses in x and y
Dxi = Exx.*t;
Dx = sum(Dxi);

Dyi = Eyy.*t;
Dy = sum(Dyi);

% Membrane shear stiffness
Dxyi = Gxy.*t;
Dxy = Dxy_glue*sum(Dxyi);

%--Calculations for out-of-plane shear stiffnesses--

% Flexural rigidity in x
EIx_B_i = Exx.*t.*(z-z_gross).^2;
EIx_B = sum(EIx_B_i);

% c-constant in xz-plane
cxz_i = (1/EIx_B).*cumsum(Exx.*t.*(z-z_gross));

% Assemble shear stiffness in x
inv_Sxz = zeros(length(t),1)';
for i = 2:length(t)
```

```
    inv_Sxz(i) = t(i)./(3*Gxz(i)).*(cxz_i(i-1).^2 + cxz_i
       (i-1)*cxz_i(i) + cxz_i(i)^2);
end

Sxz = 1/sum(inv_Sxz);

% Flexural rigidity in y
EIy_B_i = Eyy.*t.*(z-z_gross).^2;
EIy_B = sum(EIy_B_i);

% c-constant in yz-plane
cyz_i = (1/EIy_B).*cumsum(Eyy.*t.*(z-z_gross));

% Assemble shear stiffness in y
inv_Syz = zeros(length(t),1)';
for i = 2:length(t)
    inv_Syz(i) = t(i)./(3*Gyz(i)).*(cyz_i(i-1).^2 + cyz_i
       (i-1)*cyz_i(i) + cyz_i(i)^2);
end

Syz = 1/sum(inv_Syz);


%Convert stiffness matix parameters to orthotropic
   stiffnesses.
Ex_eq = 12*Bx/(sum(t)^3);
Ey_eq = 12*By/(sum(t)^3);

Gxz_eq = (6/5)*Sxz./sum(t);%Add 6/5 to consider the shear
    reduction in RFEM
Gyz_eq = (6/5)*Syz./sum(t);%Add 6/5 to consider the shear
    reduction in RFEM
Gxy_eq = Dxy/sum(t);

D = diag([Bx By Bxy Sxz Syz Dx Dy Dxy])

end
```

B.2 Equivalent stiffness using approximate shear correction factor

```
function [Ex_eq,Ey_eq,Gxy_eq,Gyz_eq,Gxz_eq] =
   CLT_plate_shearcorr(t,Exx,Eyy,Gxy,Gxz,Gyz,glue)
% Script calculating the eq. orthotropic stiffness of a
   CLT-plate
% using an approximative shear correction factor.
% The shear correction factors are taken from Wallner-
   Novak (2014),
% where approximations are used.

% Example of indata
% t = [21 21 21 21 21 21 21]*1e-3;
% Exx = [11 0.37 11 0.37 11 0.37 11]*1e9;
% Eyy = [0.37 11 0.37 11 0.37 11 0.37]*1e9;
% Gxz = [690 69 690 69 690 69 690]*1e6;
% Gyz = [69 690 69 690 69 690 69]*1e6;
% Gxy = [690 690 690 690 690 690 690]*1e6;

n = length(t);

%Shear correction factor is dependant on number of layers
   .
switch n
    case 1
        kappa = 0.83;
    case 3
        kappa = 0.21;
    case 5
        kappa = 0.24;
    case 7
        kappa = 0.26;
    case 9
        kappa = 0.27;
end


%Reduction factors
if glue == 1
    Dxy_glue = 1;
end
if glue == 0
    Dxy_glue = 1/4;
end
```

```
%Cross section centers and inertias
z_gross = sum(t)/2;
cumsum_t = cumsum(t);

for i=1:length(t)
z(i) = cumsum_t(i)-t(i)/2;
I(i) = 1*t(i)^3/12 + 1*t(i)*(z_gross-z(i))^2;
end


%Calculate RFEM input parameters
Ex_eq = sum(Exx.*I)/sum(I);
Ey_eq = sum(Eyy.*I)/sum(I);
Gxz_eq = (6/5).*kappa.*sum(t.*Gxz)./sum(t);
Gyz_eq = (6/5).*kappa.*sum(t.*Gyz)./sum(t);
Gxy_eq = Dxy_glue.*sum(Gxy.*t)/sum(t);


end
```

C

RFEM - Printout report

Erik Johansson
Lindholmsallen 25, 41753 Gothenburg

STRUCTURAL ANALYSIS

PROJECT

Sensitivity study of reference building

CLIENT

-

CREATED BY

Caroline Johansson
Erik Johansson

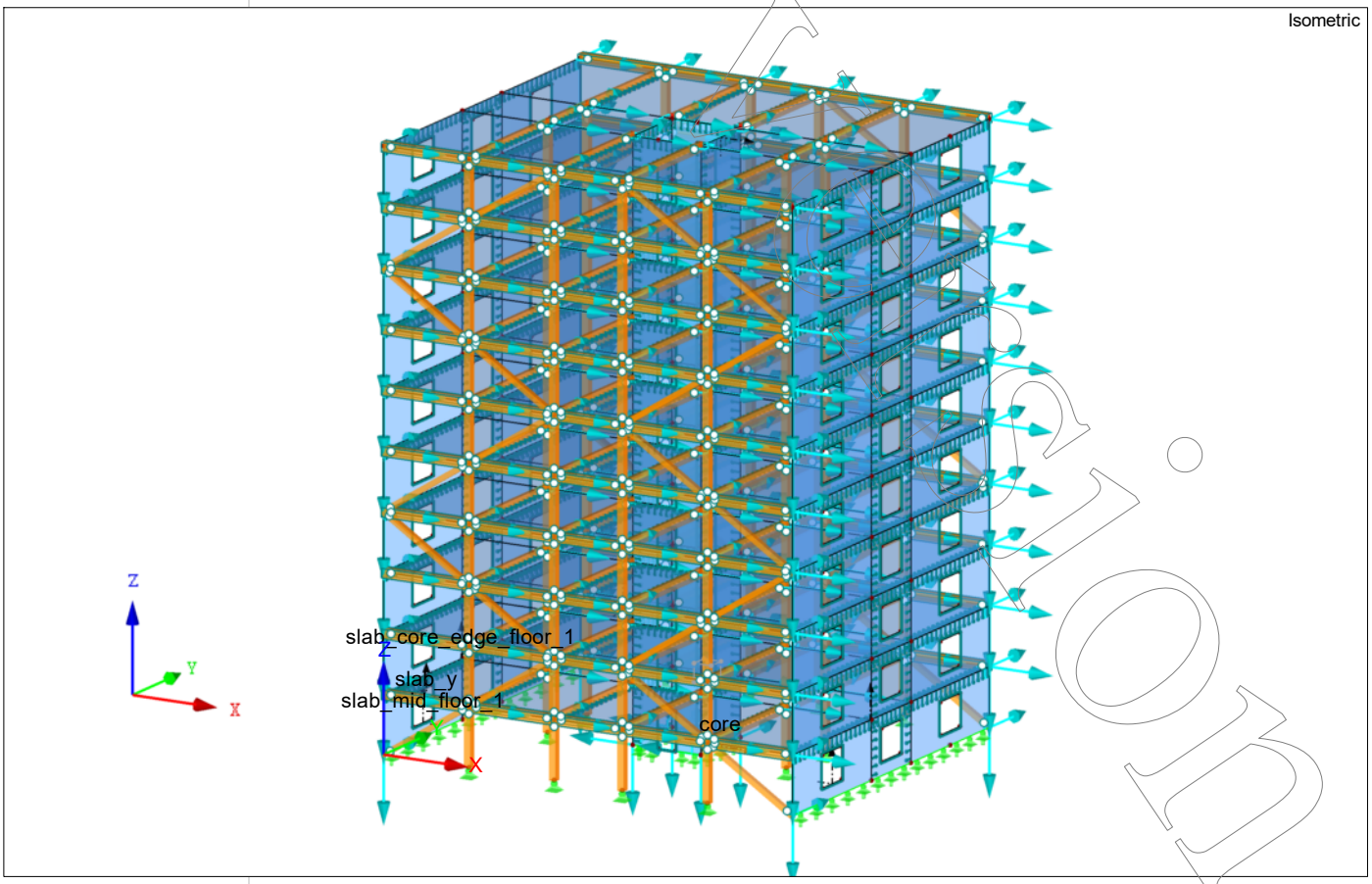

Project: Sensitivity study | Model: reference_model_testing1 | Date: 2021-05-03

MODEL - GENERAL DATA

General	Model name	:	reference_model_testing1	
	Project name	:	Sensitivity study	
	Type of model	:	3D	
	Positive direction of global axis Z	:	Upward	
	Classification of load cases and combinations	:	According to Standard: EN 1990 + EN 1995 (Wood) National Annex: SS - Sweden	
Options	☐ RF-FORM-FINDING - Find initial equilibrium shapes of membrane and cable structures			
	☐ RF-CUTTING-PATTERN			
	☐ Piping analysis			
	☐ Use CQC Rule			
	☐ Enable CAD/BIM model			
	Standard Gravity			
	g	:	10.00 m/s²	

FE MESH SETTINGS

General	Target length of finite elements	l_{FE}	:	0.400 m
	Maximum distance between a node and a line to integrate it into the line	ε	:	0.001 m
	Maximum number of mesh nodes (in thousands)		:	500
Members	Number of divisions of members with cable, elastic foundation, taper, or plastic characteristic		:	10
	☒ Activate member divisions for large deformation or post-critical analysis			
	☒ Use division for members with node lying on them			
Surfaces	Maximum ratio of FE rectangle diagonals	Δ_D	:	1.800
	Maximum out-of-plane inclination of two finite elements	α	:	0.50 °
	Shape direction of finite elements		:	Triangles and quadrangles ☒ Same squares where possible

1.3 MATERIALS

Matl. No.	Modulus E [GPa]	Modulus G [GPa]	Poisson's Ratio ν [-]	Spec. Weight γ [kN/m³]	Coeff. of Th. Exp. α [1/°C]	Partial Factor γ_M [-]	Material Model
7	Virtual work (140-5s)			4.75	0.00E+00	1.00	Orthotropic Elastic 2D...
	Additional material parameters are defined in the Material Model dialog box						
8	Virtual work (100-5s)			4.75	0.00E+00	1.00	Orthotropic Elastic 2D...
	Additional material parameters are defined in the Material Model dialog box						
10	Glulam Timber GL30c | SS-EN 14080:2013-08						
	13.000	0.650	9.000	4.30	5.00E-06	1.25	Isotropic Linear Elastic
11	Shearcorr (140-5s)			4.75	0.00E+00	1.00	Orthotropic Elastic 2D...
	Additional material parameters are defined in the Material Model dialog box						
12	Shearcorr (100-5s)			4.75	0.00E+00	1.00	Orthotropic Elastic 2D...
	Additional material parameters are defined in the Material Model dialog box						
13	Product sheet (140-5s)			4.75	0.00E+00	1.00	Orthotropic Elastic 2D...
	Additional material parameters are defined in the Material Model dialog box						
14	Product sheet (100-5s)			4.75	0.00E+00	1.00	Orthotropic Elastic 2D...
	Additional material parameters are defined in the Material Model dialog box						
15	Simple ortho (140-5s)			4.75	0.00E+00	1.00	Orthotropic Elastic 2D...
	Additional material parameters are defined in the Material Model dialog box						
16	Simple ortho (100-5s)			4.75	0.00E+00	1.00	Orthotropic Elastic 2D...
	Additional material parameters are defined in the Material Model dialog box						
17	Reduced Ey (140-5s)			4.75	0.00E+00	1.00	Orthotropic Elastic 2D...
	Additional material parameters are defined in the Material Model dialog box						
18	Isotropic (140-5s)			4.75	0.00E+00	1.00	Orthotropic Elastic 2D...
	Additional material parameters are defined in the Material Model dialog box						

1.3.5 MATERIALS - MATERIAL MODEL - ORTHOTROPIC ELASTIC 2D

Matl. No.	Modulus of Elasticity [GPa] E_x	E_y	Shear Modulus [GPa] G_{yz}	G_{xz}	G_{xy}	Poisson's Ratio[-] ν_{xy}	ν_{yx}
7	Virtual work (140-5s)						
	7.106	2.767	0.077	0.075	0.547	0.000	0.000
8	Virtual work (100-5s)						
	6.692	3.022	0.055	0.092	0.590	0.000	0.000
11	Shearcorr (140-5s)						
	7.106	2.767	0.120	0.093	0.547	0.000	0.000
12	Shearcorr (100-5s)						
	6.692	3.022	0.088	0.125	0.590	0.000	0.000
13	Product sheet (140-5s)						
	7.106	2.767	0.133	0.073	0.547	0.000	0.000
14	Product sheet (100-5s)						
	6.692	3.022	0.104	0.100	0.590	0.000	0.000
15	Simple ortho (140-5s)						
	7.106	2.767	0.069	0.069	0.690	0.000	0.000
16	Simple ortho (100-5s)						
	6.692	3.022	0.069	0.069	0.690	0.000	0.000
17	Reduced Ey (140-5s)						
	7.106	0.300	0.077	0.075	0.547	0.000	0.000
18	Isotropic (140-5s)						
	7.106	7.106	0.069	0.069	0.069	0.000	0.000

1.13 CROSS-SECTIONS

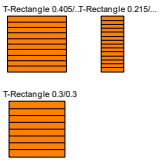

Section No.	Matl. No.	J [m⁴] A [m²]	I_y [m⁴] A_y [m²]	I_z [m⁴] A_z [m²]	Principal Axes α [°]	Rotation α' [°]	Overall Dimensions [m] Width b	Height h
1	T-Rectangle 0.405/0.38							
	10	0.003	0.002	0.002	0.00	0.00	0.405	0.380
		0.154	0.128	0.128				
2	T-Rectangle 0.215/0.54							
	10	0.001	0.003	0.000	0.00	0.00	0.215	0.540
		0.116	0.097	0.097				
3	T-Rectangle 0.3/0.3							
	10	0.001	0.001	0.001	0.00	0.00	0.300	0.300
		0.090	0.075	0.075				

2.1 LOAD CASES

Load Case	Load Case Description	Action Category	Active	Self-Weight - Factor in Direction X	Y	Z	EN 1990 + 1995 | SS Load Duration
LC1	Self-weight	Permanent	☒	0.000	0.000	-1.000	Permanent
LC2	Imposed load	Imposed - Category A: domestic, residential areas	☐				Medium-term
LC3	Wind in x	Wind	☐				Short-term
LC5	Wind in y	Wind	☐				Short-term

2.1.1 LOAD CASES - CALCULATION PARAMETERS

Load Case	Load Case Description	Calculation Parameters		
LC1	Self-weight	Method of analysis	: ⊙	Geometrically linear analysis
		Method for solving system of nonlinear algebraic equations	: ⊙	Newton-Raphson
		Activate stiffness factors of:	: ☒	Cross-sections (factor for J, I_y, I_z, A, A_y, A_z)
			: ☒	Members (factor for GJ, EI_y, EI_z, EA, GA_y, GA_z)
LC2	Imposed load	Method of analysis	: ⊙	Geometrically linear analysis
		Method for solving system of nonlinear algebraic equations	: ⊙	Newton-Raphson
		Activate stiffness factors of:	: ☒	Cross-sections (factor for J, I_y, I_z, A, A_y, A_z)
			: ☒	Members (factor for GJ, EI_y, EI_z, EA, GA_y, GA_z)
LC3	Wind in x	Method of analysis	: ⊙	Geometrically linear analysis
		Method for solving system of nonlinear algebraic equations	: ⊙	Newton-Raphson
		Activate stiffness factors of:	: ☒	Cross-sections (factor for J, I_y, I_z, A, A_y, A_z)
			: ☒	Members (factor for GJ, EI_y, EI_z, EA, GA_y, GA_z)
LC5	Wind in y	Method of analysis	: ⊙	Geometrically linear analysis
		Method for solving system of nonlinear algebraic equations	: ⊙	Newton-Raphson
		Activate stiffness factors of:	: ☒	Cross-sections (factor for J, I_y, I_z, A, A_y, A_z)
			: ☒	Members (factor for GJ, EI_y, EI_z, EA, GA_y, GA_z)

2.5 LOAD COMBINATIONS

Load Combin.	DS	Load Combination Description	No.	Factor	Load Case	
CO1		ULS wind x	1	1.10	LC1	Self-weight
			2	1.40	LC2	Imposed load
			3	0.42	LC3	Wind in x
CO2		ULS wind y	1	1.10	LC1	Self-weight
			2	1.40	LC2	Imposed load
			3	0.42	LC5	Wind in y
CO3		SLS (no wind)	1	1.00	LC1	Self-weight
			2	1.00	LC2	Imposed load
CO4		SLS (wind x)	1	1.00	LC1	Self-weight
			2	1.00	LC3	Wind in x

2.5 LOAD COMBINATIONS

Load Combin.	DS	Load Combination Description	No.	Factor	Load Case	
CO5		SLS (wind y)	1	1.00	LC1	Self-weight
			2	1.00	LC5	Wind in y

2.5.2 LOAD COMBINATIONS - CALCULATION PARAMETERS

Load Combin.	Description	Calculation Parameters	
CO1	ULS wind x	Method of analysis	: ◉ Geometrically linear analysis
		Options	: ☒ Consider favorable effects due to tension
			: ☒ Refer internal forces to deformed system for:
			☒ Normal forces N
			☒ Shear forces V_y and V_z
			☒ Moments M_y, M_z and M_T
		Activate stiffness factors of:	: ☒ Materials (partial factor γM)
			: ☒ Cross-sections (factor for J, I_y, I_z, A, A_y, A_z)
			: ☒ Members (factor for GJ, EI_y, EI_z, EA, GA_y, GA_z)
CO2	ULS wind y	Method of analysis	: ◉ Geometrically linear analysis
		Options	: ☒ Consider favorable effects due to tension
			: ☒ Refer internal forces to deformed system for:
			☒ Normal forces N
			☒ Shear forces V_y and V_z
			☒ Moments M_y, M_z and M_T
		Activate stiffness factors of:	: ☒ Materials (partial factor γM)
			: ☒ Cross-sections (factor for J, I_y, I_z, A, A_y, A_z)
			: ☒ Members (factor for GJ, EI_y, EI_z, EA, GA_y, GA_z)
CO3	SLS (no wind)	Method of analysis	: ◉ Second order analysis (P-Delta)
		Method for solving system of nonlinear algebraic equations	: ◉ Picard
		Options	: ☒ Consider favorable effects due to tension
			: ☒ Refer internal forces to deformed system for:
			☒ Normal forces N
			☒ Shear forces V_y and V_z
			☒ Moments M_y, M_z and M_T
		Activate stiffness factors of:	: ☒ Materials (partial factor γM)
			: ☒ Cross-sections (factor for J, I_y, I_z, A, A_y, A_z)
			: ☒ Members (factor for GJ, EI_y, EI_z, EA, GA_y, GA_z)
CO4	SLS (wind x)	Method of analysis	: ◉ Second order analysis (P-Delta)
		Method for solving system of nonlinear algebraic equations	: ◉ Picard
		Options	: ☒ Consider favorable effects due to tension
			: ☒ Refer internal forces to deformed system for:
			☒ Normal forces N
			☒ Shear forces V_y and V_z
			☒ Moments M_y, M_z and M_T
		Activate stiffness factors of:	: ☒ Materials (partial factor γM)
			: ☒ Cross-sections (factor for J, I_y, I_z, A, A_y, A_z)
			: ☒ Members (factor for GJ, EI_y, EI_z, EA, GA_y, GA_z)
CO5	SLS (wind y)	Method of analysis	: ◉ Second order analysis (P-Delta)
		Method for solving system of nonlinear algebraic equations	: ◉ Picard
		Options	: ☒ Consider favorable effects due to tension
			: ☒ Refer internal forces to deformed system for:
			☒ Normal forces N
			☒ Shear forces V_y and V_z
			☒ Moments M_y, M_z and M_T
		Activate stiffness factors of:	: ☒ Materials (partial factor γM)
			: ☒ Cross-sections (factor for J, I_y, I_z, A, A_y, A_z)
			: ☒ Members (factor for GJ, EI_y, EI_z, EA, GA_y, GA_z)

LC2
Imposed load

3.4 SURFACE LOADS

LC2: Imposed load

No.	On Surfaces No.	Load Type	Load Distribution	Load Direction	Load Parameters Symbol	Value	Unit
1	11-24,35-48,59-72,83-96,107-120,131-144, 155-168,179-192,203-216	Force	Uniform	ZL	p	-2.00	kN/m²

LC3
Wind in x

3.4 SURFACE LOADS

LC3: Wind in x

No.	On Surfaces No.	Load Type	Load Distribution	Load Direction	Load Parameters Symbol	Value	Unit
1	8-10,32-34,56-58,80-82,104-106,128-130	Force	Uniform	XL	p	-0.88	kN/m²
2	152-154,176-178,200-202,224-226	Force	Uniform	XL	p	-0.97	kN/m²
3	5-7,29-31,53-55,77-79,101-103,125-127	Force	Uniform	XL	p	-0.58	kN/m²
4	149-151,173-175,197-199,221-223	Force	Uniform	XL	p	-0.63	kN/m²

3.15 GENERATED LOADS

LC3: Wind in x

No.	Load Description		
1	From Area Loads on Openings		
	Area load direction	Perpendicular to the plane	: ☒ z
	Member load direction	Direction of generated member loads:	: ☒ Global in X, Y, Z
	Load distribution type:	☒ Combined	

3.15 GENERATED LOADS

LC3: Wind in x

No.	Load Description				
	Area load magnitude	☒ Constant		: -0.88	kN/m²
	Openings with area load	Openings		: 2,3,4,10,11,12,18,19, 20,26,27,28,34,35,36, 42,43,44	
	Generating total loads in direction	ΣP_{Areas}	X	: -55.314	kN
			Y	: 0.000	kN
			Z	: 0.000	kN
		ΣP_{Lines}	X	: -55.314	kN
			Y	: 0.000	kN
			Z	: 0.000	kN
	Total moment to the origin	ΣM_{Areas}	X	: 0.000	kNm
			Y	: -532.397	kNm
			Z	: 553.140	kNm
		ΣM_{Lines}	X	: 0.000	kNm
			Y	: -532.397	kNm
			Z	: 553.140	kNm
2	From Area Loads on Openings				
	Area load direction	Perpendicular to the plane		: ☒ z	
	Member load direction	Direction of generated member loads:		: ☒ Global in X, Y, Z	
	Load distribution type:	☒ Combined			
	Area load magnitude	☒ Constant		: -0.97	kN/m²
	Openings with area load	Openings		: 50,51,52,58,59,60,66, 67,68,74,75,76	
	Generating total loads in direction	ΣP_{Areas}	X	: -40.614	kN
			Y	: 0.000	kN
			Z	: 0.000	kN
		ΣP_{Lines}	X	: -40.614	kN
			Y	: 0.000	kN
			Z	: 0.000	kN
	Total moment to the origin	ΣM_{Areas}	X	: 0.000	kNm
			Y	: -1040.730	kNm
			Z	: 406.140	kNm
		ΣM_{Lines}	X	: 0.000	kNm
			Y	: -1040.730	kNm
			Z	: 406.140	kNm
3	From Area Loads on Openings				
	Area load direction	Perpendicular to the plane		: ☒ z	
	Member load direction	Direction of generated member loads:		: ☒ Global in X, Y, Z	
	Load distribution type:	☒ Combined			
	Area load magnitude	☒ Constant		: -0.58	kN/m²
	Openings with area load	Openings		: 5,6,7,13,14,15,21,22, 23,29,30,31,37,38,39, 45,46,47	
	Generating total loads in direction	ΣP_{Areas}	X	: -36.288	kN
			Y	: 0.000	kN
			Z	: 0.000	kN
		ΣP_{Lines}	X	: -36.288	kN
			Y	: 0.000	kN
			Z	: 0.000	kN
	Total moment to the origin	ΣM_{Areas}	X	: 0.000	kNm
			Y	: -349.272	kNm
			Z	: 362.880	kNm
		ΣM_{Lines}	X	: 0.000	kNm
			Y	: -349.272	kNm
			Z	: 362.880	kNm
4	From Area Loads on Openings				
	Area load direction	Perpendicular to the plane		: ☒ z	
	Member load direction	Direction of generated member loads:		: ☒ Global in X, Y, Z	
	Load distribution type:	☒ Combined			
	Area load magnitude	☒ Constant		: -0.63	kN/m²
	Openings with area load	Openings		: 53,54,55,61,62,63,69, 70,71,77,78,79	
	Generating total loads in direction	ΣP_{Areas}	X	: -26.628	kN
			Y	: 0.000	kN
			Z	: 0.000	kN
		ΣP_{Lines}	X	: -26.628	kN
			Y	: 0.000	kN
			Z	: 0.000	kN
	Total moment to the origin	ΣM_{Areas}	X	: 0.000	kNm
			Y	: -682.342	kNm
			Z	: 266.280	kNm
		ΣM_{Lines}	X	: 0.000	kNm
			Y	: -682.343	kNm
			Z	: 266.280	kNm

LC5
Wind in y

3.15 GENERATED LOADS

LC5: Wind in y

No.	Load Description				
1	From Area Loads via Plane				
	Area load direction	Global relative to the projected area:		: ☒ YP	
	Area of load application	☒ Fully closed plane			
	Load distribution type:	☒ Combined			
	Area load magnitude	☒ Constant		: 0.63	kN/m²
	Boundary of the area load plane	Corner nodes		: 898,899,503,502	
		Note		: Each row in the drop down list box denotes one plane	
	Generating total loads in direction	ΣP_{Areas}	X	: 0.000	kN
			Y	: 193.536	kN
			Z	: 0.000	kN
		$\Sigma P_{Members}$	X	: 0.000	kN
			Y	: 193.536	kN
			Z	: 0.000	kN
	Total moment to the origin	ΣM_{Areas}	X	: -4954.520	kNm
			Y	: 0.000	kNm
			Z	: 2322.430	kNm
		$\Sigma M_{Members}$	X	: -4954.520	kNm
			Y	: 0.000	kNm
			Z	: 2322.430	kNm
	Cells selected for generating	Σ number of cells		: 13	
		Σ cell area		: 307.200	m²
	Convert loads to members No.			: 137-140,159-162, 181-184,203-206, 427-430,437-440	
2	From Area Loads via Plane				
	Area load direction	Global relative to the projected area:		: ☒ YP	
	Area of load application	☒ Fully closed plane			
	Load distribution type:	☒ Combined			
	Area load magnitude	☒ Constant		: 0.58	kN/m²
	Boundary of the area load plane	Corner nodes		: 502,503,4,3	
		Note		: Each row in the drop down list box denotes one plane	
	Generating total loads in direction	ΣP_{Areas}	X	: 0.000	kN
			Y	: 267.264	kN
			Z	: 0.000	kN
		$\Sigma P_{Members}$	X	: 0.000	kN
			Y	: 267.264	kN
			Z	: 0.000	kN
	Total moment to the origin	ΣM_{Areas}	X	: -2565.730	kNm
			Y	: 0.000	kNm
			Z	: 3207.170	kNm
		$\Sigma M_{Members}$	X	: -2565.730	kNm
			Y	: 0.000	kNm
			Z	: 3207.170	kNm
	Cells selected for generating	Σ number of cells		: 17	
		Σ cell area		: 460.800	m²
	Convert loads to members No.			: 5-8,17-20,49-52,71-74, 93-96,115-118,421-426, 431-436	
3	From Area Loads via Plane				
	Area load direction	Global relative to the projected area:		: ☒ YP	
	Area of load application	☒ Fully closed plane			
	Load distribution type:	☒ Combined			
	Area load magnitude	☒ Constant		: 0.97	kN/m²
	Boundary of the area load plane	Corner nodes		: 897,896,500,501	
		Note		: Each row in the drop down list box denotes one plane	
	Generating total loads in direction	ΣP_{Areas}	X	: 0.000	kN
			Y	: 297.984	kN
			Z	: 0.000	kN
		$\Sigma P_{Members}$	X	: 0.000	kN
			Y	: 297.984	kN
			Z	: 0.000	kN
	Total moment to the origin	ΣM_{Areas}	X	: -7628.390	kNm
			Y	: 0.000	kNm
			Z	: 3575.810	kNm
		$\Sigma M_{Members}$	X	: -7628.390	kNm
			Y	: 0.000	kNm
			Z	: 3575.810	kNm
	Cells selected for generating	Σ number of cells		: 13	
		Σ cell area		: 307.200	m²
	Convert loads to members No.			: 133-136,155-158, 177-180,199-202, 407-410,417-420	

3.15 GENERATED LOADS

LC5: Wind in y

No.	Load Description				
4	From Area Loads via Plane				
	Area load direction	Global relative to the projected area:	:	☒ YP	
	Area of load application	☒ Fully closed plane			
	Load distribution type:	☒ Combined			
	Area load magnitude	☒ Constant	:	0.88	kN/m²
	Boundary of the area load plane	Corner nodes	:	501,500,1,2	
		Note	:	Each row in the drop down list box denotes one plane	
	Generating total loads in direction	ΣP_{Areas} X	:	0.000	kN
		Y	:	405.504	kN
		Z	:	0.000	kN
		$\Sigma P_{Members}$ X	:	0.000	kN
		Y	:	405.504	kN
		Z	:	0.000	kN
	Total moment to the origin	ΣM_{Areas} X	:	-3892.840	kNm
		Y	:	0.000	kNm
		Z	:	4866.050	kNm
		$\Sigma M_{Members}$ X	:	-3892.840	kNm
		Y	:	0.000	kNm
		Z	:	4866.050	kNm
	Cells selected for generating	Σ number of cells	:	17	
		Σ cell area	:	460.800	m²
	Convert loads to members No.		:	1-4,13-16,27,30,47,48, 67-70,89-92,111-114, 401-406,411-416	

4.0 RESULTS - SUMMARY

Description	Value	Unit	Comment
Load Case LC1 - Self-weight			
Sum of loads in X	0.000	kN	
Sum of support reactions in X	0.000	kN	
Sum of loads in Y	0.000	kN	
Sum of support reactions in Y	0.000	kN	
Sum of loads in Z	-4762.190	kN	
Sum of support reactions in Z	-4762.190	kN	Deviation 0.00%
Resultant of reactions about X	0.000	kNm	At center of gravity of model (X:12.000, Y:10.000, Z:17.240 m)
Resultant of reactions about Y	0.000	kNm	At center of gravity of model
Resultant of reactions about Z	0.000	kNm	At center of gravity of model
Max. displacement in X	0.42	mm	Member No. 410, x: 2.968 m
Max. displacement in Y	0.13	mm	FE Mesh Node No. 62806 (X: 24.000, Y: 20.000, Z: 25.600 m)
Max. displacement in Z	-9.90	mm	FE Mesh Node No. 54112 (X: 16.692, Y: 16.000, Z: 32.000 m)
Max. vector displacement	9.90	mm	FE Mesh Node No. 54112 (X: 16.692, Y: 16.000, Z: 32.000 m)
Max. rotation about X	0.19	°	FE Mesh Node No. 53510 (X: 7.308, Y: 20.000, Z: 32.000 m)
Max. rotation about Y	0.18	°	FE Mesh Node No. 62962 (X: 0.000, Y: 15.600, Z: 28.800 m)
Max. rotation about Z	-0.05	°	FE Mesh Node No. 1112 (X: 24.000, Y: 20.000, Z: 0.000 m)
Maximum member strain	0.00019	-	Member No. 88, x: 4.000 m
Maximum surface strain	0.00118	-	FE Mesh Node No. 699 (X: 24.000, Y: 0.000, Z: 25.600 m)
Method of analysis	Linear		Geometrically linear analysis
Reduction of stiffness			Cross-sections, Members, Surfaces
Number of load increments	1		
Number of iterations	1		
Maximum value of element of stiffness matrix on diagonal	2.266E+14		
Minimum value of element of stiffness matrix on diagonal	1.E+03		
Stiffness matrix determinant	6.131E+2999637		
Infinity Norm	4.532E+14		
Load Case LC2 - Imposed load			
Sum of loads in X	0.000	kN	
Sum of support reactions in X	0.000	kN	
Sum of loads in Y	0.000	kN	
Sum of support reactions in Y	0.000	kN	
Sum of loads in Z	-8352.000	kN	
Sum of support reactions in Z	-8352.000	kN	Deviation 0.00%
Resultant of reactions about X	0.000	kNm	At center of gravity of model (X:12.000, Y:10.000, Z:17.240 m)
Resultant of reactions about Y	0.000	kNm	At center of gravity of model
Resultant of reactions about Z	0.000	kNm	At center of gravity of model
Max. displacement in X	0.15	mm	FE Mesh Node No. 49661 (X: 14.000, Y: 11.819, Z: 29.181 m)
Max. displacement in Y	0.21	mm	FE Mesh Node No. 62806 (X: 24.000, Y: 20.000, Z: 25.600 m)
Max. displacement in Z	-25.49	mm	FE Mesh Node No. 46460 (X: 16.692, Y: 4.400, Z: 28.800 m)
Max. vector displacement	25.49	mm	FE Mesh Node No. 46460 (X: 16.692, Y: 4.400, Z: 28.800 m)
Max. rotation about X	0.55	°	FE Mesh Node No. 42933 (X: 7.308, Y: 20.000, Z: 25.600 m)
Max. rotation about Y	0.53	°	FE Mesh Node No. 62358 (X: 0.000, Y: 15.600, Z: 25.600 m)
Max. rotation about Z	0.13	°	FE Mesh Node No. 1148 (X: 14.000, Y: 20.000, Z: 19.200 m)
Maximum member strain	0.00051	-	Member No. 88, x: 4.000 m
Maximum surface strain	0.00227	-	FE Mesh Node No. 699 (X: 24.000, Y: 0.000, Z: 25.600 m)
Method of analysis	Linear		Geometrically linear analysis
Reduction of stiffness			Cross-sections, Members, Surfaces
Number of load increments	1		
Number of iterations	1		
Maximum value of element of stiffness matrix on diagonal	2.266E+14		
Minimum value of element of stiffness matrix on diagonal	1.E+03		
Stiffness matrix determinant	6.131E+2999637		
Infinity Norm	4.532E+14		
Load Case LC3 - Wind in x			
Sum of loads in X	-968.192	kN	
Sum of support reactions in X	-968.192	kN	Deviation -0.00%
Sum of loads in Y	0.000	kN	
Sum of support reactions in Y	0.000	kN	
Sum of loads in Z	0.000	kN	
Sum of support reactions in Z	0.000	kN	
Resultant of reactions about X	0.000	kNm	At center of gravity of model (X:12.000, Y:10.000, Z:17.240 m)
Resultant of reactions about Y	839.060	kNm	At center of gravity of model
Resultant of reactions about Z	0.006	kNm	At center of gravity of model
Max. displacement in X	-24.75	mm	FE Mesh Node No. 50934 (X: 24.000, Y: 11.000, Z: 30.425 m)
Max. displacement in Y	1.24	mm	FE Mesh Node No. 59828 (X: 24.000, Y: 0.000, Z: 12.800 m)
Max. displacement in Z	3.03	mm	FE Mesh Node No. 1125 (X: 24.000, Y: 20.000, Z: 12.800 m)
Max. vector displacement	24.75	mm	FE Mesh Node No. 50934 (X: 24.000, Y: 11.000, Z: 30.425 m)
Max. rotation about X	-0.28	°	FE Mesh Node No. 18435 (X: 24.000, Y: 20.000, Z: 12.750 m)
Max. rotation about Y	-0.45	°	FE Mesh Node No. 34797 (X: 24.000, Y: 10.000, Z: 19.623 m)
Max. rotation about Z	0.17	°	FE Mesh Node No. 40209 (X: 24.000, Y: 9.000, Z: 24.025 m)
Maximum member strain	0.00021	-	Member No. 411, x: 0.000 m
Maximum surface strain	0.01390	-	FE Mesh Node No. 304 (X: 24.000, Y: 20.000, Z: 12.800 m)
Method of analysis	Linear		Geometrically linear analysis
Reduction of stiffness			Cross-sections, Members, Surfaces
Number of load increments	1		
Number of iterations	1		
Maximum value of element of stiffness matrix on diagonal	2.266E+14		
Minimum value of element of stiffness matrix on diagonal	1.E+03		
Stiffness matrix determinant	6.131E+2999637		
Infinity Norm	4.532E+14		
Load Case LC5 - Wind in y			
Sum of loads in X	0.000	kN	

4.0 RESULTS - SUMMARY

Description	Value	Unit	Comment
Sum of support reactions in X	0.000	kN	
Sum of loads in Y	1164.290	kN	
Sum of support reactions in Y	1164.290	kN	Deviation 0.00%
Sum of loads in Z	0.000	kN	
Sum of support reactions in Z	0.000	kN	
Resultant of reactions about X	1030.560	kNm	At center of gravity of model (X:12.000, Y:10.000, Z:17.240 m)
Resultant of reactions about Y	0.000	kNm	At center of gravity of model
Resultant of reactions about Z	0.000	kNm	At center of gravity of model
Max. displacement in X	5.80	mm	FE Mesh Node No. 896 (X: 0.000, Y: 0.000, Z: 32.000 m)
Max. displacement in Y	39.14	mm	Member No. 419, x: 3.392 m
Max. displacement in Z	2.77	mm	FE Mesh Node No. 28340 (X: 0.000, Y: 0.000, Z: 18.000 m)
Max. vector displacement	39.48	mm	Member No. 419, x: 3.392 m
Max. rotation about X	0.40	°	FE Mesh Node No. 1 (X: 0.000, Y: 0.000, Z: 0.000 m)
Max. rotation about Y	0.17	°	FE Mesh Node No. 196 (X: 12.500, Y: 12.000, Z: 3.200 m)
Max. rotation about Z	0.40	°	FE Mesh Node No. 1003 (X: 0.000, Y: 0.000, Z: 0.000 m)
Maximum member strain	0.00047	-	Member No. 414, x: 2.736 m
Maximum surface strain	0.00666	-	FE Mesh Node No. 59828 (X: 24.000, Y: 0.000, Z: 12.800 m)
Method of analysis	Linear		Geometrically linear analysis
Reduction of stiffness			Cross-sections, Members, Surfaces
Number of load increments	1		
Number of iterations	1		
Maximum value of element of stiffness matrix on diagonal	2.266E+14		
Minimum value of element of stiffness matrix on diagonal	1.E+03		
Stiffness matrix determinant	6.131E+2999637		
Infinity Norm	4.532E+14		
Load Combination CO1 - ULS wind x			
Sum of loads in X	-406.641	kN	
Sum of support reactions in X	-406.641	kN	Deviation 0.00%
Sum of loads in Y	0.000	kN	
Sum of support reactions in Y	0.000	kN	
Sum of loads in Z	-16931.20	kN	
Sum of support reactions in Z	-16931.20	kN	Deviation 0.00%
Resultant of reactions about X	-0.01	kNm	At center of gravity of model (X:12.00, Y:10.00, Z:17.24 m)
Resultant of reactions about Y	352.46	kNm	At center of gravity of model
Resultant of reactions about Z	0.02	kNm	At center of gravity of model
Max. displacement in X	-11.29	mm	FE Mesh Node No. 50934 (X: 24.000, Y: 11.000, Z: 30.425 m)
Max. displacement in Y	0.36	mm	FE Mesh Node No. 62806 (X: 24.000, Y: 20.000, Z: 25.600 m)
Max. displacement in Z	-52.38	mm	FE Mesh Node No. 46448 (X: 16.692, Y: 4.000, Z: 28.800 m)
Max. vector displacement	53.08	mm	FE Mesh Node No. 46448 (X: 16.692, Y: 4.000, Z: 28.800 m)
Max. rotation about X	1.08	°	FE Mesh Node No. 42933 (X: 7.308, Y: 20.000, Z: 25.600 m)
Max. rotation about Y	-1.01	°	FE Mesh Node No. 63005 (X: 24.000, Y: 4.400, Z: 28.800 m)
Max. rotation about Z	-0.30	°	FE Mesh Node No. 1103 (X: 10.000, Y: 20.000, Z: 19.200 m)
Maximum member strain	0.00089	-	Member No. 81, x: 4.000 m
Maximum surface strain	0.00995	-	FE Mesh Node No. 59701 (X: 0.000, Y: 0.000, Z: 12.800 m)
Method of analysis	Linear		Geometrically linear analysis
Reduction of stiffness			Materials, Cross-sections, Members, Surfaces
Number of load increments	1		
Number of iterations	1		
Maximum value of element of stiffness matrix on diagonal	1.818E+14		
Minimum value of element of stiffness matrix on diagonal	1.E+03		
Stiffness matrix determinant	1.681E+2996664		
Infinity Norm	3.636E+14		
Load Combination CO2 - ULS wind y			
Sum of loads in X	0.000	kN	
Sum of support reactions in X	0.000	kN	
Sum of loads in Y	489.001	kN	
Sum of support reactions in Y	489.001	kN	Deviation 0.00%
Sum of loads in Z	-16931.20	kN	
Sum of support reactions in Z	-16931.20	kN	Deviation 0.00%
Resultant of reactions about X	432.83	kNm	At center of gravity of model (X:12.00, Y:10.00, Z:17.24 m)
Resultant of reactions about Y	0.00	kNm	At center of gravity of model
Resultant of reactions about Z	0.00	kNm	At center of gravity of model
Max. displacement in X	3.38	mm	Member No. 410, x: 2.968 m
Max. displacement in Y	17.50	mm	Member No. 419, x: 3.392 m
Max. displacement in Z	-52.57	mm	FE Mesh Node No. 49068 (X: 16.692, Y: 16.000, Z: 28.800 m)
Max. vector displacement	54.36	mm	FE Mesh Node No. 49068 (X: 16.692, Y: 16.000, Z: 28.800 m)
Max. rotation about X	1.08	°	FE Mesh Node No. 42933 (X: 7.308, Y: 20.000, Z: 25.600 m)
Max. rotation about Y	1.01	°	FE Mesh Node No. 62890 (X: 0.000, Y: 4.400, Z: 28.800 m)
Max. rotation about Z	0.38	°	FE Mesh Node No. 1126 (X: 19.000, Y: 20.000, Z: 9.600 m)
Maximum member strain	0.00089	-	Member No. 125, x: 4.000 m
Maximum surface strain	0.00819	-	FE Mesh Node No. 62689 (X: 0.000, Y: 0.000, Z: 25.600 m)
Method of analysis	Linear		Geometrically linear analysis
Reduction of stiffness			Materials, Cross-sections, Members, Surfaces
Number of load increments	1		
Number of iterations	1		
Maximum value of element of stiffness matrix on diagonal	1.818E+14		
Minimum value of element of stiffness matrix on diagonal	1.E+03		
Stiffness matrix determinant	1.681E+2996664		
Infinity Norm	3.636E+14		
Load Combination CO3 - SLS (no wind)			
Sum of loads in X	0.000	kN	
Sum of support reactions in X	0.000	kN	

4.0 RESULTS - SUMMARY

	Description	Value	Unit	Comment
	Sum of loads in Y	0.000	kN	
	Sum of support reactions in Y	-0.000	kN	
	Sum of loads in Z	-13114.20	kN	
	Sum of support reactions in Z	-13114.20	kN	Deviation 0.00%
	Resultant of reactions about X	-0.23	kNm	At center of gravity of model (X:12.00, Y:10.00, Z:17.24 m)
	Resultant of reactions about Y	1.18	kNm	At center of gravity of model
	Resultant of reactions about Z	0.00	kNm	At center of gravity of model
	Max. displacement in X	0.73	mm	Member No. 410, x: 2.968 m
	Max. displacement in Y	0.49	mm	FE Mesh Node No. 62806 (X: 24.000, Y: 20.000, Z: 25.600 m)
	Max. displacement in Z	-39.76	mm	FE Mesh Node No. 46448 (X: 16.692, Y: 4.000, Z: 28.800 m)
	Max. vector displacement	39.76	mm	FE Mesh Node No. 46448 (X: 16.692, Y: 4.000, Z: 28.800 m)
	Max. rotation about X	0.82	°	FE Mesh Node No. 48389 (X: 7.308, Y: 20.000, Z: 28.800 m)
	Max. rotation about Y	0.76	°	FE Mesh Node No. 62962 (X: 0.000, Y: 15.600, Z: 28.800 m)
	Max. rotation about Z	0.22	°	FE Mesh Node No. 1148 (X: 14.000, Y: 20.000, Z: 19.200 m)
	Maximum member strain	0.00068	-	Member No. 176, x: 4.000 m
	Maximum surface strain	0.00494	-	FE Mesh Node No. 699 (X: 24.000, Y: 0.000, Z: 25.600 m)
	Method of analysis	2nd Order		Second order analysis (Nonlinear, Timoshenko)
	Internal forces referred to deformed system for...	☒		N, V_y, V_z, M_y, M_z, M_T
	Reduction of stiffness			Materials, Cross-sections, Members, Surfaces
	Consider favorable effects of tensile forces	☒		
	Divide results by CO factor	☐		
	Number of load increments	1		
	Number of iterations	3		
	Maximum value of element of stiffness matrix on diagonal	1.818E+14		
	Minimum value of element of stiffness matrix on diagonal	1.E+03		
	Stiffness matrix determinant	7.984E+2996591		
	Infinity Norm	3.636E+14		
Load Combination CO4 - SLS (wind x)				
	Sum of loads in X	-968.192	kN	
	Sum of support reactions in X	-968.192	kN	Deviation 0.00%
	Sum of loads in Y	0.000	kN	
	Sum of support reactions in Y	0.000	kN	
	Sum of loads in Z	-4762.190	kN	
	Sum of support reactions in Z	-4762.190	kN	Deviation 0.00%
	Resultant of reactions about X	-0.04	kNm	At center of gravity of model (X:12.00, Y:10.00, Z:17.24 m)
	Resultant of reactions about Y	777.58	kNm	At center of gravity of model
	Resultant of reactions about Z	0.01	kNm	At center of gravity of model
	Max. displacement in X	-27.63	mm	FE Mesh Node No. 50934 (X: 24.000, Y: 11.000, Z: 30.425 m)
	Max. displacement in Y	1.11	mm	FE Mesh Node No. 59828 (X: 24.000, Y: 0.000, Z: 12.800 m)
	Max. displacement in Z	-11.50	mm	FE Mesh Node No. 54112 (X: 16.692, Y: 16.000, Z: 32.000 m)
	Max. vector displacement	27.65	mm	FE Mesh Node No. 50934 (X: 24.000, Y: 11.000, Z: 30.425 m)
	Max. rotation about X	-0.29	°	FE Mesh Node No. 22870 (X: 0.000, Y: 0.000, Z: 12.850 m)
	Max. rotation about Y	-0.46	°	FE Mesh Node No. 34797 (X: 24.000, Y: 10.000, Z: 19.623 m)
	Max. rotation about Z	0.17	°	FE Mesh Node No. 34753 (X: 24.000, Y: 9.000, Z: 20.825 m)
	Maximum member strain	0.00026	-	Member No. 0, x: 0.000 m
	Maximum surface strain	0.01476	-	FE Mesh Node No. 59701 (X: 0.000, Y: 0.000, Z: 12.800 m)
	Method of analysis	2nd Order		Second order analysis (Nonlinear, Timoshenko)
	Internal forces referred to deformed system for...	☒		N, V_y, V_z, M_y, M_z, M_T
	Reduction of stiffness			Materials, Cross-sections, Members, Surfaces
	Consider favorable effects of tensile forces	☒		
	Divide results by CO factor	☐		
	Number of load increments	1		
	Number of iterations	3		
	Maximum value of element of stiffness matrix on diagonal	1.818E+14		
	Minimum value of element of stiffness matrix on diagonal	1.E+03		
	Stiffness matrix determinant	3.373E+2996634		
	Infinity Norm	3.636E+14		
Load Combination CO5 - SLS (wind y)				
	Sum of loads in X	0.000	kN	
	Sum of support reactions in X	-0.000	kN	
	Sum of loads in Y	1164.290	kN	
	Sum of support reactions in Y	1164.290	kN	Deviation 0.00%
	Sum of loads in Z	-4762.190	kN	
	Sum of support reactions in Z	-4762.190	kN	Deviation 0.00%
	Resultant of reactions about X	948.40	kNm	At center of gravity of model (X:12.00, Y:10.00, Z:17.24 m)
	Resultant of reactions about Y	0.21	kNm	At center of gravity of model
	Resultant of reactions about Z	0.90	kNm	At center of gravity of model
	Max. displacement in X	6.61	mm	Member No. 410, x: 3.392 m
	Max. displacement in Y	41.67	mm	Member No. 419, x: 3.392 m
	Max. displacement in Z	-12.03	mm	FE Mesh Node No. 54113 (X: 16.308, Y: 16.000, Z: 32.000 m)
	Max. vector displacement	42.03	mm	Member No. 419, x: 3.392 m
	Max. rotation about X	0.54	°	FE Mesh Node No. 4 (X: 0.000, Y: 20.000, Z: 0.000 m)
	Max. rotation about Y	-0.27	°	FE Mesh Node No. 57238 (X: 10.000, Y: 12.000, Z: 3.200 m)
	Max. rotation about Z	0.44	°	FE Mesh Node No. 1075 (X: 0.000, Y: 20.000, Z: 0.000 m)
	Maximum member strain	0.00049	-	Member No. 411, x: 2.968 m
	Maximum surface strain	0.00727	-	FE Mesh Node No. 62689 (X: 0.000, Y: 0.000, Z: 25.600 m)
	Method of analysis	2nd Order		Second order analysis (Nonlinear, Timoshenko)
	Internal forces referred to deformed system for...	☒		N, V_y, V_z, M_y, M_z, M_T
	Reduction of stiffness			Materials, Cross-sections, Members, Surfaces
	Consider favorable effects of tensile forces	☒		
	Divide results by CO factor	☐		
	Number of load increments	1		
	Number of iterations	3		
	Maximum value of element of stiffness matrix on diagonal	1.818E+14		
	Minimum value of element of stiffness matrix on d	1.E+03		

4.0 RESULTS - SUMMARY

	Description	Value	Unit	Comment
	diagonal			
	Stiffness matrix determinant	6.918E+2996634		
	Infinity Norm	3.636E+14		
Summary				
	Max. displacement in X	-27.63	mm	CO4, FE Mesh Node No. 50934 (X: 24.000, Y: 11.000, Z: 30.425 m)
	Max. displacement in Y	41.67	mm	CO5, Member No. 419, x: 3.392 m
	Max. displacement in Z	-52.57	mm	CO2, FE Mesh Node No. 49068 (X: 16.692, Y: 16.000, Z: 28.800 m)
	Max. vector displacement	54.36	mm	CO2, FE Mesh Node No. 49068 (X: 16.692, Y: 16.000, Z: 28.800 m)
	Max. rotation about X	1.08	°	CO1, FE Mesh Node No. 42933 (X: 7.308, Y: 20.000, Z: 25.600 m)
	Max. rotation about Y	1.01	°	CO2, FE Mesh Node No. 62890 (X: 0.000, Y: 4.400, Z: 28.800 m)
	Max. rotation about Z	0.44	°	CO5, FE Mesh Node No. 1075 (X: 0.000, Y: 20.000, Z: 0.000 m)
	Other Settings:			
	Number of 1D finite elements	4225		
	Number of 2D finite elements	62637		
	Number of 3D finite elements	0		
	Number of FE mesh nodes	63992		
	Number of equations	383952		
	Internal forces referred to deformed system for...:			
	Max. number of iterations	100		
	Number of divisions for member results	10		
	Division of cable/foundation/tapered members	10		
	Number of member divisions for searching maximum values	10		
	Subdivisions of FE mesh for graphical results	0		
	Percentage of iterations according to Picard method in combination with Newton-Raphson method	5	%	
	Options:			
	Activate shear stiffness of members (Ay, Az)	☒		
	Activate member divisions for large deformation or post-critical analysis	☒		
	Activate entered stiffness modifications	☒		
	Ignore rotational degrees of freedom	☐		
	Check of critical forces of members	☒		
	Nonsymmetric direct solver if demanded by nonlinear model	☐		
	Method for the system of equations	Direct		
	Plate bending theory	Mindlin		
	Solver version	64-bit		
	Precision and Tolerance:			
	Change default setting	☐		

DEPARTMENT OF ARCHITECTURE AND CIVIL ENGINEERING
CHALMERS UNIVERSITY OF TECHNOLOGY
Gothenburg, Sweden
www.chalmers.se

CHALMERS
UNIVERSITY OF TECHNOLOGY